Universitat de Lleida

Sistemas solares innovadores basados en membranas poliméricas combinadas con tecnologías fotovoltaicas orgánicas para integración arquitectónica

Álex Moreno Bellostes

Universitat de Lleida

TESI DOCTORAL

Sistemas solares innovadores basados en membranas poliméricas combinadas con tecnologías fotovoltaicas orgánicas para integración arquitectónica

Álex Moreno Bellostes

Memòria presentada per optar al grau de Doctor per la Universitat de Lleida

Programa de Doctorat en Enginyeria i Tecnologies de la Informació

Director

Daniel Chemisana Villegas

Tutor/a

Daniel Chemisana Villegas

Agradecimientos

Resumen

El objetivo de la presente tesis es desarrollar un sistema fotovoltaico para ser integrado arquitectónicamente que, basado en membranas poliméricas y células orgánicas semitransparentes, promueva la consecución de edificios más eficientes mediante la generación de electricidad, el control lumínico y la mejora de la eficiencia energética de los cerramientos semitransparentes.

Los sistemas solares integrados en edificios representan unos elementos que cumplen una doble función. Por un lado actúan como elemento constructivo y por el otro son elementos generadores. Esta ambivalencia les posición como imprescindibles para cumplir los requisitos establecidos por la comisión Europea en materia de eficiencia energética en edificios. El sistema objeto de la tesis pueden ser incluido en zonas que requieren un material translucido o transparente como son ventanas, tragaluces o cualquier cerramiento transparente. Normalmente, los elementos translucidos que encontramos en la construcción de edificios están basados en vidrio, aunque existen otros materiales que pueden ofrecer prestaciones similares como son los polímeros. Un polímero con unas propiedades muy adecuadas para esta aplicación es el etileno tetrafluoroetileno (ETFE). La integración de sistemas fotovoltaicos en elementos translucidos exige la necesidad de cierta semitrasnparencia, este hecho ha propiciado que en los últimos años sea una propiedad muy estudiada en este campo de la física. Para explorar estos avances se ha realizado una revisión de las tecnologías fotovoltaicas semitransparentes. Se seleccionó la tecnología fotovoltaica orgánica (OPV) para integrarla conjuntamente con el ETFE, ya que los avances logrados en investigaciones previas muestran que es la tecnología más avanzada y prometedora para este fin.

Para llevar a cabo el análisis del nuevo sistema ETFE/OPV se ha realizado una caracterización de los diferentes materiales para determinar su comportamiento lumínico y eléctrico. La caracterización lumínica del ETFE y de las OPVs se ha realizado midiendo sus propiedades ópticas para un espectro ancho de hasta 50 μm, obteniéndose las principales características ópticas. Referente a las OPVs, se ha realizado una caracterización eléctrica en condiciones reales de operación, no solo para determinar su eficiencia sino también su estabilidad. A partir de aquí, se ha podido realizar un modelo y simulación dinámica de un sistema ETFE/OPV plano que permite ver el grado de aportación energética, la influencia en la demanda térmica y la afectación en el confort lumínico al ser integrado como cerramiento translucido.

Finalmente, partiendo de las propiedades ópticas, se ha realizado un modelo numérico que permite determinar el comportamiento térmico y eléctrico de las OPVs incorporadas en sistemas cojín multicapa de ETFE.

Summary

The objective of this thesis is to develop a photovoltaic system to be building integrated that, based on polymeric membranes and semi-transparent organic cells, promotes the achievement of more efficient buildings through the generation of electricity, light control and the improvement of energy efficiency in semitransparent glazing.

Solar systems integrated in buildings represent elements that serve a dual function. On the one hand, they act as a constructive element and, on the other hand, they are generating elements. This ambivalence positions them as essential to meet the requirements established by the European Commission regarding energy efficiency in buildings. The system object of the thesis can be included in zones that require a translucent or transparent material such as windows, skylights or any transparent enclosure. Normally, the translucent elements that we find in the construction of buildings are based on glass, albeit other materials that can offer similar benefits such as polymers exist. A polymer with very suitable properties for this application is ethylene tetrafluoroethylene (ETFE). The integration of photovoltaic systems in translucent elements requires certain semitransparency, this fact has led the transparency to be a property that has been widely studied in this field of physics in recent years. To explore these advances, a review of semitransparent photovoltaic technologies has been carried out. Organic photovoltaic (OPV) technology was selected to be integrated together with ETFE, since the advances made in previous research did show that it is the most advanced and promising technology to this purpose.

In order to perform an analysis of the new ETFE / OPV system, a characterization of the different materials has been conducted to determine their luminous and electrical performance. The luminous characterization of ETFE and OPVs has been carried out by measuring their optical properties for a wide spectrum of up to 50 μm, obtaining the main optical characteristics. Regarding the OPVs, an electrical characterization has been executed under real operating conditions, not only to determine its efficiency but also its stability. From here, it has been possible to build a model for the dynamic simulation of a flat ETFE/OPV system that reveals the degree of energy input, the influence on thermal demand and the effect on light comfort when the system is integrated as a translucent glazing.

Finally, based on the optical properties, a numerical model has been implemented that allows determining the thermal and electrical behavior of the OPVs incorporated in ETFE multilayer cushion systems.

Resum

L'objectiu de la present tesi és desenvolupar un sistema fotovoltaic per a ser integrat arquitectònicament que, basat en membranes polimèriques i cèl·lules orgàniques semitransparents, promogui la consecució d'edificis més eficients mitjançant la generació d'electricitat, el control lumínic i la millora de l'eficiència energètica dels tancaments semitransparents.

Els sistemes solars integrats en edificis representen uns elements que compleixen una doble funció. D'una banda actuen com a element constructiu i de l'altra són elements generadors. Aquesta ambivalència els posiciona com a imprescindibles per complir els requisits establerts per la Comissió Europea en matèria d'eficiència energètica en edificis. El sistema objecte de la tesi pot ser inclòs en zones que requereixen un material translúcid o transparent com són finestres, lluernes o qualsevol tancament transparent. Normalment, els elements translúcids que trobem en la construcció d'edificis estan basats en vidre, encara que existeixen altres materials que poden oferir prestacions similars com són els polímers. Un polímer amb unes propietats molt adequades per a aquesta aplicació és l'etilè tetrafluoroetilè (ETFE). La integració de sistemes fotovoltaics en elements translúcids exigeix la necessitat d'una certa semitransparència, aquest fet ha propiciat que en els últims anys sigui una propietat molt estudiada en aquest camp de la física. Per explorar aquests avenços s'ha realitzat una revisió de les tecnologies fotovoltaiques semitransparents. Es va seleccionar la tecnologia fotovoltaica orgànica (OPV) per integrar-la conjuntament amb l'ETFE, ja que els avenços aconseguits en investigacions prèvies mostren que és la tecnologia més avançada i prometedora per a aquest fi.

Per dur a terme l'anàlisi del nou sistema ETFE / OPV s'ha realitzat una caracterització dels diferents materials per determinar el seu comportament lumínic i elèctric. La caracterització lumínica de l'ETFE i de les OPV s'ha realitzat mesurant les seves propietats òptiques per a un espectre ample de fins a 50 micres, obtenint les principals característiques òptiques. Pel que fa a les OPV, s'ha realitzat una caracterització elèctrica en condicions reals d'operació, no només per determinar la seva eficiència sinó també la seva estabilitat. A partir d'aquí, s'ha pogut realitzar un model i simulació dinàmica d'un sistema ETFE / OPV pla que permet veure el grau d'aportació energètica, la influència en la demanda tèrmica i l'afectació en el confort lumínic a l'ésser integrat com a tancament translúcid.

Finalment, partint de les propietats òptiques, s'ha realitzat un model numèric que permet determinar el comportament tèrmic i elèctric de les OPV incorporades en sistemes coixí multicapa d'ETFE.

Tabla de contenido

Capítulo 1. Introducción

1. Contexto

El Acuerdo de París de 2015 [1] y la Agenda 2030 [2] de Desarrollo Sostenible de Naciones Unidas marcan el inicio de una agenda global sostenible, en respuesta la Unión Europea (UE) se ha comprometido a establecer un sistema energético sostenible, competitivo, seguro y descarbonizado hasta el año 2030. Mediante la Directiva 2018/844 [3] se establecen unos compromisos ambiciosos con horizonte de consecución 2030 en la Unión Europea para reducir las emisiones de gases de efecto invernadero (al menos un 40 % de aquí a 2030, en comparación con los niveles registrados en 1990), aumentar la proporción de energía renovable consumida (al menos un 32% de cuota de energías renovables) y conseguir un ahorro energético (al menos un 32,5% de mejora de la eficiencia energética). Esta directiva actualiza y fusiona las Directivas 2010/31/UE [4], relativa a la eficiencia energética de los edificios (EPBD), y la 2012/27/UE [5], relativa a la eficiencia energética.

La EPBD cubre una amplia gama de políticas y medidas de apoyo que ayudarán a los gobiernos nacionales de la UE a impulsar el rendimiento energético de los edificios y mejorar el stock de edificios existentes. Entre sus principales objetivos está el lograr un stock de edificios altamente eficientes y descarbonizados para el año 2050, edificios de consumo casi nulo (NZEB), ya requeridos desde 2019 en edificios públicos y, a partir de 2021 en viviendas de nueva construcción. Cabe puntualizar que en la actualidad todavía no ha aplicado de forma completa lo estipulado en la directiva EPBD. . Las directrices marcadas, tanto en nuevos edificios como en los ya existentes, sometidos a las reformas pertinentes se articula en una serie de normas e informes técnicos conocidos como las normas EPBD [6]. El organismo estatal encargado de gestionar esta normativa es el Comité Nacional de Normalización (CEN).

Uno de los conceptos ligados al EPBD es el de los Edificios de Consumo Casi Nulo, cuyo acrónimo inglés es NZEB. Para conseguir que un edificio sea considerado NZEB, puede contar con soluciones pasivas (aislamiento, rotura de puentes térmicos, control de infiltraciones, etc.) y activas, tales como la incorporación de sistemas de generación renovables. El EPBD no especifica qué tipos de energías renovables deberían usarse, pero los paneles fotovoltaicos son la opción más común, teniéndose en cuenta que el sol es el recurso energético más abundante, seguro y limpio y que la generación directa de electricidad tiene un alto valor y practicidad [7]. Por otro lado, destacar que los módulos solares térmicos son una tecnología de igual forma muy extendida, siendo utilizados en un número sustancial de edificios y, en el caso de España propiciados por la normativa vigente. Otras fuentes de energía renovables utilizadas en los edificios son sistemas geotérmicos (de bombas de calor de origen), de biomasa y de calefacción urbana centralizada con alta aportación de energía renovable [8]. Los módulos fotovoltaicos, FV, (y solares en general) pueden estar integrados arquitectónicamente BIPV-Building Integrated Photovoltaics) o añadidos al edificio (BAPV-Building Applied Photovoltaics)

durante la construcción o después de la fase de construcción. El concepto de BIPV lleva asociada una multifuncionalidad del elemento fotovoltaico, que además de generar, debe de cumplir una función arquitectónica (cerramiento, cubierta, etc.). En el caso de los sistemas BAPV esta doble función no es un requisito. Actualmente la tasa de utilización de los BIPV está alrededor del 3% [9], pero la necesidad y la idoneidad para poder contribuir a los propósitos NZEB la hacen una tecnología necesaria y con muchas expectativas. Como ya se ha introducido anteriormente, los sistemas BIPV pueden ser incluidos como elementos constructivos de las zonas opacas, cubriendo diferentes necesidades tales como tejados, fachadas, elementos de aislamiento, de protección [10] o en zonas acristaladas, zonas que requieren de un material translucido o semitransparente. Las tecnologías fotovoltaicas presentan diversos tipos de materiales que pueden satisfacer esta propiedad, catalogados como sistemas semitransparentes. Las células solares semitransparentes (ST) son un tipo de tecnología que combina los beneficios de permitir el paso de la luz visible la conversión de luz en electricidad.
Una de las mayores oportunidades para tales tecnologías, es su integración como ventanas y tragaluces o cualquier cerramiento translucido dentro de los edificios energéticamente sostenibles [11].

Teniéndose en cuenta lo anteriormente mencionado, la presente tesis aborda el desarrollo de un sistema semitransparente que combina células fotovoltaicas orgánicas y membranas poliméricas para ser integrado arquitectónicamente.

Una vez contextualizada la temática de la tesis, se definen los objetivos de esta tesis.

2. Objetivos

El objetivo principal de esta tesis es desarrollar un sistema fotovoltaico para ser integrado arquitectónicamente, que basado en membranas poliméricas y células orgánicas semitransparentes, promueva la consecución de edificios más eficientes mediante la generación de electricidad, el control lumínico y la mejora de la eficiencia energética de los cerramientos semitransparentes.

Para alcanzar este objetivo principal, se marcan una serie de objetivos parciales que se enuncian a continuación:

• Realizar una revisión bibliográfica de las membrana poliméricas de etileno tetrafluoroetileno (ETFE) y de los sistemas fotovoltaicos semitransparentes susceptibles de ser integrados arquitectónicamente. Mediante la elaboración del estado del arte, se ha conseguido adquirir una visión amplia de la funcionalidad del ETFE a través de sus propiedades como material utilizado en la construcción de envolventes de edificios. Por otro lado, se ha alcanzado una perspectiva sobre sistemas FV que permiten ser integrados o utilizados como elementos constructivos translúcidos que han facilitado las etapas

siguientes de la tesis. Una vez valoradas las diferentes tecnologías fotovoltaicas semitransparentes, se ha seleccionado como óptima la basada en células orgánicas (OPV).

•. Caracterizar y analizar el comportamiento eléctrico y óptico de los módulos solares orgánicos. Además, monitorizar durante un periodo de tiempo suficiente para poder la evolución temporal de su rendimiento y propiedades ópticas (estudio de estabilidad).

•. Caracterizar experimentalmente las propiedades ópticas de diferentes láminas de ETFE y módulos OPV para a partir de estas determinar las características luminosas, solares, radiativas y sus propiedades de color.

• Modelar y simular energética y lumínicamente un sistema semitransparente formado por ETFE y OPV como cerramiento translúcido en una vivienda tipo y para varias condiciones climáticas a lo largo de un año. De esta forma se conocerá la potencialidad de esta configuración a partir de su comportamiento en frente de las necesidades térmicas, eléctricas y lumínicas.

• Desarrollar de un modelo que permita determinar el comportamiento e interacción térmica y eléctrica de las células orgánicas incorporadas en sistemas multicapa de ETFE para un rango amplio de longitudes de onda que comprenda desde el ultravioleta-visible y hasta el infrarrojo lejano.

3. Estructura de la tesis

Los objetivos anteriormente plasmado se abordan en los siguientes cinco capítulos de la tesis (capítulos 2 al 6). Cada uno de ellos corresponde a un documento científico publicado o enviado a una revista pendiente de revisión de un alto impacto, excepto la revisión de las tecnologías FV que permiten lograr cierto grado de transparencia. Si bien este capítulo no se ha enviado a publicar, su contenido ha sido totalmente necesario para poder decidir sobre la tecnología fotovoltaica a adoptar. El orden de los capítulos corresponde a un orden lógico y orgánico de evaluación de un nuevo sistema constructivo. Se empieza por una revisión de los materiales que se quieren utilizar en el nuevo cerramiento, el análisis de las tecnologías FV que permiten su uso para sistemas translucidos seguido de un estado del arte del material polimérico para membranas arquitectónicas etileno tetrafluoroetileno (ETFE). Posteriormente se caracterizan estos materiales eléctrica y ópticamente para después poder llevar a cabo un análisis térmico y una simulación energética. La estructura desglosada de la tesis es la siguiente.

Capítulo 2: Estado del arte sobre tecnologías FV semitransparentes. En este capítulo se revisan las diferentes tecnologías FV que son susceptibles de poder ser utilizadas o incorporadas como elementos constructivos translúcidos. Se revisan los avances tecnológicos en cada una de las tecnologías, lo que nos permite entender y determinar el potencial de cada una de ellas para la presente aplicación.

Capítulo 3 Estado del arte sobre membranas poliméricas de ETFE. Este capítulo presenta una revisión bibliográfica de las características principales que hacen de este material un elemento constructivo emergente y con elevada proyección. Tales como sus propiedades mecánicas, lumínicas, acústicas, ambientales y sus principales usos en la arquitectura actual como envolvente de edificios. Este capítulo ha sido publicado con el título "Ethylene tetrafluoroethylene (ETFE) material: Critical issues and applications with emphasis on buildings" en la revista Renewable and Sustainable Energy Reviews en Febrero del 2018.

Capítulo 4. Análisis de eficiencia y estabilidad de tecnologías OPV. En este capítulo se realizan las medidas experimentales que permiten determinar la transmitancia, reflectancia y absortancia espectrales mediante espectrofotometría y el rendimiento eléctrico mediante trazado de curvas de intensidad-voltaje y monitorización bajo condiciones de operación en punto de máxima potencia de tres tecnologías FV orgánicas. Se ha realizado una campaña de monitorización lo suficientemente dilatada para poder evaluar la estabilidad y degradación de estas tecnologías y poder discernir en sus efectos sobre sus propiedades ópticas y eléctricas. Este capítulo está publicado con el título "Performance and stability of semitransparent OPVs for building integration: A benchmarking analysis" en la revista Renewable Energy en Julio de 2019.

Capítulo 5. Eficiencia energética y lumínica de envolventes de ETFE/OPV. En este capítulo, a partir de las mediante las mediciones espectrales del ETFE y un módulo fotovoltaico orgánico se realiza una modelización óptica que nos permite realizar una simulación dinámica anual para evaluar el comportamiento térmico/eléctrico/lumínico del sistema combinado ETFE/OPV semitransparente. Este capítulo está publicado con el título "Energy and Luminous Performance Investigation of an OPV/ETFE Glazing Element for Building Integration" publicado en la revista Energies en Abril de 2019

Capítulo 6. Análisis óptico y térmico de membranas ETFE/OPV en forma de cojín. En este capítulo se realiza un trazado de rayos espectral para determinar el intercambio radiativo entre las diferentes capas que componen una estructura ETFE/OPV tipo cojín hinchable, a diferencia del capítulo anterior en el que se analizan sistemas planos. Mediante este análisis se puede determinar el comportamiento térmico y eléctrico para diferentes configuraciones o disposición de la célula orgánica integrada en la estructura tipo cojín. Este capítulo está enviado al congreso 15th SDEWES "Design and modelling of an OPV-ETFE cushion for semi-transparent glazing".

Capítulo 7. Conclusiones e investigaciones futuras. Las conclusiones globales, discusión y oportunidades para futuros trabajos están incluidos en este capítulo como parte final de la tesis.

4. Referencias

[1] OECD, National Climate Change Adaptation. OECD, 2015.

[2] R. Bluth, The Sustainable Development Goals Report 2019. UN, 2019.

[3] DIRECTIVE (EU) 2018/844, "Directive 2018/844/EU Energy performance of buildings," Off. J. Eur. Union, vol. 2018, no. October 2012, pp. 75–91, 2018.

[4] EU, "Directive 2010/31/EU of the European Parliament and of the Council of 19 May 2010 on the energy performance of buildings (recast)," Off. J. Eur. Union, pp. 13–35, 2010.

[5] Comisión Europea, "Directiva 2012/27/UE del parlamento Europeo y del Consejo," D. Of. la Unión Eur., pp. 1–56, 2012.

[6] Comité técnico CTN 100 and Asociación Española de Normalización, "Eficiencia energética de los edificios Evaluación global de la eficiencia energética de los edificios Parte 1: Marco general y procedimientos (ISO 52000-1:2017)," p. 163, 2019.

[7] P. K. Nayak, S. Mahesh, H. J. Snaith, and D. Cahen, "Photovoltaic solar cell technologies: analysing the state of the art," Nat. Rev. Mater., vol. 4, no. 4, pp. 269–285, 2019.

[8] T. Building-integrated, "D2 . 3 - nZEB building concepts for the application of BIPV building elements," no. January 2016, 2020.

[9] T. M. R. Research, "Global, Transparency Market Research: Building Integrated Photovoltaics (BIPV) Market. Industry Analysis, Size, Share, Growth, Trends 2013–2019.," 2014.

[10] H. Kaan and T. Reijenga, "Photovoltaics in an architectural context," Prog. Photovoltaics Res. Appl., vol. 12, no. 6, pp. 395–408, 2004.

[11] J. Sun and J. J. Jasieniak, "Semi-transparent solar cells," J. Phys. D. Appl. Phys., vol. 50, no. 9, 2017.

Capítulo 2. Estado del arte sobre tecnologías fotovoltaicas semitransparentes

1. Células solares semitransparentes

Las principales tecnologías fotovoltaicas que pueden cumplir funciones de elemento semitransparente se muestran en la figura 1. Se han clasificado las mismas en función de su madurez y cronología en su desarrollo.

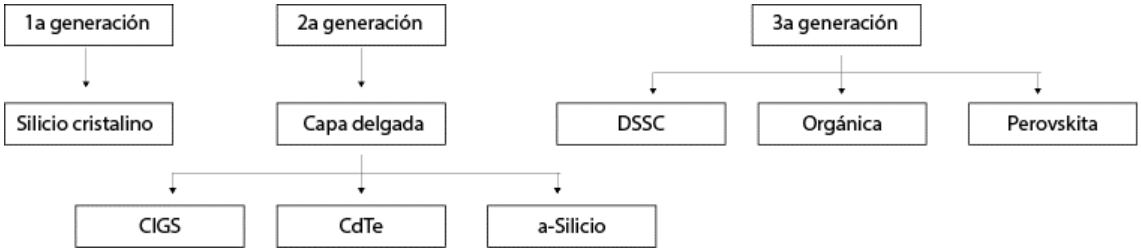

Figura 1. Tecnologías FV semitransparentes.

Según el método por el cual se consigue la semitransparencia en las células solares se pueden clasificar en células o módulos solares (entiendo un módulo como un conjunto de células interconectadas) de tipo apertura y células/módulos de tipo penetración (Figura 2). La célula/módulo de tipo apertura está formada por micro agujeros en la estructura de la célula solar, esto significa que partes de la célula solar son activas convirtiendo la irradiancia solar en electricidad, mientras que las otras regiones, las cuales no tienen material semiconductor, permiten que la luz pase. El nivel de transparencia de estas células depende del ratio entre la zona descubierta y el área total de apertura. En las tecnologías de capa (lámina) delgada los agujeros se pueden crear con cualquier forma mediante el procesado laser o por grabado químico; sin embargo, en los sistemas basados en silicio cristalino se requiere un mecanizado de precisión que elimine de forma efectiva el mayor espesor de semiconductor. Referente a las células tipo penetración, se consigue la semitransparencia reduciendo el grosor de la película fotoactiva, de esta forma una parte del rango visible será absorbido y el otro pasara a su través. La ventaja de la célula solar de tipo penetración sobre la célula solar de tipo apertura es que en la primera la potencia de salida no está fuertemente influenciada por el cambio en la transparencia. Usando este enfoque, la semitransparencia se puede introducir en todo tipo de células solares de película delgada. [1]

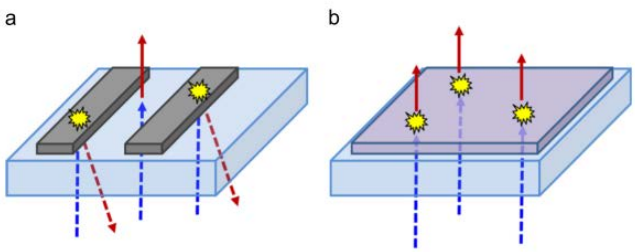

Figura 2. a) célula solar tipo apertura. b) célula solar tipo penetración.[2]

Las tecnologías de película delgada abren nuevas oportunidades para el diseño de dispositivos fotovoltaicos para ser integrados arquitectónicamente, es decir, células solares flexibles, que ofrecen una fuente de energía alternativa conveniente para aplicaciones en interiores y exteriores. Los módulos fotovoltaicos flexibles se pueden integrar fácilmente con infraestructuras de varias formas y tamaños, en consecuencia, estimulando el diseño de productos innovadores generadores de energía. Además, estos módulos flexibles son livianos y, por lo tanto, adecuados para aplicaciones donde el peso es importante. Económicamente, suponen una recuperación de la inversión mucho más rápida que los módulos fotovoltaicos convencionales y medioambientalmente son considerablemente más sostenibles [3]. Hasta la actualidad, se han desarrollado muchos materiales fotovoltaicos diferentes con diversos métodos de deposición en una variedad de sustratos flexibles para fabricar células solares flexibles. En consecuencia, según los materiales fotovoltaicos utilizados, las células solares flexibles se clasifican generalmente como: (1) células solares flexibles basadas en Si, (2) células solares flexibles y compuestas y (3) células solares orgánicas

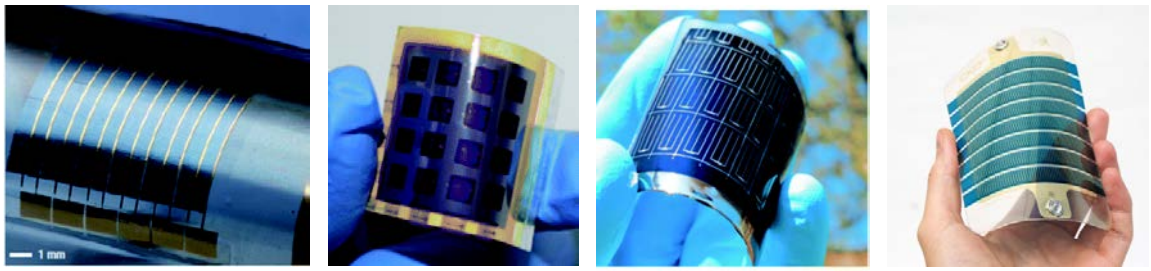

Figura 3. a) c-Si flexible. [4] b) a-Si [4]c) CGIS [4] d) célula solar orgánica[5]

A continuación se realizará una descripción sobre el uso de las diferentes tecnologías FV semitransparentes y flexibles que potencialmente pueden ser integradas arquitectónicamente. La primera tecnología que se incluye es la basada en silicio cristalino, siguiendo con las tecnologías de capa fina y, finalizando con tecnologías de tercera generación. En estas tecnologías (ver Fig. 1) se hará énfasis en la tecnología de células solares orgánicas debido a su utilización en la presente tesis.

2. Tecnologías de primera generación.

2.1. Silicio cristalino

Las células de silicio cristalino son las primeras candidatas atendiendo a su conocida estabilidad y alta eficiencia. Sin embargo su opacidad inherente dificulta su utilización como tecnología semitransparente. Por ese motivo, el uso de células de silicio cristalino como elementos constructivos de cerramientos semitransparente se ha basado en el uso de las matrices de ventanas BIPV estampadas basadas en alternar zonas con células

solares y zonas transparentes. La figura 4.a. muestra dos ejemplos de esta configuración [6], [7].

Recientemente se están utilizando micro células solares de silicio que permiten una mejor visibilidad a su través del vidrio. En 2019, Peng *et al.* [8] utilizaron células solares de silicio cristalino estándar en tiras muy estrechas que soldadas e interconectadas se laminaron entre un doble vidrio. Las transmisiones promedias en el rango del espectro solar y en la zona visible son 0.16 y 0.42, respectivamente. La eficiencia del área de laminado PV bajo condiciones estándar de test (STC) fue del 7% (solo alrededor de un tercio del laminado estaba cubierto por células solares). La figura 4.b contiene una fotografía de esta tecnología.

Lee *et al.* [9] demostraron un enfoque alternativo para construir un sustrato de c-Si transparente con un color neutro similar al vidrio, colocando ventanas de transmisión de luz en forma de micro agujeros, que no son visibles a simple vista, mostrando una eficiencia de conversión (PCE-Power Conversion Efficiency) de un 12.2% para una transmitancia del 20%(ver figura4.c).

Kang *et al.* [10] evaluaron una célula solar transparente flexible de color neutro y de alta eficiencia basada en una forma independiente de n microhilos de silicio (SiMWs-Silicon MicroWires). Los SiMWs de punta plana con espaciado controlable se fabricaron mediante grabado iónico reactivo profundo y se integraron en una matriz de polímero transparente independiente. La transmitancia de la luz se puede ajustar de alrededor del 10% al 55% ajustando el espacio entre los microhilos. Una celula solar transparente basada SiMW de punta inclinada demostró una eficiencia del 8% con una transparencia visible del 10% y con flexibilidad. Esta eficiencia es la más alta entre los semiconductores transparentes basados en Si y comparable con la de tecnologías de color neutro de última generación basados en perovskita híbrida orgánica-inorgánica y orgánicas.

a

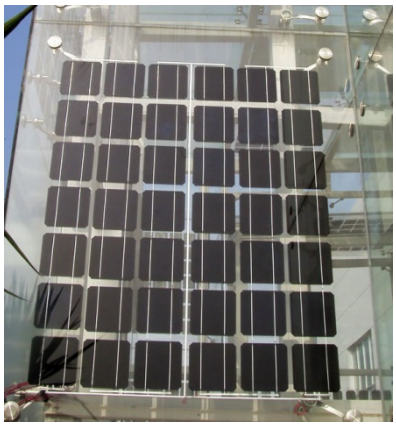

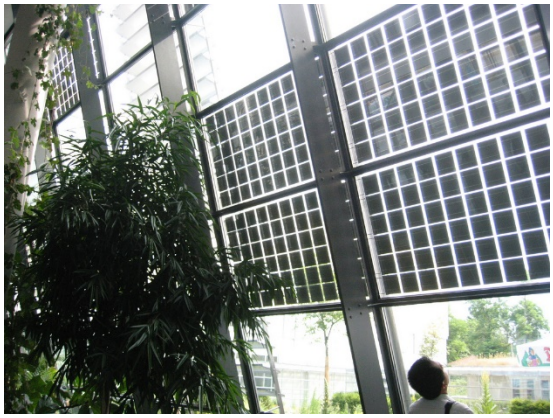

b

c

Figura 4. Sistemas semitransparentes de c-Si. a) Matrices de c-Si [11] b) c-Si [9] micro perforado c) c-Si SiMW..[8]

3. Tecnologías de segunda generación.

3.1. CdTe

La segunda generación de células solares está integrada por las células de lámina delgada. Esta lámina o láminas se pueden depositar sobre varios sustratos tales como vidrio, plástico o metal. Será entonces el sustrato el que confiera a la tecnología una determinada flexibilidad. Las células solares de película delgada se utilizan comercialmente en varias tecnologías, incluyendo teluro de cadmio (CdTe), diseleniuro de cobre, indio y galio (CIGS) y silicio amorfo (a-Si). Las células solares de película delgada (TFs-Thin Films) han pasado la adolescencia y están listas para hacer una contribución sustancial a la generación de electricidad en el mundo. Pueden tener ventajas sobre los módulos solares de c-Si, posibilidad de áreas más grandes, fabricación de menor costo y en versatilidad para ser utilizadas en varios tipos de aplicaciones.[12].

El teluro de cadmio es un compuesto cristalino estable formado a partir de cadmio y teluro. La película delgada CdTe tiene mucho potencial para la aplicación fotovoltaica debido a que es un semiconductor de band gap directo con un intervalo de energías prohibidas de 1.45 eV, que coincide estrechamente con la máxima intensidad del espectro solar. Para construir células solares CdTe transparentes, se deben alcanzar dos pasos cruciales de desarrollo para permitir la transmisión de la luz incidente: el contacto posterior metálico no transparente debe ser reemplazado por un contacto posterior

transparente [13]. Debido al intervalo de banda fijo y al alto coeficiente de absorción del CdTe, la cantidad de luz transmitida por debajo de 860 nm solo puede aumentarse disminuyendo su espesor por debajo de 1 μm [14].

Plotnikov *et al.*[15] realizaron una estructura de vidrio de cal sodada / TCO / HRT / CdS / CdTe / BC, donde el contacto transparente (TCO-Transparent Conductive Oxide) era SnO2:F, la capa transparente de alta resistividad (HRT-High Resistivity Transparent) era típicamente SnO2 de 50 a 100 nm de espesor, el CdS pulverizado tenía espesores de 40 a 80 nm y el espesor de CdTe se varió de 250 nm a 2500 nm. Utilizaron una serie de materiales como contacto posterior (BC-Back Contact), de los que no se especifican las características. Esta configuración consiguió alcanzar eficiencias en el rango del 8% al 12.6. Si bien en el artículo se muestran diversos módulos semitransparentes, los autores no indican las transmitancias de los mismos.

Durante el mismo año que los autores anteriores, 2013, Heisler *et al.* [14] estudiaron el rendimiento de las células solares CdTe con diferentes espesores de capa absorbente de CdTe depositados a dos temperaturas de sustrato diferentes. Variaron el grosor de CdTe de 0.2 a 5 μm ajustando el tiempo de deposición y utilizando como contacto posterior de óxido de cinc y aluminio para lograr una célula solar CdTe transparente. Para un espesor de absorbente de 0.25 μm, las células solares del proceso de baja temperatura mostraron eficiencias del 4%. En la figura 5.a se muestran los valores de eficiencia eléctrica para diferentes grosores de CdTe y diferentes temperaturas del sustrato. En la figura 5. b se muestran los valores de transmisión del espectro solar para diferentes grosores de la capa de CdTe.

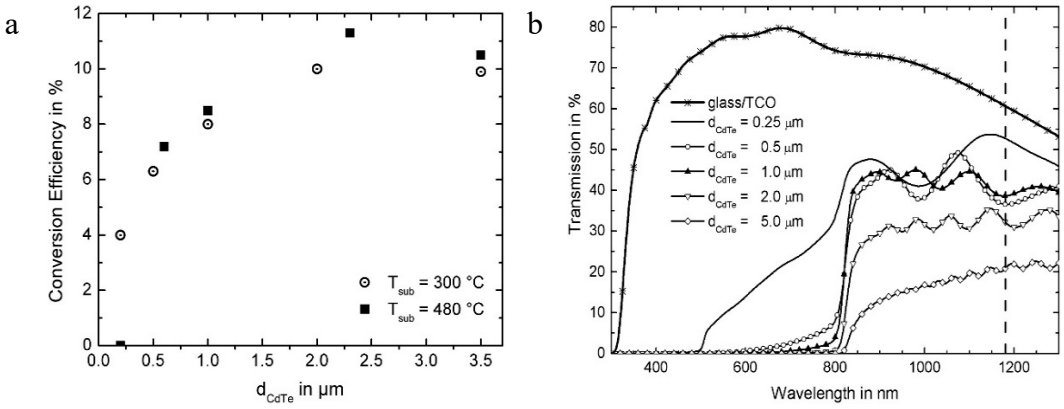

Figura 5. a) Eficiencia de las células solares con capas absorbentes de CdTe de alta y baja temperatura y diferentes espesores absorbentes b) Transmitancia espectral del vidrio con TCO y de las agrupaciones de capa de vidrio / TCO / CdS / CdTe con diferentes espesores de capa de CdTe entre 0.25 y 5 μm [14].

Sun *et al.* [16] evaluaron mediante los programas informáticos Energyplus y Radiance el comportamiento en una oficina incorporando por ventanas semitransparentes fotovoltaicas. Seleccionaron el acristalamiento con células solares CdTe de película

delgada integradas con un 10% de transmitancia. En este caso, la transparencia fue conseguida mediante la eliminación de parte del material activo. Sabry *et al.* [17] analizaron unos módulos de CdTe de superficie 1200 × 600 mm^2, con diferentes potencias pico 48W, 64W, y 72W y, en concordancia con diferentes transmisiones del espectro visible: 40%, 20%, y 10%, respectivamente. Meng *et al.*[18] ensayaron el rendimiento energético de CdTe semitransparente para integración en edificios. Compararon una ventana con CdTe y una con a-Si. Los resultados muestraron una producción de la ventana de a-Si y la ventana de CdTe de 41.8 kWh/m^2 y 52.3 kWh/m^2, respectivamente.. Recientemente, Liu *et al.* (2019) [19] midieron las transmisiones espectrales de cuatro configuraciones de ventanas de CdTe con un 20%, 30%, 40% y50% de parte transparente (sin material activo) y determinaron las propiedades de color de las ventanas mediante los indicadores temperatura de color correlacionada(CCT) y el índice de reproducción cromática (CRI). Determinaron que las ventanas de CdTe pueden lograr un valor de CCT recomendado (3300-5000K) cuando la fuente de luz diurna está en el rango de 4000K y 6500K. El CRI de todas las ventanas se puedo mantener en un rango de comodidad superior a 90. Las mediciones espectrales de la transmisión visible CdTe-20%, CdTe-30%, CdTe-40% y CdTe-50% son 8%, 13%, 19% y 29%, respectivamente

Finalmente, comentar que Alrashidi *et al.* (2020) [13] han analizado por primera vez el rendimiento térmico de una ventana de CdTe, siendo comparada con un acristalamiento simple. Han determinado el coeficiente de transferencia térmica y la ganancia solar. De la medición espectral obtuvo una transmisión visible del 25% y una transmisión solar del 12%. Se encontró un coeficiente global de transferencia de calor (valor U) de 2.7 W/m^2K frente los 5.7 W/m^2K del acristalamiento simple y una ganancia solar del 20% frente al 72.8% del acristalamiento simple. En la Figura 6.a se muestra la medidas espectrales del rango solar y en la figura 6.b las dos muestras analizadas; el acristalamiento simple y la ventana CdTe.

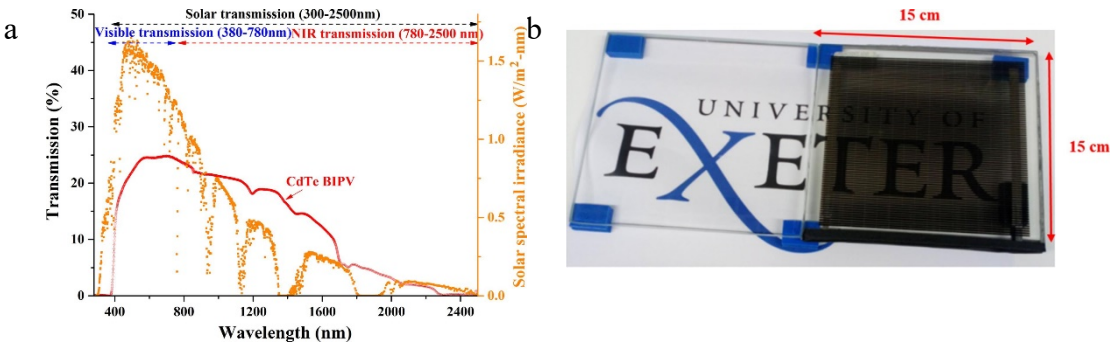

Figura 6. a) Transmitancia de la célula semitransparente de CdTe b) Fotografía del vidrio simple y una célula semitransparente de CdTe. [13]

3.2. CIGS

Las células solares de película delgada basadas en calcopirita como Cu (In_x, Ga_{1-x}) Se_2 (CIGS) y Cu (In_x, Ga_{1-x}) (Sy, Se_{1-y}) (CIGSSe) se han considerado alternativas prometedoras al silicio cristalino debido a su alto coeficiente de absorción, separación de banda sintonizable y flexibilidad, logrando eficiencias de célula de hasta el 22.9% [20]. Para este tipo de células solares, las referencias de sistemas semitransparentes son menores a las halladas sobre células de teluro de cadmio. A continuación se describe las más representativas.

Moon *et al.* [21] examinaron tres películas absorbentes CIGS con diferentes niveles de espesor (400, 800, 1200 nm) con el fin de investigar el rendimiento de la célula solar en función del espesor de la capa activa de CIGS. Para el caso con la película absorbente más delgada, la transmisión media en el rango 600–750 nm fue del 20%, registrando una eficiencia del 1.7%. Saifullah *et al.* [22] realizaron un trabajo sobre una célula solar CIGS de 230 nm de espesor modificada con una capa de AgGa sulfurizado previo al contacto posterior de óxido de estaño e indio de 45 nm de espesor. Esta configuración exhibió una eficiencia del 5.94% con una transmitancia visible promedio de más del 25%. Esta es la eficiencia más alta reportada para una celda solar semitransparente de CIGS. En la figura 7.a se muestra la composición de la célula y en la figura 7. b los valores de transmitancia. El último de los estudios incluidos, es el presentado por Sidali *et al.* [23], en el que presentan un proceso experimental para preparar células solares de CIGS para aplicaciones ST BIPV por el método de micro perforación utilizando como sustrato Mo. Los valores de eficiencia que reportaron son del 7.7%, con una transmitancia del 37%.

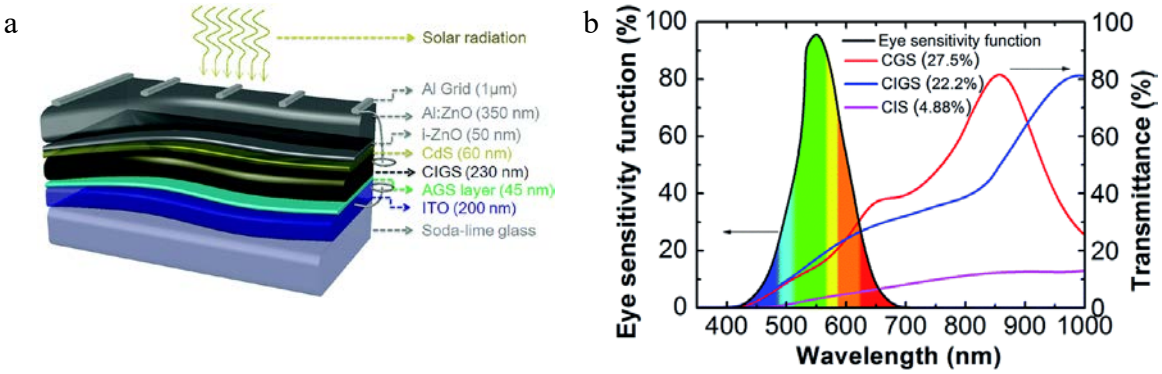

Figura 7. a) Esquema de un dispositivo basado en CIGS de 230 nm de espesor b) Curva de respuesta de sensibilidad ocular y transmitancias del dispositivo CIGS. [22]

3.3. a-Si

La celda solar de unión simple de silicio amorfo hidrogenado (a-Si:H) típica se compone de cinco capas principales: diodo de Si p-i-n intercalado entre dos capas conductoras. Apilando dos células a-Si: H/μc-Si: H una encima de la otra forma la estructura de unión en tándem, que también se intercala entre los contactos frontal y posterior.

Muchas células solares semitransparentes basadas en a-Si:H son de apertura. Las celdas de apertura se componen de rejillas rectangulares fabricadas por procesos de diseño complicados, como los que utilizan un láser para perforar o eliminar parcialmente las películas a-Si:H y las capas de contacto posterior [2].

Wook *et al.*[2] utilizaron un absorbente i-a-Si:H muy delgado de 115 nm de grosor para fabricar células solares a-Si: H semitransparentes por el método de penetración. Analizaron el comportamiento al utilizar diferentes capas con bandgaps elevado como capas de interfaz n/i para reducir la pérdida por resistencia en paralelo y mejorar la colección de portadores para este absorbedor ultra delgado. Investigaron las propiedades eléctricas y ópticas, obteniendo unos valores de transmitancia visible del 23.6% y un rendimiento eléctrico del 6.92%. En la. Yang *et al.* [24] desarrollaron una célula de óxido de silicio amorfo hidrogenado de capa p-i-n (a-SiOx: H) para mejorar su transmitancia en rangos el rango visibles de 500–800 nm para su aplicación en BIPV. Variaron el flujo de gas CO_2 / SiH_4 (R) de 0 a 0.6 durante el proceso de deposición de vapor con plasma para investigar el efecto de la adición de oxígeno. La configuración óptima se obtuvo para un flujo de gas, R, de 0.2, alcanzando una eficiencia eléctrica del 5.71% y una transmitancia del 18.94% para el rango espectral anteriormente mencionado. Recientemente, Cho *et al.* (2019) llevaron a cabo un estudio de una célula solar bifacial y semitransparente de a-Si: H. Fabricaron células con contactos transparentes utilizando deposición química de vapor mejorada con plasma (PECVD). Se investigaron las influencias de las diferentes capas (contactos transparentes (TCO), capas i, capas dopadas n y dopadas p) en los parámetros de rendimiento de las células solares bifaciales. Obtuvieron valores de eficiencia del 6.01% y una transmitancia del 22.76% [25].

4. Células solares de tercera generación.

Las tecnologías solares de tercera generación incluyen principalmente las OPVs (Organic solar cells), las células solares tipo perovskita y células solares sensibilizadas por colorantes (DSSC). Existen otras tecnologías de tercera generación como son las kesteritas o las células que incorporan puntos o pozos cuánticos que no se incluyen en el presente apartado. La energía fotovoltaica de tercera generación cuenta con la potencialidad de producir dispositivos de conversión de fotones a electricidad de alta

eficiencia a un costo de producción más económico, igual que las células de capa delgada su bajo espesor permiten su uso como material flexible

4.1. DSSC

DSSCs o también conocida como la célula de Grätzel en honor a su inventor, consiste en una capa transparente conductora de óxido (TCO) en sustratos de vidrio, un colorante, un fotoánodo, electrolitos y un contraelectrodo (CE). La figura 8 muestra un esquema que ilustra la estructura y comportamiento de un célula DSSC.

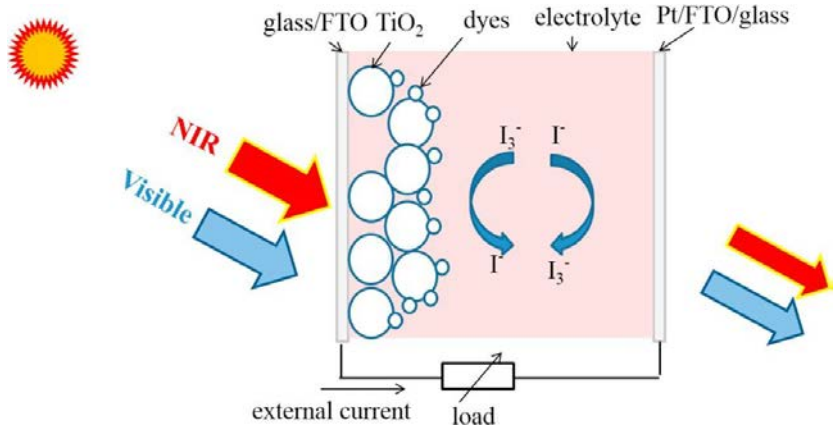

Figura 8. Ilustración esquemática de una célula DSSC [26]

Cuando la luz solar incide en la célula solar, los sensibilizadores de tinte en la superficie de la película de TiO_2 se excitan y los electrones a su vez se inyectan en la banda de conducción del TiO_2. Dentro de la película de TiO_2, los electrones inyectados se difunden completamente a través de la película mesoporosa hacia el ánodo y se utilizan para realizar un trabajo útil en la carga externa. Finalmente, para completar el ciclo, estos electrones son recogidos por el electrolito en el contraelectrodo que a su vez son absorbidos para regenerar el sensibilizador de tinte. [27]

Entre las células o módulos solares transparentes, las DSSC (célula solar sensibilizada por colorante) tienen un costo de producción relativamente bajo en comparación con las células solares a base de silicio y proporcionan una gama de colores muy adecuada para su integración de edificios. La transparencia de los DSSCs puede modificarse ajustando el tamaño de las nanopartículas de dióxido de titanio (TiO_2) y el grosor de la película. Además, la célula DSSC posee un coeficiente de temperatura positivo, en contraste con las células solares cristalinas[28].

El primer acristalamiento DSSC fue desarrollado por [29], conectando en serie células solares de TiO_2 sensibilizadas con colorante alcanzando valores de transmitancia media en el ancho de banda visible del 60% con un V_{oc} de 5.7 V y una J_{sc} de 220 mA.. En 2013, el mismo grupo determinaron las características térmicas y ópticas de las ventanas

DSSC utilizando unos tintes verdes (33% transparencia) y rojos (28% de transparencia) mediante el programa WINDOW 6.0. [30].

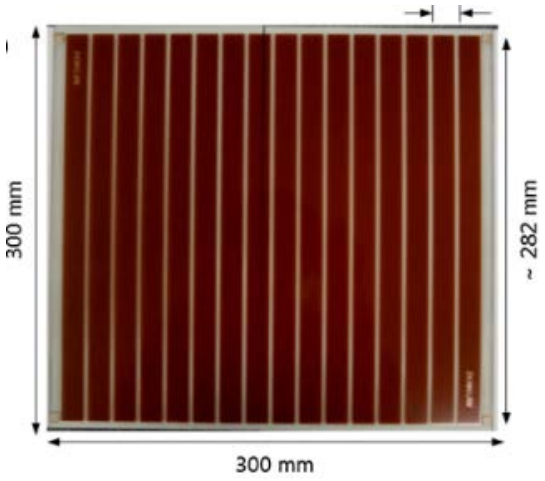

Figura 9. Módulo solar de DSSCs con colorante rojo [30].

Kim *et al*. (2017) presentaron las metodologías de diseño de un módulo DSSC transparente de área 300 × 300 mm^2 par a ser integrado en edificios. Mediante el programa informático PSpice realizaron un modelo equivalente 2D a partir del cual se estimó una eficiencia del 3.19% [31]. El mismo año, Morini *et al*. [32] realizaron una investigación sobre las características ópticas, térmicas y eléctricas de un módulo DSSC con los softwares Zemax, WINDOW y COMSOL. El estudio se centró en tres configuraciones principales que representan las principales posiciones posibles del módulo dentro de una ventana de doble acristalamiento: en la superficie exterior, en la superficie interna del vidrio expuesta al sol y dentro de la cavidad. Obtuvieron valores de transmitancia visible alrededor del 11% en todos los casos.

En 2018, Lee and Yoon *et al.* [33] realizaron un análisis del rendimiento energético de ventanas BIPV con DSSCs para dos inclinaciones de instalación diferentes. La eficiencia de potencia operativa de la ventana vertical varió de 2.65 a 4.14% con un promedio de 3.40%, mientras que la de la ventana inclinada se mantuvo en el rango 2.64–3.63% con una media de 3.01%. Ghosh *et al.* [26] estudiaron seis configuraciones de células DSSC a pequeña escala, variando el grosor de TiO_2, obteniendo valores de PCE que van desde 5.15 % cuando la capa de TiO_2 es más ancha y 2.1% cuando esta tiene 3.5 micrómetros. De forma opuesta a la tendencia en la eficiencia, al reducir el espesor de la capa de TiO_2 aumenta el valor de la transmitancia, que varía de aproximadamente el 53% al 25% cuando la capa de TiO_2 es más ancha. Cornaro *et al.* [34] reportaron una caracterización térmica y eléctrica un módulo DSM (Dye-Sensitized Module) en condiciones reales de funcionamiento, determinando el valor de

la transmitancia térmica (Valor *U*) y coeficiente de ganancia de calor solar (SHGC) de un prototipo DSM. El dispositivo exhibió un valor U de 3.6 W/m^2K y un SHGC de 0.2. La caracterización eléctrica mostro un aumento de la potencia del módulo con respecto a la temperatura, exhibiendo un coeficiente de temperatura de la potencia de 0.6 %/ºC. La eficiencia promedio durante el período de prueba fue de 1.69%, siendo la medida en condiciones estándar de 3.28%.

En 2019, Knott *et al.* [35] realizaron una trazado de rayos 3D basado en el algoritmo de Monte-Carlo para evaluar diferentes geometrías piramidales de TiO_2, obteniendo entre un 15-25% de mejora en la absorción de la luz. A partir de las simulaciones, encontraron unas transmisiones de la ventana DSSC con geometría piramidal y de la ventana DSSC plana del 11% y 29% respectivamente. Roy *et al.* [28] estudiaron el comportamiento lumínico de unas células DSSC de 0.2528 cm^2 con diferentes espesores de TiO_2 durante un periodo de 2 años, los espesores de estas células fueron de 3.5, 6 y 10 μm sobre vidrio FTO (Fluorine doped Tin Oxyde). Los dispositivos al inicio de la monitorización exhibieron eficiencias de conversión (PCE) de 2.51%, 4.49% y 5.93% en condiciones estándar. La transmitancia visible promedio (AVT) después de dos años cambió de 35 a 31%, 44 a 26% y 42 a 28% para los tres espesores de células comentados anteriormente. Cabe mencionar que el estudio estaba centrado en los parámetros lumínicos, únicamente reportando la eficiencia eléctrica del inicio del estudio. Además de reportar la evolución en la transmitancia en el rango visible, también analizan la variación del CCT y el CRI para las tres células

4.2. Perovskita

Una célula solar de perovskita (PSC) es un tipo de célula solar que incluye un compuesto estructurado tipo perovskita, más comúnmente un material híbrido orgánico-inorgánico a base de plomo o haluro de estaño, como la capa activa de captación de luz. La figura 10 muestra un esquema de célula tipo perovskita. Las perovskitas son materiales descritos por la fórmula ABX_3, donde X es un anión y A y B son cationes de diferentes tamaños (siendo A más grande que B). El catión más grande A es orgánico, generalmente el compuesto utilizado es el metilamonio ($CH_3NH_{3\ +}$) con un radio iónico de 0.18 nm, aunque el etilamonio ($CH_3CH_2NH_{3+}$), con un radio de 0.23 nm) y el formamidinio ($NH_2CH{=}NH_2$ +), con un radio iónico intermedio de entre 0.19 nm y 0.22 nm. El anión X es un halógeno, generalmente anión iodo (radio iónico = 0.220 nm), aunque el Br^- i Cl^- también se usan comúnmente (Radios de 0.196 nm y 0.181 nm respectivamente). De forma habitual en haluros mixtos, el catión B ha sido universalmente Pb (R_B = 0.119 nm) y Sn (R_B = 0.110 nm), que forma compuestos similares con bandgaps menores y teóricamente mejores [36].

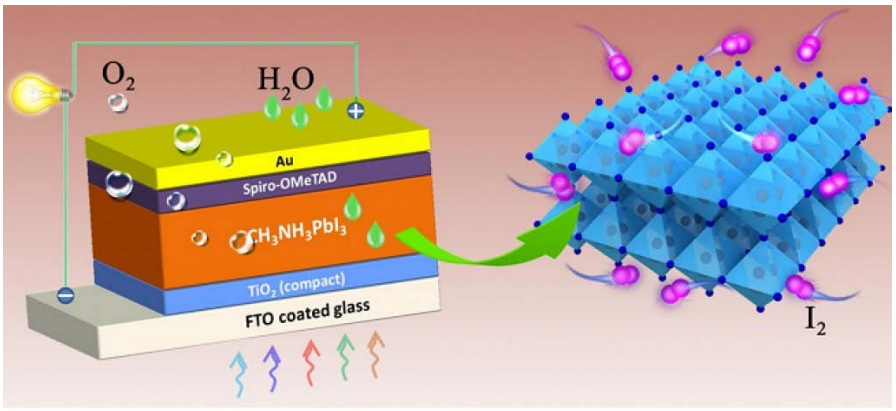

Figura 10. Esquema de una célula de perovskita [37].

Actualmente se han desarrollado células con una eficiencia del 21.6% [38]. Su coeficiente de absorción es aproximadamente un orden de magnitud mayor que el del c-Si y su grosor puede ser fácilmente controlado para fabricar una película delgada... Aunque se crearon varios colores de perovskitas semitransparentes a través de ingeniería sobre la banda prohibida de los materiales incluidos en la estructura de perovskita, el color varía solo de rojizo marrón a amarillo, acompañando con la fluctuación PCE del dispositivo. Para abordar estos desafíos, se ha demostrado que las microcavidades ópticas, los cristales fotónicos y otros métodos efectivos de gestión de la luz pueden integrarse con ST-PSC para lograr el ajuste de color sin sacrificar PCE [39]

En 2014 Roldán-Carmona *et al.* [40] fabricaron una célula solar flexible sobre un sustrato de polietileno tereftalato (PET) altamente eficiente basada en perovskita de yoduro de plomo y metilamonio con capas intercaladas entre dos capas de transporte de carga orgánica. Después de doblarse 50 veces, no se encontró un deterioro evidente del rendimiento, y los dispositivos conservaron un PCE del 7%.

Un año más tarde, en 2015, *Della et al.* [41] desarrollaron células solares de perovskita eficientes con alta transparencia en el espectro visible al combinar la deposición de capa CH3NH3PbI3 controlable con una estructura de electrodo DMD (dispositivo digital de microespejos), logrando un PCE de entre 5.5% y 13.6% para dispositivos con valores promedio de transmitancia visible (AVT) del 31 % y 7%, respectivamente. Ese mismo año Jung *et al.* [42] utilizando como HTL (Hole Transport Layer) CuSCN, obtuvieron dispositivos semitransparentes. Cuando el espesor de la capa de perovskita estaba entre 140 y 240 nm, la transmitancia visible promedio del dispositivo se pudo sintonizar en el rango entre 37.5% y 13.0%. Una célula semitransparente con 180 nm de perovskita ha mostrado un PCE muy prometedor de 10.3% y una AVT de 25.1. Ramirez Quiroz *etal.* [43] informaron de dos protocolos robustos para el procesamiento de películas de perovskita de menos de 100 nm, permitiendo un ajuste de la capa activa sin comprometer la cristalinidad y la calidad del semiconductor. Obtuvieron células con

AVT del y PCE de 7.8%. Eperon *et al.* [44] desarrollaron cátodos transparentes que les permitió la fabricación de células solares semitransparentes de color neutro por primera vez. Dichos dispositivos obtuvieron más del 5% de PCE con AVTs promedio de casi el 30%.

En 2016, Hörantner *et al.* [45] presentaron una técnica química donde aplicaron un post tratamiento molecular de películas de perovskita en sustratos de TiO_2, evitando la formación de caminos de derivación. Este tratamiento actuó como bloqueador selectivo de las vías de derivación, mejorando el rendimiento de la célula solar con un PCE del 6.1% para una semitransparencia de color neutro con AVT cercana al 40%.

En 2018, Deluca *et al*. [46] fabricaron electrodos transparentes cuasi interdigitados (t-QIDE) reemplazando los componentes opacos de los QIDE existentes con óxido de indio y estaño (ITO). Para lograr eficiencias de conversión de energía de hasta 11.5% y 13.3% cuando se ilumina desde la cara frontal y posterior, respectivamente. Para láminas de perovskita de 250 nm, se calculó una AVT del 32%. Los valores de PCE correspondientes se pronosticaron como del 5.9% para iluminación frontal y del 7.5% para iluminación trasera.

4.3. OPV

Las ventajas potenciales de las células solares de polímeros son numerosas, incluida la flexibilidad, la capacidad de procesamiento, el bajo costo del material y la independencia de los recursos escasos. La ventaja de la flexibilidad es compartida con las tecnologías fotovoltaicas de película delgada, y es una característica que permite incorporar las células solares en un gran abanico de aplicaciones. Los módulos solares que se pueden desplegar sobre un techo u otras superficies son una opción. La procesabilidad es otro punto importante en la competitividad de las células solares orgánicas. Las células solares de primera y segunda generación dependen, muchas de ellas, de métodos de deposición al vacío que requieren grandes cantidades de energía. Las células solares orgánicas, por otro lado, se procesan a partir de la solución y las células procesadas en solución completa son una posibilidad

4.3.1. Historia

El descubrimiento del efecto fotovoltaico (PV) se atribuye comúnmente a Becquerel, quien descubrió una fotocorriente cuando electrodos de platino, cubiertos con bromuro de plata o cloruro de plata, se iluminaban en solución acuosa (estrictamente hablando esto es un efecto fotoelectroquímico) [47]. En 1873, el ingeniero eléctrico inglés Willoughby Smith descubrió que el selenio tenía potencial fotoconductor, lo que significa que se vuelve eléctricamente conductor cuando absorbe la luz [48]. Tres años más tarde, en 1976, este descubrimiento llevó a William Grylls Adams y Richard Evans

Day a la conclusión de que el selenio crea electricidad cuando se expone a la luz solar, sin calor ni partes móviles que puedan descomponerse fácilmente [49].

La primera observación de fotoconductividad en compuestos orgánicos (antraceno) fue reportada en 1906 por Pochettino [50], En 1958, Kearns y Calvin fabricaron células solares de ftalocianinas de magnesio (MgPh), produciendo una fotovoltaje de 200 mV [51]. Durante el mismo período, se desarrollaron las primeras células fotovoltaicas inorgánicas en los laboratorios Bell [52]. En 1986 se produjo un gran avance sobre el desarrollo de una célula fotovoltaica orgánica de dos capas, que tenía una gran densidad de fotocorriente, del orden de mA/cm^2, y una eficiencia del 1 %. Esto fue como resultado de la sensibilización donante-receptor informada por Tang [53]. En 1991, Hiramoto *et al.* propusieron una unión combinada para células de molécula pequeña [54]. En 1992, Sariciftci *et al.* informaron sobre una célula de heterounión de polímero compuesta de C60 y MEH-PPV (poli [2-metoxi-5- (2-etilhexiloxi) -1,4-fenilenvinileno]) [55],. En el año 2000, Alan MacDiarmid, Alan Heeger y Hideki Shirakawa descubrieron que los plásticos podrían ser conductores y también aislantes. La importancia del descubrimiento fue reconocida el año 2000 con la adjudicación del Premio Nobel de Química a los tres investigadores. Según estos estudios fundamentales, después del año 2000, la eficiencia aumentó del 1 % y comenzó a aumentar rápidamente hasta alcanzar el 13.45 % en 2019 [38].

4.3.2. Principios básicos de las células solares orgánicas [56], [57]

El principio básico detrás de la célula solar orgánicas y otras formas de células solares es el mismo, es decir, la transformación de la energía en forma de radiación electromagnética (luz) en energía eléctrica (una corriente y un voltaje. Esta conversión de energía es posible con el uso de semiconductores. Los semiconductores están a medio camino entre un conductor normal y un aislante. En el caso del conductor las bandas de valencia y conducción están energéticamente indiferenciadas y en un aislante tienen una separación energética superior a los 10 eV. El semiconductor tiene una proximidad entre la banda de valencia y la de conducción (< 2 eV en los aplicados en células solares) y, de esta manera, el fotón incidente puede excitar un electrón para que salte energéticamente a la banda de conducción.

Como material semiconductor orgánico se utiliza un polímero conjugado o moléculas pequeñas. Un polímero es molécula compuesta por gran cantidad de monómeros. Por el contrario, las moléculas pequeñas u oligómero es una molécula que consiste en un número reducido de monómeros. La mayoría de las células fotovoltaicas orgánicas son células solares de polímero. Las moléculas orgánicas tienen (en una frecuencia decreciente de apariencia) átomos de C, H, O y N. La habilidad de los semiconductores

orgánicos para el transporte de carga y absorción de radiación luminosa en la región del visible-UV se debe a la hibridación sp2 que ocurre en los átomos de carbono.

Los semiconductores moleculares y poliméricos surgen de su estructura química conjugada. Esto significa que los enlaces entre átomos de carbono en el conjunto de los polímeros están alternados simples o dobles (conjugación). En materiales conjugados, tres orbitales híbridos sp^2 forman enlaces covalentes: uno con cada uno de los átomos de carbono contiguos, y el tercero con un átomo de hidrógeno u otro grupo. El electrón restante ocupa un p_z orbital. La superposición mutua de los orbitales p_z crea enlaces π a lo largo del conjugado vertebral, por esa deslocalización de electrones π a lo largo de todo el camino conjugado. El orbital π más alto lleno se denomina orbital molecular ocupado más alto (HOMO, de sus siglas en inglés Highest Occupied Molecular Orbital) y el orbital vacío más bajo π∗ se denomina el orbital molecular desocupado más bajo (LUMO- lowest unoccupied molecular orbital). La diferencia de energía entre el HOMO y LUMO se denomina hueco HOMO-LUMO (del inglés HOMO-LUMO gap). El HOMO es a los semiconductores orgánicos, lo que la banda de valencia es a los semiconductores inorgánicos. La misma analogía existe entre el LUMO y la banda de conducción. La diferencia de energía entre el HOMO y LUMO es la energía de la banda prohibida.

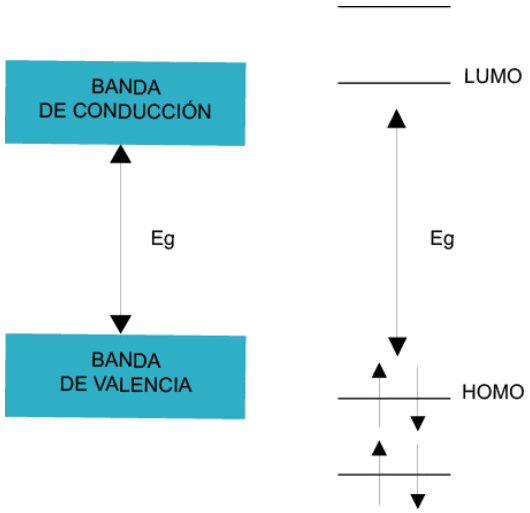

Figura 11. Diagrama de nivel de energía que compara un semiconductor a granel con su análogo molecular

Si ampliamos los sistemas π agregando más anillos, por ejemplo, la deslocalización aumenta, ya que disminuye la distancia HOMO-LUMO.

La absorción de fotones por semiconductores inorgánicos produce electrones y huecos libres, mientras que la absorción de fotones por semiconductores orgánicos produce excitones, que es una cuasipartícula que integra un electrón y un hueco ligados.. La

separación de carga es más difícil en semiconductores orgánicos debido a su baja constante dieléctrica.

4.3.3. Principio de operación [56], [57]

Para entender mejor su funcionamiento explicaremos la estructura básica de una célula orgánica, la cual se compone de una capa de transporte de electrones, una capa de transporte de huecos, y el material activo. El material activo tiene dos constituyentes. El polímero que absorbe la luz (donador) que tiene una gran afinidad por los huecos y un material aceptador que tiene una gran afinidad por los electrones.

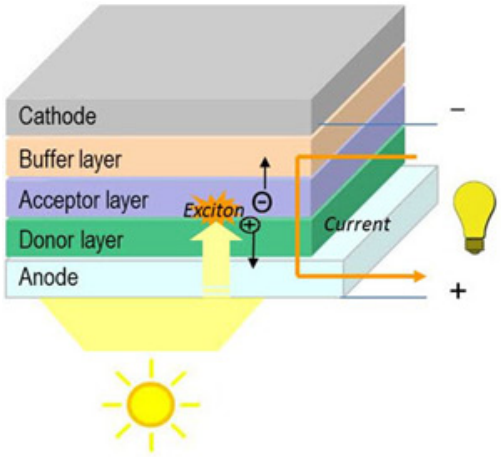

Figura 12. Esquema de una célula orgánica [58].

Cuando la célula está expuesta a la se producen un conjunto de eventos (figuras 13 y 14) que empiezan por una absorción de los fotones por la capa activa. Los fotones con una energía más grande que la del gap crean un par electrón-hueco ligados (excitón). El donador del polímero sirve como el principal absorbedor de la luz solar y portador de huecos y el aceptor es el encargado de transportar los electrones, por lo tanto, un amplio rango de absorción, grandes coeficientes de extinción y grandes movilidades portadoras son requisitos básicos de la capa activa. Después, se produce la difusión del excitón a través de un límite de fase entre el donante el aceptor, la vida de este excitón es limitada, la distancia que puede recorrer es muy pequeña, entre los 10 a 20 nm antes de recombinarse. Esto significa que el tamaño óptimo del material activo debe ser de ese orden, para para aumentar la disociación del excitón, se hace lo que se llama una unión heterogénea (figura 13.b). Las hetereouniones se construían en una geometría de dos capas (figura 13.c), esto suponía igualmente que el excitón tenía que viajar a gran distancia. Este hecho se ha mitigado realizando una mezcla (organic blend) a granel o separada por microfase, proporcionando una gran área interficial para la separación de cargas y reducción de la recombinación del excitón debido a la menor distancia en la

que el electrón se difunde hacia el cátodo y los huecos se difunden hacia el ánodo. El excitón puede separarse gracias al potencial en la interfaz donador-aceptor, formando dos transportistas libres, uno positivo y otro negativo (también llamados polarons). Una vez las cargas están separadas, viajan del donador y el aceptor hacia los electrodos correspondientes.

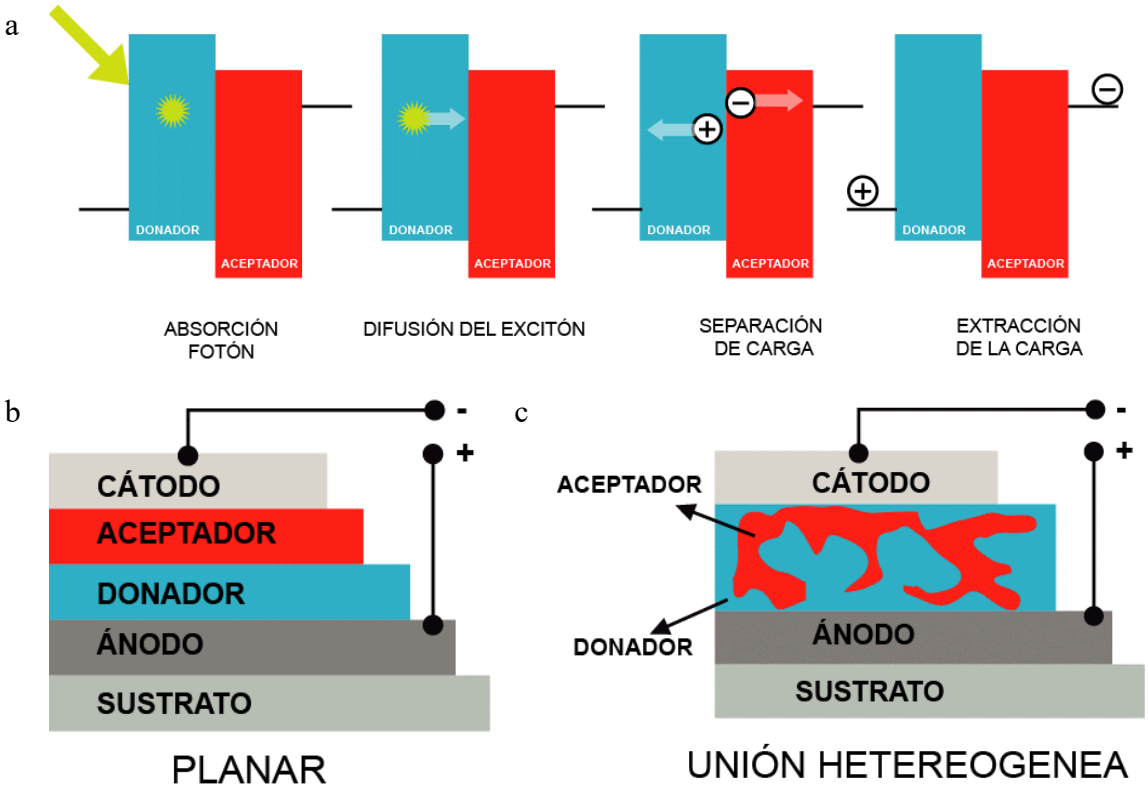

Figura 13. a) Unión planar b) Unión hetereogenea.

A menudo, las células solares de heterounión a granel se construyen sobre un sustrato transparente recubierto con un material de electrodo conductor y transparente que hace la función de ánodo. Debido a su excelente transparencia y conductividad, el ITO (óxido de indio y estaño) se aplica en la mayoría de dispositivos. En la llamada configuración estándar, figura 14.a, el ITO está recubierto con una capa de transporte de agujeros (HTL). La HTL suele consistir en películas delgadas de polímero conjugado dopado como el PEDOT: PSS (poli (3,4-etilendioxitiofeno) poli (estirenosulfonato)) o una capa delgada de óxido (por ejemplo, MoO_3). En la parte superior del HTL, se recubre con la capa fotoactiva, una mezcla de material donante y aceptor ("blenda"), seguida de una capa opcional de transporte de electrones (ETL) y un electrodo de baja función de trabajo. Los materiales ETL son a menudo óxidos como el óxido de zinc o

dióxido de titanio. El electrodo de baja función de trabajo que hace la función de cátodo normalmente es aluminio. A esta disposición de los elementos se le denomina configuración estándar. En la configuración invertida, figura 14.b, se invierte la secuencia de capas de la OPV convencional para evitar el uso de metales fácilmente oxidables en el cátodo expuesto, mejorar la estabilidad del dispositivo y mejorar el rendimiento general del dispositivo. En esta configuración el electrodo transparente recubierto sobre el sustrato actúa como un cátodo. Ya sea modificando la función de trabajo del material del electrodo, aplicando una capa interficial o utilizando óxidos transparentes como el óxido de zinc o el dióxido de titanio. En la parte superior de la capa activa se ha utiliza un HTL como PEDOT: PSS o una capa delgada de óxido (por ejemplo, MoO_3) y el dispositivo está finalizado con un material de electrodo de alta función de trabajo estable al aire como plata u oro. Ambas arquitecturas de dispositivos permiten la preparación de células solares de heterounión a granel de alto rendimiento. El diseño invertido ofrece ventajas de procesado (no se requiere proceso de vacío) y muestra una mejor estabilidad ambiental debido a la ausencia de un electrodo de baja función de trabajo[59].

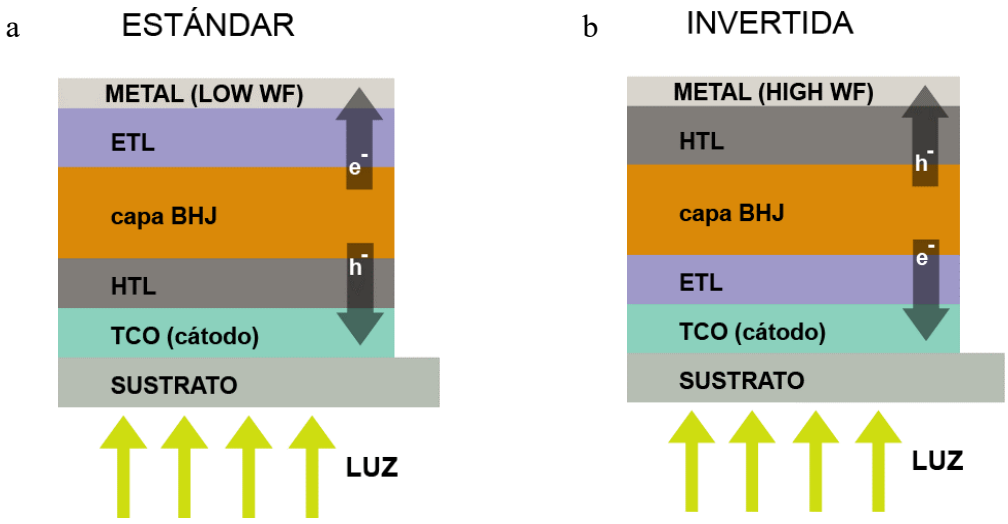

Figura 14. a) Configuración estándar b) Configuración invertida.

4.3.4. **Física de la célula solar orgánica** [56], [57]

En el apartado previo, hemos hablado de los procesos que suceden para que las células orgánicas, mediante el efecto fotovoltaico, conviertan la luz en electricidad; la cantidad de fotones que una vez alcanzan la célula solar creando excitones, y son efectivamente

separados y recogidos en los electrodos define la eficiencia cuántica de la célula solar. En particular, la relación de los electrones recolectados dividida por el número de fotones incidentes, para una energía incidente dada, define la Eficiencia Cuántica Externa (EQE). De modo análogo también se puede definir como el producto de las eficiencias de cada subproceso que ocurre en la célula orgánica para poder generar corriente. η_A se refiere a la eficiencia de absorción, η_{ED} la eficiencia de difusión, η_{CT} la eficiencia de transferencia de carga, η_{CD} eficiencia de la disociación de la carga, η_{CP} la eficiencia del transporte de la carga y la η_{CC} eficiencia de recolección de portadores de carga.

$$EQE = \frac{cantidad\ electrones\ recolectados}{numero\ incidente\ de\ fotones} \qquad \mathrm{EQE} = \eta_A\,\eta_{ED}\,\eta_{CT}\,\eta_{CD}\,\eta_{CP}\,\eta_{CC}$$

La eficiencia de absorción de luz, η_A, depende del coeficiente de absorción α (hω) de la molécula absorbente. Adicionalmente a los fotones transmitidos, los fotones reflejados se pierden. Puesto que el grosor de las capas de las células solares orgánicas está en el rango de la longitud de coherencia de la luz solar, además del grosor del absorbedor, su posición dentro de la distribución del campo óptico creada por interferencia determina la eficiencia pico de absorción η_{PA} (hω). Por lo tanto, una optimización de η_{PA} significa encontrar moléculas con alta absorción en el rango espectral deseado y una optimización de la agrupación "stack" con respecto a la óptica.

La eficiencia de absorción puede ser ajustada mediante la elección de materiales con determinada banda prohibida, mejorando el empaquetamiento intermolecular y mejorando la absorción mediante la aplicación de plasmones superficiales.

La Difusión de excitón con eficiencia η_{ED}. El excitón para ser separado tiene que alcanzar una interfaz D-A. Durante este proceso, la difusión y la relajación compiten. Una alta difusividad D y vida útil τ conducen a una gran longitud de difusión de excitones $L_D = \sqrt{D\tau}$. Por lo tanto, η_{ED} se determina principalmente por el ratio de L_D y el espesor de la capa absorbente. Los valores comunes de L_D de películas orgánicas amorfas están en el rango de 10 nm. La optimización del dispositivo conduce a una compensación con η_{PA}, que requiere capas con espesores de 50 a 100 nm (para $\alpha \approx 10^5$ cm^{-1}). Para superar este problema se cambia a una estructura de heterounión. La absorción parasitaria en regiones también influye en la eficiencia de extracción de excitones.

Transferencia de carga con eficiencia η_{CT}. Este proceso es muy eficiente y rápido (45 a varios cientos de femtosegundos) para varias combinaciones de donantes y aceptores.

Para una transferencia de carga eficiente se requiere una compensación en las afinidades electrónicas (potenciales de ionización) para la transferencia electrónica entre el donante y aceptor, que es más grande que la energía de unión del excitón.

Disociación del par electrón-agujero con eficiencia η_{CD}. Este paso se considera esencial en una célula solar orgánica, aunque todavía no se comprende completamente. La pregunta principal es si la disociación ocurre a través de un estado intermedio, un llamado excitón de transferencia de carga (CT) que es el primer estado excitado de un complejo de transferencia de carga en la heterounión. La otra propuesta es que la energía obtenida se utiliza para generar directamente portadores de carga libres a través de excitónes calientes.

Transporte de carga con eficiencia η_{CP}. Una vez separados, las cargas tienen que ser transportados a través de los materiales orgánicos a los electrodos. La única pérdida posible es la recombinación entre electrones y huecos. Una medida común para η_{CP} es el producto movilidad-tiempo de vida ($\mu\tau$), que expresa la distancia promedio que recorre un portador de carga en un campo eléctrico fijo antes de que se recombine.

Recolección de carga en los electrodos con eficiencia η_{CC}. Esta es solo una pérdida directa si los contactos no son selectivos y un portador de carga llega al contacto "incorrecto", donde se recombina.

El EQE dividido por η_{PA} se llama eficiencia cuántica interna (IQE) y contiene solo los procesos eléctricos internos del dispositivo.

A partir de la EQE, traduciendo la eficiencia en respuesta espectral mediante el factor $q\lambda/hc$ y multiplicando por el espectro solar incidente obtenemos de forma directa la densidad de corriente de corto circuito, J_{sc}. El voltaje de circuito abierto se puede calcular a partir de la energía del gap, es decir, la diferencia de energías entre el LUMO y el HOMO. Además se ha de tener en cuenta la densidad de estados, la probabilidad de disociación y la generación de pares electrón-hueco.

4.3.5. Métodos de fabricación

En términos generales, el proceso de fabricación se puede dividir en técnicas de recubrimiento, que son adecuadas para la fabricación a gran escala en laboratorios y técnicas de impresión. Algunas de éstas son totalmente compatibles con procesado R2R (Roll to Roll), que es el método de manufactura de células orgánicas donde el sustrato está en un rollo. El proceso generalmente comprende: desenrollado del sustrato, el recubrimiento de las diferentes capas que comprenden la célula mediante una técnica de recubrimiento o impresión y el rebobinado de materia. Dentro de los métodos por recubrimiento encontramos el recubrimiento de cuchilla, recubrimiento de ranura, el recubrimiento de inmersión y el recubrimiento de alambre. Las técnicas de impresión

comprenden la impresión de pantalla, la impresión flexográfica, la impresión hueco-grabado y la impresión inkjet o chorro de tinta. Algunos de estos métodos son compatibles con el roll to roll y en otros es difícil su implementación. En la literatura se pueden encontrar diferentes artículos de revisión que repasan de forma detallada las diferentes técnicas de fabricación. [60], [61]. En la siguiente figura 15 se muestran algunas de las técnicas principales.

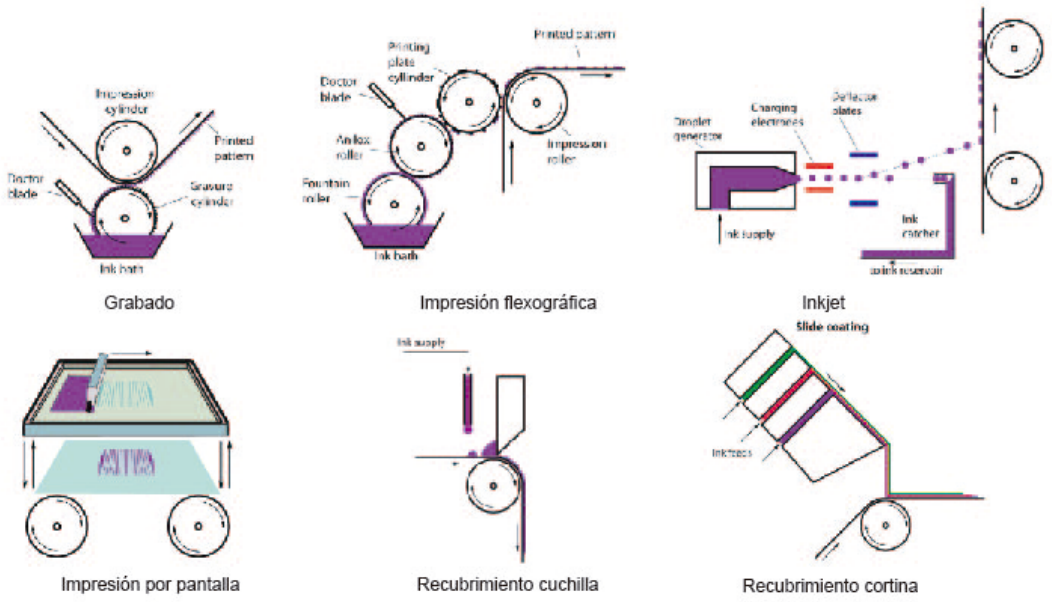

Figura 15. Técnicas de impresión y recubrimiento de células orgánicas mediante Roll-to-Roll. [61]

4.3.6. Estado del arte sobre células orgánicas

Una de las propiedades inherentes de las células solares orgánicas es su semitransparencia y la capacidad de ajustar su color a través del polímero absorbente. Estas características hacen las células orgánicas el principal candidato para aplicaciones en sistemas fotovoltaicos integrados en edificios (BIPV). La energía fotovoltaica orgánica semitransparente (ST-OPV) ofrece una alternativa atractiva debido a su espectro de absorción que puede permitir la transmisión de luz visible junto con la absorción ultravioleta (UV) / infrarrojo cercano (NIR) a través de la elección de la composición molecular y de la región activa del dispositivo.

Tal como se ha hecho anteriormente con las otras tecnologías, a continuación se muestra un pequeño estado del arte de los avances e hitos conseguidos en células orgánicas semitransparentes.

En 2012, Environ *et al.* [62] fabricaron un dispositivo, basado en PBDTTT-C-T y PC71BM como materiales activos, para explorar su potencial para aplicaciones en ventanas. Demostraron las extraordinarias capacidades de reproducción del color (CRI > 96). Variaron el grosor del electrodo de metal reflectante, consiguiendo eficiencias de conversión de potencia (PCE) entre el 7.56% y el 4.25%, con una transparencia correspondiente del 2% al 36%

En 2017, Li *et al*. [63] desarrollaron un aceptor de sin fullereno absorbente de NIR (infrarrojo cercano) (BT-CIC) con cuatro átomos de cloruro en sitios moleculares definidos. Su trabajo proporcionó nuevas vías en el diseño de aceptadores NIR obteniendo una PCE de 11.2% y un CRI de91. Cui *et al.* [64], en consonancia con el anterior grupo, diseñaron y sintetizaron un aceptor sin fullereno de banda ultrabaja, "IEICO-4Cl", cuyo espectro de absorción se encuentra principalmente en la región del infrarrojo cercano. Investigaron el uso de tres tipos de dadores (J52, PBDB - T y PTB7 - Th), al usar 15 nm de Au como electrodo, los OPV semitransparentes basadas en estas tres mezclas mostraron unos PCEs de 6.37%, 6.24%, y 6.97% con alta transmitancia visible promedio (AVT) de 35.1%, 35.7% y 33.5%, respectivamente. También estudiaron la influencia del grosor de Au, observando que al reducir este alcanza se podía alcanzar una eficiencia 8.38% con un AVT de 25.7%. El mismo año *Liu et al.* [65] desarrollaron un nuevo material aceptor de electrones con elevada absorción en el NIR, entre 600 y 940 nm, obteniendo valores de PCE de 7,7% con una alta transparencia, del 37%. Wang *et al*. [66] desarrollaron un aceptor de electrones hexacíclico fusionado, IHIC, basado en dithienocyclopentathieno[3,2-b]thiophene. El IHIC exhibe una fuerte absorción en el infrarrojo cercano. Las ST-OPV basadas en mezclas de un dador de polímero de banda estrecha de banda PTB7-Th y el aceptador IHIC de banda estrecha muestran una eficiencia de conversión de potencia de campeón de 9.77% con una transmitancia visible promedio del 36% y una excelente estabilidad del dispositivo.

En 2018, Li *et al*., [67] fabricaron una célula basada en tris(tiotiofeno) fusionado (3TT), diseñado y sintetizado con fuertes propiedades de donación de electrones y de empaquetamiento molecular, donde tres unidades de tiotiofeno se condensan con dos anillos de ciclopentadienilo.. Estas células mostraron un PCE de hasta 10.3% con una transmitancia visible promedio del 37.4%.

Xie *et al*. [68] fabricaron una célula solar ternaria utilizando un dador de polímero de banda ancha (Eg = 2.10 eV), PBT1-S, como el tercer componente. Hallaron que la adición de una pequeña cantidad de PBT1-S a PTB7 -Th: la mezcla de PC71BM tenía una influencia insignificante en su transmitancia visible promedio (AVT) y la percepción del color. Se alcanza un PCE de 9.2% para el dispositivo ternario con 20% AVT. En la misma línea, Ma *et al.* [69] llevaron a cabo células solares de polímero

ternario semitransparente con un donador de banda prohibida estrecha (PTB7-Th) y dos aceptadores de banda prohibida ultra estrecha (COi8DFIC e IEICO-4F). Las células ternarias semitransparentes optimizadas mostraron una PCE de 8.23% y una transmitancia visible promedio (de 370 nm a 740 nm) del 20.78%. El mismo año, Ma *et al.* [69], aplicaron una mejora empleando un espejo dieléctrico y una capa fotoactiva ternaria con absorción de infrarrojo cercano para ajustar la percepción del color y el rendimiento del ST-OPV con precisión. Como resultado, lograron una ST-OSC de color neutro con un PCE de 9.37% y un AVT de más del 20%.

Mencionar que en la actualidad se pueden encontrar numerosísimos estudios que reportan pequeñas mejoras en los diferentes procesos en pro de la transparencia y/o la eficiencia de conversión.

En la siguiente Tabla 1, se incluye un resumen sobre algunas de las diferentes eficiencias y transmitancias comentadas en el presente capítulo. Se ha de tener en cuenta que las transmitancias mostradas no están todas referidas al mismo rango espectral.

Tabla1. Resumen de las eficiencias eléctricas y la transmitancia visiblede las investigaciones citadas en este documento.

Referencia	Tecnología	PCE	Transmitancia
[8]	c-Si	7%	42%
[9]	c-Si	12.2%	20%
[10]	c-Si	8%	10%
[14]	CdTe	4%	
[16]	CdTe		10%
[17]	CdTe		40-10%
[19]	CdTe		CRI > 90%
[13]	CdTe		25%
[21]	CIGS	1.7%	20%
[22]	CIGS	5.94%	25%
[23]	CIGS	7.7%	37%
[2]	a-Si	6.92%	23.6%
[24]	a-Si	4.91 -5.57	17.49% -20.99%
[25]	a-Si	6.01%	22.76%
[31]	DSSC	3.6%	
[32]	DSSC		11%
[33]	DSSC	3.40%	

[26]	DSSC	5.15%-2.1%	25%-53%
[28]	DSSC	5.93%-2.51%	
[40]	Perovskita	7%	
[41]	Perovskita	5.5%-13.6%	31%-7%
[42]	Perovskita	10.3 %	25.1%
[43]	Perovskita	7.8%	37%
[44]	Perovskita	5%	30%
[45]	Perovskita	6.1%	40%
[46]	Perovskita	5.9%	32%
[62]	Orgánicas	7.56-4.25	2-36%
[63]	Orgánicas	11.2%	
[64]	Orgánicas	6.37%-6.24%-6.97%	35.1%-35.7%-33.56%
[65]	Orgánicas	7.7%	37%
[66]	Orgánicas	9.77%	36%
[67]	Orgánicas	10.3%	37.4%
[68]	Orgánicas	9.2%	20%
[69]	Orgánicas	8.23%	
[69]	Orgánicas	9.37%	20%
[71]	Orgánicas	8%-5.8%	44.2%-44%

5. Referencias

[1] M. Saifullah and J. Ho, “present status , and future prospects for building-,” pp. 8512–8540, 2016.

[2] J. Wook, M. Shin, D. Jung, S. Hyun, and S. Jin, “Solar Energy Materials & Solar Cells Highly transparent amorphous silicon solar cells fabricated using thin absorber and high-bandgap-energy n / i-interface layers,” *Sol. Energy Mater. Sol. Cells*, vol. 128, pp. 301–306, 2014.

[3] C. Lamnatou and D. Chemisana, *Life-cycle assessment of photovoltaic systems*. 2019.

[4] F. Article, “Flexible photovoltaic technologies,” pp. 1233–1247, 2014.

[5] Infinity, “OPV.” .

[6] T. Y. Y. Fung and H. Yang, “Study on thermal performance of semi-transparent building-integrated photovoltaic glazings,” *Energy Build.*, vol. 40, no. 3, pp. 341–350, 2008.

[7] M. Chen *et al.*, “Experimental and numerical evaluation of the crystalline silicon PV window under the climatic conditions in southwest China,” *Energy*, vol. 183, pp. 584–598, 2019.

[8] J. Peng, D. C. Curcija, A. Thanachareonkit, E. S. Lee, H. Goudey, and S. E. Selkowitz, “Study on the overall energy performance of a novel c-Si based semitransparent solar photovoltaic window,” *Appl. Energy*, vol. 242, no. August 2018, pp. 854–872, 2019.

[9] K. Lee *et al.*, “Neutral-Colored Transparent Crystalline Silicon Photovoltaics,” *Joule*, vol. 4, no. 1, pp. 235–246, 2020.

[10] S. B. Kang, J. Kim, C. U. Kim, and C. Kim, “Stretchable and colorless freestanding microwire arrays for transparent solar cells with fl exibility,” *Light Sci. Appl.*, 2019.

[11] Web, “Custom Overlay Solar Cells n Custom Make Solar Panels.” .

[12] M. GREEN *et al.*, “Solar cell efficiency tables (version 40),” *Ieee Trans Fuzzy Syst*, vol. 20, no. 6, pp. 1114–1129, 2012.

[13] H. Alrashidi, A. Ghosh, W. Issa, N. Sellami, T. K. Mallick, and S. Sundaram, “Thermal performance of semitransparent CdTe BIPV window at temperate climate,” *Sol. Energy*, vol. 195, no. December 2019, pp. 536–543, 2020.

[14] C. Heisler *et al.*, “Transparent CdTe solar cells with a ZnO:Al back contact,” *Thin Solid Films*, vol. 548, pp. 627–631, 2013.

[15] V. V. Plotnikov *et al.*, “Semitransparent PV windows with sputtered CdS/CdTe thin films,” *Conf. Rec. IEEE Photovolt. Spec. Conf.*, pp. 405–408, 2013.

[16] Y. Sun *et al.*, “Integrated semi-transparent cadmium telluride photovoltaic glazing into windows: Energy and daylight performance for different architecture designs,” *Appl. Energy*, vol. 231, no. September, pp. 972–984, 2018.

[17] Y. H. Sabry, W. Z. W. Hasan, A. H. Sabry, M. Z. A. A. Kadir, M. A. M. Radzi, and S. Shafie, “Measurement-based modeling of a semitransparent CdTe Thin-Film PV Module Based on a Custom Neural Network,” *IEEE Access*, vol. 6, pp. 34934–34947, 2018.

[18] W. Meng, P. Jinqing, Y. Hongxing, and L. Yimo, “Performance evaluation of semi-transparent CdTe thin film PV window applying on commercial buildings in Hong Kong,” *Energy Procedia*, vol. 152, pp. 1091–1096, 2018.

[19] D. Liu, Y. Sun, X. Liu, R. Wilson, and Y. Wu, “Evaluation of the colour properties of CdTe PV windows,” *Energy Procedia*, vol. 158, pp. 3088–3093, 2019.

[20] Y. Wang, T. Wu, and Y. Chueh, “A critical review on flexible Cu (In , Ga) Se 2 (CIGS) solar cells,” *Mater. Chem. Phys.*, vol. 234, no. April, pp. 329–344, 2019.

[21] S. H. Moon *et al.*, “Printable, wide band-gap chalcopyrite thin films for power generating window applications,” *Sci. Rep.*, vol. 4, pp. 1–6, 2014.

[22] M. Saifullah *et al.*, “Development of semitransparent CIGS thin-film solar cells modified with a sulfurized-AgGa layer for building applications,” *J. Mater. Chem. A*, vol. 4, no. 27, pp. 10542–10551, 2016.

[23] T. Sidali *et al.*, “Semi-transparent photovoltaic glazing based on electrodeposited CIGS solar cells on patterned molybdenum/glass substrates,” *EPJ Photovoltaics*, vol. 9, pp. 3–9, 2018.

[24] J. Yang, H. Jo, S. Choi, D. Kang, and J. Kwon, “All p-i-n hydrogenated amorphous silicon oxide thin fi lm solar cells for semi- transparent solar cells,” *Thin Solid Films*, vol. 662, no. April, pp. 97–102, 2018.

[25] J. Cho *et al.*, “Solar Energy Materials and Solar Cells Energy harvesting performance of bifacial and semitransparent amorphous silicon thin- fi lm solar cells with front and rear transparent conducting oxide contacts,” *Sol. Energy Mater. Sol. Cells*, vol. 202, no. August, p. 110078, 2019.

[26] A. Ghosh, P. Selvaraj, S. Sundaram, and T. K. Mallick, “The colour rendering index and correlated colour temperature of dye-sensitized solar cell for adaptive glazing application,” *Sol. Energy*, vol. 163, no. February, pp. 537–544, 2018.

[27] J. Gong, K. Sumathy, Q. Qiao, and Z. Zhou, “Review on dye-sensitized solar cells (DSSCs): Advanced techniques andresearch trends,” *Renew. Sustain. Energy Rev.*, vol. 68, no. October 2016, pp. 234–246, 2017.

[28] A. Roy, A. Ghosh, S. Bhandari, P. Selvaraj, S. Sundaram, and T. K. Mallick, “Color Comfort Evaluation of Dye-Sensitized Solar Cell (DSSC) Based Building-Integrated Photovoltaic (BIPV) Glazing after 2 Years of Ambient Exposure,” *J. Phys. Chem. C*, vol. 123, no. 39, pp. 23834–23837, 2019.

[29] M. G. Kang, N. Park, and Y. J. Park, “Manufacturing method for transparent electric windows using dye-sensitized TiO 2 solar cells,” vol. 75, pp. 475–479, 2003.

[30] J. Kang, J. Kim, and J. Kim, “Performance Evaluation of DSC Windows for Buildings,” vol. 2013, 2013.

[31] H. Kim, J. Jo, G. Lee, M. Shin, and J. Lee, “Design and analysis of a highly reliable large-area Z-type transparent module for dye-sensitized solar cells,” *Sol. Energy*, vol. 155, pp. 585–592, 2017.

[32] M. Morini and R. Corrao, “Energy optimization of BIPV glass blocks : a multi-software study,” *Energy Procedia*, vol. 111, no. September 2016, pp. 982–992, 2017.

[33] H. M. Lee and J. H. Yoon, “Power performance analysis of a transparent DSSC BIPV window based on 2 year measurement data in a full-scale mock-up,” *Appl. Energy*, vol. 225, no. April, pp. 1013–1021, 2018.

[34] C. Cornaro, L. Renzi, M. Pierro, A. Di Carlo, and A. Guglielmotti, “Thermal and electrical characterization of a semi-transparent dye-sensitized photovoltaic module under real operating conditions,” *Energies*, vol. 11, no. 1, 2018.

[35] A. Knott, X. Liu, O. Makarovskiy, C. Tuck, and Y. Wu, “Design and optical characterisation of an efficient light trapping structure for dye-sensitized solar cell integrated windows,” pp. 41–49, 2019.

[36] M. A. Green, A. Ho-baillie, and H. J. Snaith, “The emergence of perovskite solar cells,” vol. 8, no. July, 2014.

[37] Web, “Stability Challenge in Perovskite Solar Cell Technology | Okinawa Institute of Science and Technology Graduate University OIST.” .

[38] M. A. Green, E. D. Dunlop, J. Hohl-Ebinger, M. Yoshita, N. Kopidakis, and A. W. Y. Ho-Baillie, “Solar cell efficiency tables (Version 55),” *Prog. Photovoltaics Res. Appl.*, vol. 28, no. 1, pp. 3–15, Jan. 2020.

[39] L. Shen, H. Yip, F. Gao, and L. Ding, “Semitransparent Perovskite Solar Cells for Smart Windows,” *Sci. Bull.*, 2020.

[40] C. Roldán-Carmona *et al.*, “Flexible high efficiency perovskite solar cells,” *Energy Environ. Sci.*, vol. 7, no. 3, pp. 994–997, 2014.

[41] E. Della *et al.*, “Ultra-thin high ef fi ciency semitransparent perovskite solar cells,” *Nano Energy*, vol. 13, pp. 249–257, 2015.

[42] J. W. Jung, C. Chueh, and A. K. Jen, “High-Performance Semitransparent Perovskite Solar Cells with 10 % Power Conversion Effi ciency and 25 % Average Visible Transmittance Based on Transparent CuSCN as the Hole-Transporting Material,” pp. 1–7, 2015.

[43] C. O. Ramírez Quiroz *et al.*, “Pushing efficiency limits for semitransparent perovskite solar cells,” *J. Mater. Chem. A*, vol. 3, no. 47, pp. 24071–24081, 2015.

[44] G. E. Eperon *et al.*, “E ffi cient, Semitransparent Neutral-Colored Solar Cells Based on Microstructured Formamidinium Lead Trihalide Perovskite,” 2015.

[45] M. T. Hörantner *et al.*, “Shunt-Blocking Layers for Semitransparent Perovskite Solar Cells,” pp. 1–7, 2016.

[46] G. Deluca *et al.*, “Transparent Quasi-Interdigitated Electrodes for Semitransparent Perovskite Back-Contact Solar Cells,” pp. 1–6, 2018.

[47] A. E. Becquerel, “Recherches sur les effets de la radiation chimique de la lumiere solaire au moyen des courants electriques,” *Comptes Rendus L{\textasciiacute}Academie des Sci.*, vol. 9, pp. 145–149, 1839.

[48] W. Smith, “Effect of Light on Selenium During the Passage of An Electric Current*,” *Nature*, vol. 7, no. 173, p. 303, 1873.

[49] R. E. D. Adams, W. G., “THE FIRST DEMONSTRATION THAT ELECTRICITY COULD BE PRODUCED FROM LIGHT WITHOUT MOVING PARTS AND LED TO THE MODERN SOLAR CELL,” *R. Soc. London*, vol. 25, pp. 113–117, 1877.

[50] A. Pochettino, A.; Sella, “Photoelectric behavior of anthracene,” vol. 15, pp. 355–363, 1906.

[51] D. Kearns and M. Calvin, “Photovoltaic Effect and Photoconductivity in Laminated Organic Systems,” vol. 950, pp. 6–8, 1958.

[52] D. M. Chapin, C. S. Fuller, and G. L. Pearson, “A New Silicon p-n Junction Photocell for Converting Solar Radiation into Electrical Power,” *J. Appl. Phys.*, vol. 676, no. 1954, pp. 22–24, 1954.

[53] C. W. Tang, “Two-layer organic photovoltaic cell,” *Appl. Phys. Lett.*, vol. 183, 1986.

[54] M. Hiramoto, H. Fujiwara, M. Yokoyama, M. Hiramoto, H. Fujiwara, and M. Yokoyama, “Threelayered organic solar cell with a photoactive interlayer of codeposited pigments Three-layered organic solar cell with a photoactive of codeposited pigments,” vol. 1062, 1991.

[55] N. S. Sariciftci, L. Smilowitz, A. J. Heeger, and F. Wudi, “Photoinduced Electron Transfer from a Conducting Polymer to Buckminsterfullerene,” 1992.

[56] E. D. Głowacki, N. S. Sariciftci, and C. W. Tang, *Organic Solar Cells organic*

solar cell. 2013.

[57] W. Tress, “Device Physics of Organic Solar Cells.”

[58] “Rafi Shikler’s Lab.” .

[59] M. C. Scharber and N. S. Sariciftci, “Progress in Polymer Science Efficiency of bulk-heterojunction organic solar cells,” *Prog. Polym. Sci.*, vol. 38, no. 12, pp. 1929–1940, 2013.

[60] F. C. Krebs, “Solar Energy Materials & Solar Cells Fabrication and processing of polymer solar cells : A review of printing and coating techniques,” vol. 93, pp. 394–412, 2009.

[61] D. Angmo, T. T. Larsen-olsen, and F. C. Krebs, “Roll-to-roll fabrication of polymer solar cells As the performance in terms of power conversion efficiency and operational,” vol. 15, no. 1, pp. 36–49, 2012.

[62] E. Environ, H. Yip, L. Huo, and A. K. Jen, “Environmental Science window applications †,” pp. 9551–9557, 2012.

[63] Y. Li *et al.*, “High E ffi ciency Near-Infrared and Semitransparent Non-Fullerene Acceptor Organic Photovoltaic Cells,” pp. 17114–17119, 2017.

[64] Y. Cui *et al.*, “Efficient Semitransparent Organic Solar Cells with Tunable Color enabled by an Ultralow-Bandgap Nonfullerene Acceptor,” vol. 1703080, pp. 1–7, 2017.

[65] F. Liu *et al.*, “Efficient Semitransparent Solar Cells with High NIR Responsiveness Enabled by a Small-Bandgap Electron Acceptor,” vol. 1606574, 2017.

[66] W. Wang *et al.*, “Fused Hexacyclic Nonfullerene Acceptor with Strong Near-Infrared Absorption for Semitransparent Organic Solar Cells with 9 . 77 % Efficiency,” vol. 1701308, pp. 1–7, 2017.

[67] T. Li *et al.*, “Fused Tris (thienothiophene) -Based Electron Acceptor with Strong Near-Infrared Absorption for High-Performance As-Cast Solar Cells,” vol. 1705969, pp. 1–7, 2018.

[68] Y. Xie *et al.*, “High-Performance Semitransparent Ternary Organic Solar Cells,” vol. 1800627, pp. 1–7, 2018.

[69] X. Ma *et al.*, “Simultaneously improved e ffi ciency and average visible transmittance of semitransparent polymer solar cells with two ultra-narrow bandgap,” pp. 21485–21492, 2018.

[70] P. Selvaraj, A. Ghosh, T. K. Mallick, and S. Sundaram, “Investigation of semi-transparent dye-sensitized solar cells for fenestration integration,” *Renew. Energy*, vol. 141, pp. 516–525, 2019.

[71] Y. Li *et al.*, “Enhanced Light Utilization in Semitransparent Organic Photovoltaics Using an Optical Outcoupling Architecture,” vol. 1903173, pp. 1–8, 2019.

Capítulo 3. Estado del arte sobre membranas poliméricas de ETFE

Chr. Lamnatou, A. Moreno, D. Chemisana, F. Reitsma and F. Clariá. Ethylene tetrafluoroethylene (ETFE) material: Critical issues and applications with emphasis on buildings, Renewable and Sustainable Energy Reviews, Manuscrito aceptado y publicado

Ethylene tetrafluoroethylene (ETFE) material: Critical issues and applications with emphasis on buildings

Chr. Lamnatou[1], A. Moreno[1], D. Chemisana[1*], F. Reitsma[2], F. Clariá[3]

[1] Applied Physics Section of the Environmental Science Department, University of Lleida, Jaume II 69, 25001 Lleida, Spain

[2] IASO, Av. de l'Exèrcit 35-37, 25194 Lleida, Spain

[3] Industrial Engineering and Computer Science Department, University of Lleida, Jaume II 69, 25001 Lleida, Spain

Abstract

The present article is a critical review about ETFE (ethylene tetrafluoroethylene) material, with emphasis on building applications since ETFE is promising for the building sector, offering multiple advantages (elastic and low-weight structures, etc.) from different points of view. Selected references about ETFE properties are presented, revealing that ETFE material presents resistance to temperature/aging, mechanical strength and chemical resistance. In addition, studies about light transmission/insulation of ETFE material for building applications are included, showing that ETFE cushion insulating characteristics can be further improved by utilizing additional layers while some studies refer to ETFE decay in terms of light and solar transmittance performances after some months of exposure. Investigations which compare ETFE with glass are also presented, revealing that ETFE offers many advantages, in comparison with glass, from different points of view. A separate part of the article is about ETFE environmental profile and the literature review demonstrates that most of the investigations (which include LCA (life cycle assessment)/environmental issues about ETFE) evaluate embodied energy (the findings show values from 26.5 to 210 MJ/kg). Concerning ETFE applications, the literature review reveals that ETFE can be used for different applications (roofs, façades, atria, in combination with PV (photovoltaic) technology, etc.). Moreover, additional issues (acoustics, shading, etc.) are presented and critically discussed. Furthermore, a separate part with case studies is included. In this way, the present article offers useful information about ETFE, based on different factors, focusing on ETFE applications for buildings and constructions.

Keywords: ETFE (ethylene tetrafluoroethylene); Material properties; Roofs, façades, atria; LCA (life cycle assessment)/environmental issues; Buildings, Constructions; Case studies

LIST OF SYMBOLS AND ABBREVIATIONS

BI	Building-integrated

BIPV	Building-integrated photovoltaic
BIPVT	Building-integrated photovoltaic/thermal
CFD	Computational fluid dynamics
CML	CML method
ECTFE	Ethylene chlorotrifluoroethylene
ETFE	Ethylene tetrafluoroethylene
FEM	Finite element method
FEP	Fluorinated ethylene propylene
IR	Infrared
LCA	Life cycle assessment
LED	Light-emitting diode
PE	Polyethylene
PET	Polyethylene terephthalate
PTFE	Polytetrafluoroethylene
PV	Photovoltaic
PVB	Polyvinyl butyral
PVC	Polyvinyl chloride
PVDF	Polyvinylidene difluoride
PVT	Photovoltaic/thermal
TFE	Tetrafluoroethylene
THV	Tetrafluoroethylene-hexafluoropropylene-vinylidene fluoride
TPO	Thermoplastic polyolefin
UV	Ultraviolet

1. Introduction

Plastics in buildings offer lightweight and low-cost alternative solutions to glass and other claddings; in this way, plastic materials are useful for building applications, for example for commercial buildings [1]. During the last years, new plastics have been developed, resistant to UV radiation and without showing decoloration, and there is a growth in the variety of the plastics while their lifespan and quality increase. Among

these plastics, ETFE (ethylene tetrafluoroethylene) is a promising material that can be adopted as cladding for buildings (and, in general, for multiple architectural constructions), offering around 95% light transmission, flexibility and inspiration for new concepts influencing building structural design [2]. Nowadays, ETFE is considered as one of the most innovative materials in the frame of modern architecture [3] as well as in lightweight architecture with creations of spectacular buildings of various geometric and unusual forms [4].

The development of ETFE, and in general the development of fluoropolymers (polymer materials containing fluorine atoms in their chemical structures), has started several years ago. An overview of the history of fluoropolymers, from the discovery of the polytetrafluoroethylene (30s) till nowadays has been presented by Teng [5]. Moreover, in the work of Teng [5] it was noted that the existing products can satisfy most of the requirements for industrial applications and the current efforts give emphasis on the reduction of the production cost as well as on the expansion of the market.

In the literature several studies about ETFE material have been presented. These studies examine ETFE from different points of view. For example, some investigations give emphasis on ETFE mechanical behavior [6-9] while other studies focus on issues related with light transmission and insulation [10-13]. In addition, some authors examined ETFE material from LCA (life cycle assessment)/environmental point of view [14-17]. On the other hand, in the literature there are some works which: 1) compare ETFE with glass [15, 18], 2) present issues about the acoustics of ETFE structures [19, 20], 3) examine shading and thermal comfort of ETFE structures [21, 22], 4) discuss issues about the inspection of ETFE foils [23]. In terms of ETFE applications, several studies have been presented, including multiple applications such as ETFE façades [24], ETFE roofs [14], ETFE atria [25] as well as configurations which combine ETFE with PV (photovoltaic) technology [26-28].

Based on the above mentioned, it can be seen that ETFE material presents interesting characteristics and useful applications, including the building sector. In the literature, there are few review articles about ETFE: Hu et al. [29] presented an overview about buildings with ETFE foils with emphasis on material properties, architectural performance, structural behavior and sustainable ETFE structures; Hu et al. [30] conducted a review about the production and the market of ETFE; Chilton [31] presented a state-of-the art about lightweight envelopes based on ETFE. Thereby, there is a need for more review articles which present an overview of ETFE material from different points of view. In the frame of this scope, the present article is a critical review about ETFE material, discussing different issues:

1) General characteristics for high-performance materials/configurations for buildings.

2) Requirements specifically for membrane configurations (roofs, façades, etc., in terms of issues such as material selection for membranes).

3) Mechanical and other critical properties of ETFE material (light transmission, insulation, etc.).
4) Acoustics related to structures which are based on ETFE.
5) Shading issues about configurations including ETFE components.
6) Inspection of transparent construction materials.
7) Issues about ETFE material from LCA/environmental point of view.
8) Applications (requirements in terms of claddings; studies about ETFE façades, roofs and atria; combination of ETFE with PV or PVT (photovoltaic/thermal), etc.).
9) Case studies based on ETFE systems (for buildings and architectural constructions) that have been already developed.
In addition, a critical discussion is provided and by considering that:
1) There is a need for reduction of the energy consumption in the building sector in order to reduce CO_2 emissions. Passive design approaches can offer multiple advantages (energy savings with low extra investment, etc.) towards green buildings and sustainable constructions [32].

2) ETFE is a promising material in the frame of environmentally-friendly buildings and constructions [2].

3) In the literature there are few review articles about ETFE, it can be seen that the present study provides useful information about ETFE, based on different points of view.
More specifically, in the present article, the major part focuses on building applications and environmental issues, taking into account the importance of eco-friendly constructions in the building sector. Within the frame of this concept, multiple ETFE configurations and examples which combine ETFE with PVs are presented, highlighting the role of renewable energy sources in the frame of sustainable constructions and buildings. Finally, the part of the case studies verifies, based on projects that have been already developed and applied in practice, the connection of ETFE material with renewable energy systems and eco-friendly constructions.

2. Literature review

2.1. Characteristics of high-performance materials/configurations for building applications

Paech [24] noted that structural high-performance materials present high ratio of structural strength to dead load and the application of these materials is optimal when they are under pure tension (utilizing the full structural capacity by omission of bending moments and any stability issues). However, high-performance is not only about the

structural properties. High-performance is also related, for example, with the fact that a material or composite of materials is designed and produced to have specific characteristics (e.g. specific color, acoustic damping, transparency or translucency, air permeability, etc.). Moreover, Paech [24] mentioned that selective coatings are sometimes part of high-performance materials in order to affect the properties of a specific building (example: coatings for the improvement of the interior climate conditions).

Related with the above mentioned factors, some additional issues are following presented:

- Design considerations for the roof-to-wall interface (the roof and wall design should be able to resist the fundamental forces as outlined by the applicable building code. Parameters such as building overall height, use, roof slope, location, structural type and shape should be taken into account for the development of the roof-to-wall interface) [33].
- Heat, air and moisture factors (for the protection of the quality of the interior environment and building enclosure assemblies from the deleterious effects of moisture and air) [33].
- Adaptive or moveable elements impose specific demands in terms of the selected materials (sometimes is necessary to have specific geometrical arrangements) [24].
- Adopting membrane materials for façades is a more economical solution than using traditional cladding materials, especially when there are reduced requirements on the envelope system (for example, pure shading or balancing of thermal peak loads and simple wind or visual barrier) [24].
- Use of advanced façades which are cost effective and they offer environmental quality, life-cycle savings and energy efficiency [34].
- Façades should be able to respond and adapt to the variable exterior conditions and to the needs of the occupants [34].
- Specific requirements depending e.g. on the height of the building (specific case: for example, high-rise buildings) are necessary for certain cases [34].
- Adoption of solutions which combine façade with ventilation [34].
- Use of systems that include combination of a façade with production of energy (active façade systems) [34].
- Utilization of façades that offer solar control and/or daylighting [34].

The degree of influence of the above mentioned parameters is associated with the specific case of a building/construction. As a general comment it can be said that the high-performance materials/configurations in the building sector include multiple issues, ranging from the structural strength of the materials to strategies which propose multifunctional façades (for ventilation, daylighting control, energy production, etc.).

In the report of BASF [1] it was noted that the envelope of a building should control heat flow, moisture flow and air flow and at the same time it should offer structural integrity and protection from wind, rain, snow, hail, dust, pollutants, allergens and pests. A high-performance building envelope is defined by its ability to achieve these goals [1].

Based on the above mentioned issues, it can be seen that there are different factors which influence the performance of materials for buildings/constructions such as their structural strength, acoustic damping, heat/air/moisture factors, color/transparency, type of application (façade, roof, etc.), size of the building and cost. Furthermore, it should be taken into account that usually membrane materials offer more economic solutions than other types of cladding materials.

2.2. Requirements specifically for membrane configurations (roofs, façades, etc.)

2.2.1. Material selection for membranes

Paech [24] noted that different products have been developed in the field of membranes that can be used e.g. for façade applications. In general, there are two types of membranes: 1) textile membranes (consisting of a woven-base cloth), 2) foils (very thin extrusions with a thickness less than 0.4 mm). It was mentioned [24] that since single-layer membrane configurations have relatively low mass and thickness, they present a relatively high U-value and thereby, the single-layer structural membranes are mainly adopted as exterior sun screens, for wind and rain protection, as skins for semi-air-conditioned zones or to create a visual barrier between the interior and the exterior. Certainly, multi-layer membrane configurations show better thermal performance (in terms of the U-values). The multi-layer systems can be for example inflated membrane cushions or two-layer systems (with intermediate insulation) [24].

Additional issues/concepts, related with membrane architecture, have been presented in the report of Dyneon [35]. Some of these are following presented:

- Translucent membranes which absorb and reflect daylight with a unique fashion.
- Transparent air-filled membrane cushions (including ETFE).
- Configurations with different shapes (rectangular, etc.).
- Membranes with weatherproofed surfaces.
- Films made of ETFE which allow light and UV permeability.
- Glass fibre membranes.
- Highly-transparent films made of ETFE.
- Membrane spans.
- Membrane awnings.
- Structures composed of concave elements.

- Elastic structures.

In the frame of membrane architecture, Dyneon [35] proposed some film membranes made of 3M™ Dyneon™ ETFE which offer multiple advantages such as:

- High transparency.
- Printability.
- High UV transmission.
- Freedom of design.
- Low weight.
- Cost-effectiveness.
- Long lifetime.
- Self-cleaning surface.
- Weather and UV resistance.
- Resistance to fire.
- Wide temperature range in use phase.
- Variety of colors.
- Recyclability.

In addition, IASO proposed ETFE films (for «transparent architecture» applications) with the following advantages/characteristics [3]:

• Low weight.
• Possibility of coloring, printing and light guiding.
• High transparency (95% for the visible light and 85% for UV light).
• Excellent behavior in terms of the fire.
• Impermeable, self-cleaning with rainwater, low maintenance.
• Permeable to UV-A rays (but they do not allow UV-C rays to pass).
• Extremely durable and recyclable.
• Good resistance in terms of hail, etc.
• No visible mechanical damage, no discoloring, no hardening.

On the other hand, in the work of Kawaguchi [36] it was highlighted another important advantage of ETFE: the fact that ETFE components are lightweight means that they provide protection in case of earthquakes (in contrast with the heavy ceilings).

By taking into account the above mentioned issues, it can be noted that the requirements for membranes for buildings include different parameters, ranging from characteristics which are important during use phase (thermal performance, temperature range, lifetime, self-cleaning, transparency, shape, elasticity, weatherproofing, etc.) to characteristics which are important at the end-of-life/disposal (recyclability, etc.).

2.2.2. Textile membranes

Different types of textile membranes can be found, depending on their «mesh». Mesh membranes can be adopted for applications such as sun screens but also for architectural

building envelopes. Different patterns of meshes can be found, various colors (for certain cases) and some products are printable and they present different strength classes [24]. During the last years, laminated open mesh membranes have been developed: for example, glass/PTFE (polytetrafluoroethylene) (mesh membrane with a continuous lamination of a transparent fluorpolymer (ETFE, PTFE, etc.). For this case, the advantage that they offer is relatively high transparency (> 50%) in combination with material strength [24].

2.2.3. Foils

Foil, primarily in the form of ETFE, is a membrane material that offers new design possibilities and an alternative solution to woven fabrics [37]. In the work of Zhao et al. [38] it was noted that as a construction and building material, ETFE foil is widely-used. However, it is still a new material compared with other materials (steel, wood, concrete, etc.). It was also mentioned that when ETFE foil is adopted for structures, it is often used in the form of inflated cushion [38].

Robinson [2] presented a work about ETFE foil cushions as building cladding. It was noted that ETFE foil cushions consist of alternating layers of ETFE film and air cavities and an inflation system pressurizes the foil cushions. It was highlighted [2] that ETFE cushion is a lightweight plastic which shows considerable benefits in comparison to traditional cladding materials. Moreover, ETFE foil cushions are highly transparent to light, self-cleaning, resistant to weathering. In addition, they can be manufactured in almost any shape and size, offering an efficient and low-maintenance structure for the building (alternative to glass for cases such as atria and shopping malls) [2].

With respect to foils, Paech [24] noted that ETFE offers thin films with very high transparency (up to 96%), but in comparison to textile membranes, ETFE has significantly reduced strength and the material properties are more sensitive under conditions of elevated temperatures. The thickness of the ETFE foils for the case of architectural applications is between 100 to 300 μm, while individual foil segments can be welded and seemed in order to form larger panels. In addition, ETFE foils allow printing. On the other hand, an alternative solution to ETFE foils are ECTFE (ethylene chlorotrifluoroethylene) foils. In the field of architectural applications, this is a relatively new product with abrasion resistance, excellent corrosion resistance and very good fire resistance. In general, ECTFE has similar material properties to ETFE but the major advantage of ECTFE is that the material has higher solar transmission and clarity [24].

Toniolo and Carella [39] present a work about ECTFE film for new buildings structures and it was noted that Halar® High Clarity ECTFE films from Solvay are the ideal

substitute for glass and outperform ETFE while currently they are considered as the best polymeric alternatives.

2.3. Mechanical and other properties of ETFE material

2.3.1. Mechanical properties

Galliot and Luchsinger [6] investigated the mechanical behavior of ETFE foils under uniaxial tension, standard biaxial extension and bubble inflation. The experiments which were conducted based on a biaxial machine showed that the load ratio has no influence on the elastic properties at small strains and there is no major advantage of using biaxial testing over uniaxial testing for the evaluation of the material initial behavior. It was also noted [6] that uniaxial tensile tests are easier to conduct and they do not require much material and time. It was highlighted that the main disadvantage of the uniaxial tests is the fact that with standard equipment it is not possible to evaluate Poisson´s ratio. This can be solved by using an additional device in order to measure the transverse strain in the sample. Another issue related with uniaxial tests is that the failure happens at very large strains which are not representative of the strains that the foil undergoes under large biaxial stresses [6]. On the other hand, bubble inflation tests should be adopted in order to study the biaxial failure of the foil. For design analysis, a linear or bilinear elastic model can be utilized as a first estimation of the material behavior up to the second yield point. For more accurate predictions, it is critical to include rate- and temperature-dependent behavior. The experiments [6] showed that the material behavior is non-homogeneous after the second yield point. It is also expected that the material behavior becomes anisotropic because of the reorientation of the molecular chains at large strains. Finally, it was noted that further studies are necessary to better understand the viscoelastic and plastic behavior of ETFE foils and using prestressing of the foil to increase the first yield stress would be interesting for the improvement of the load-bearing capability of ETFE foil structures [6].

Charbonneau et al. [7] conducted an experimental study about the mechanical behavior of ETFE foils. Creep tensile tests for different stress levels and for different time frames as well as tensile stress–strain tests were performed. Moreover, a one-dimensional creep model based on multi-Kelvin and power law modelling was presented. ETFE films show short-term creep under levels of stress expected in structural applications and the creep strain of the foils increases with the stress level. More analytically, at 2 MPa very little creep strain (0.015–0.033%) occurred in a basis of 24 h. Nevertheless, at 14 MPa the 24-h creep strains were 3.6–10.4%. Moreover, differences between the responses of films tested in the longitudinal and transverse directions were observed. In general terms, the films tested in the transverse direction experienced higher elastic and creep strains. It was noted [7] that the extrusion of the films and the molecular structure of ETFE could be the reasons for this behavior. In addition, the different types of film

presented differences in terms of the creep behavior. Moreover, constitutive models were developed in order to represent the observed creep behavior. Furthermore, nonlinear viscoelastic and viscoplastic models were developed for each creep test and for the 24-h tests the viscoelastic models showed a very close representation of the data for all the studied cases. The viscoplastic models offered a good representation at low stress levels; however, often deviated from the results at higher stress levels. Furthermore, tensile tests on the ETFE film were performed. In general, the findings showed that the films yielded and failed at higher stresses in the longitudinal direction than the transverse direction, but they were more ductile in the transverse direction. In terms of the average yield stresses, for all the films these ranged from 24 to 29 MPa (the average failure stresses ranged from 42 to 70 MPa). In Fig. 1 a schematic of an ETFE cushion is illustrated [7].

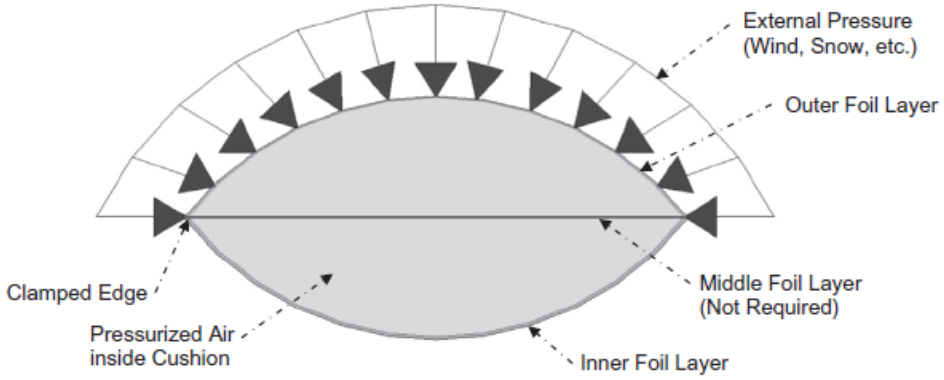

Figure 1. A schematic of an ETFE cushion (Source: Charbonneau et al. [7]).

Zhao et al. [38] demonstrated the technical feasibility of the flat-patterning method, as an efficient technique to find the form of ETFE cushion with the advantages of material cost efficiency, simple fabrication and easy installation. The main findings of Zhao et al. [38] are the following:

1. During the process of the whole form-developing, the stresses and strains of the ETFE cushion were found to be non-uniform. The maximum stresses were in the region from the center part to the middle parts of the three edges.
2. In terms of the creep phase, the internal pressure of the ETFE cushion was constant, but the rise and shape were increasing under the constant internal pressures of 4 kPa.
3. During the phase of creep-recovery, the shrinkage of the ETFE foils was proved by the variations in terms of the rise, internal pressure, stress and strain.

Wu et al. [40] carried out a model experiment on ETFE foil spring cushion. A temporary experimental hall using ETFE foil cushions as its roof was also constructed. It was demonstrated that the new structural system is easy in terms of the construction, it needs no air supply and control equipment, no running energy and low maintenance. Moreover, during the service time period of the experimental hall, the ETFE foil was tensioned very well by the compressed spring and no wrinkling of the foil was observed.

Hu et al. [8] investigated the uniaxial cyclic tensile mechanical properties of ETFE foils that are widely adopted in the frame of mechanical and construction industries. The experiments included eight cases with loading stress amplitudes from 4 to 21 MPa. The experimental findings demonstrated that the yield stress is a main mechanical property as the hysteresis loop and ratcheting strains become remarkable after the yield stress and that the elastic modulus, hysteresis loop and ratcheting strains evolve with the number of cycles and loading stress amplitude. In order to quantify these mechanical properties, a Matlab model was also developed [8].

Moreover, Hu et al. [9] presented a work about uniaxial tensile mechanical properties and model parameters determination of ETFE foils, adopted in structural engineering for membrane structures such as claddings and roofs. A series of uniaxial tensile tests under a wide range of temperatures and constant loading speeds were performed. The experimental findings were processed with mathematical methods in order to evaluate mechanical properties, such as first yield stress and elastic modulus. It was found that the first yield stress and elastic modulus decrease with increasing temperature but increase with the increasing loading speed. It was demonstrated [9] that the effect of temperature on the mechanical properties is stronger than that of the loading speed when considering the normal working conditions. In addition, a constitutive model based on viscoelasticity–plasticity of semicrystalline polymers was adopted for ETFE foils. The numerical results were in good agreement with the experimental findings. Related with the above mentioned issues about ETFE for building applications, in the work of Attipou [41] it was noted that ETFE is resistant to different temperatures and pressures.

ETFE foils present very high durability (in comparison to other transparent plastic materials). The basic characteristics of ETFE foils are: high tensile strength, high tear and impact strength. Moreover, ETFE is a very ductile material and it shows good failure behavior because of its large deformations before breaking point. In addition, ETFE foils are alkali resistant and solvent resistant (to a great extent) [42].

In the study of McKeen [43] it was noted that ETFE is a fluoroplastic with excellent electrical, chemical and mechanical properties. It was also highlighted that ETFE is especially suitable for applications which include high mechanical strength and adequate chemical, thermal, and/or electrical properties for a constructive material [43].

Moreover, it was mentioned that the mechanical properties of ETFE are superior to those of PTFE and FEP (fluorinated ethylene propylene). More specifically, the following characteristics/properties of ETFE were presented [43]:

- Excellent resistance to extremes temperatures (ETFE presents a wide range of working temperatures: from −200°C to 150°C).
- Mechanical strength (ETFE shows excellent tensile strength and elongation and it presents superior physical properties in comparison with most of the fluoropolymers).
- Excellent chemical resistance.
- Low smoke and flame characteristics.
- High resistance to weather and aging, excellent dielectric properties and nonstick characteristics.

In the study of McKeen [43] it was also mentioned that manufacturers and trade names include: DuPont™ Tefzel®, Asahi Glass Fluon® and 3M Dyneon™. In addition, uses and applications include: stadium roofing, electrical and fiber-optic wiring, liner in pipes, tanks and vessels.

In Table 1, selected literature references (years: 2011-2016) about ETFE properties (with emphasis on the mechanical properties) are presented. From Table 1, it can be seen that:

1) There are different studies which examine ETFE properties, with emphasis on its mechanical properties, and these studies are based on different methods.
2) A considerable part of these investigations is about ETFE foils appropriate for cladding and roofing applications.
3) The results show that ETFE material shows resistance to temperature/aging as well as mechanical strength and chemical resistance.

Table 1. Selected studies about ETFE properties, focusing on mechanical properties.

Study/year	Main content of the study	Studied material	Methods/tests	Findings	Additional comments/results
Galliot and Luchsinger (2011) [6]	Uniaxial and biaxial mechanical properties	ETFE foils e.g. for claddings and roofs	Three commonly used test methods were compared: uniaxial tension, biaxial extension of cruciform samples, bubble inflation (bursting test)	All methods showed very similar results (the selection of a test procedure depends on its advantages and limitations)	Uniaxial tensile tests: the strain-rate in the material varied in the range of 0.4–200%/min; the elastic modulus of the material was between 1000 and 1200 MPa and the first yield stress between 14 and 20 MPa
Charbonneau et al. (2014) [7]	Mechanical properties of ETFE foils, based on testing and modelling	ETFE foils e.g. for claddings and roofs	ASTM D882-09 standard test method for tensile properties of thin plastic sheeting	At 2 MPa, very little creep strain was presented, in the range of 0.015–0.033% in 24 h (nevertheless, at 14 MPa, 24-h creep strains showed values of 3.6–10.4%)	Average yield stresses for all the films varied from 24 to 29 MPa (average failure stresses varied from 42 to 70 MPa)
Zhao et al. (2016) [38]	Mechanical models of ETFE cushion based on flat-patterning method	ETFE foils (inflated cushion)	Forming design method of flat-patterning	Over the whole form-developing process, the stresses and strains of the ETFE cushion are non-uniform, with the maximum stresses in the region from the center part to the middle parts of the three edges and the minimum stresses in the three corners of the ETFE cushion	During the creep phase, the internal pressure of the ETFE cushion is constant (nevertheless, the rise and shape are increasing under constant internal pressures (4 kPa) and as a result, the stresses of the ETFE cushion are decreasing)
Wu et al. (2011) [40]	ETFE foil spring cushion structure and its analytical method	ETFE foil cushion structures (for greenhouses, sport facilities, etc.)	Analytical method, numerical method	The structural behavior of the spring cushion system was experimentally studied; It was found that the new structural system is easy in construction, needing no air supply and control equipment, little maintenance, no running energy	During service period of the experimental hall, the ETFE foil was tensioned very well by the compressed spring (no wrinkling of the foil was observed)
Hu et al.	Uniaxial cyclic	ETFE foils for	Methods in	The experimental	The fact that the

(2014) [8]	tensile mechanical properties of ETFE foils under eight loading cases	mechanical and construction industries	the MATLAB program	results revealed that the yield stress is a major mechanical property as the hysteresis loop and ratcheting strains become noticeable after the yield stress	first loading elastic modulus differs from subsequent loading/unloading elastic modulus gives explanations to the discrepancies found between the numerical findings calculated based on the uniaxial mechanical properties and the experimental results under field loading conditions
Hu et al. (2015) [9]	Uniaxial tensile mechanical properties and model parameters for ETFE foils	ETFE foils e.g. for claddings and roofs	Mathematical methods, numerical	The effect of temperature on the mechanical properties is stronger than that of loading speed for normal working conditions	Uniaxial tensile tests were conducted and the experimental findings were processed with mathematical methods in order to evaluate the mechanical properties
Blum et al. (2016) [44]	Elastic range, yielding conditions, break and the influence on the analysis of ETFE-structures	Structures made of ETFE films	Uniaxial tensile test; Biaxial tensile tests: square samples; Multiaxial tests on circular samples	Biaxial tensile tests (square samples): a cross sample always has a tendency to deform into the shape of a circle; Multiaxial tests on circular samples: the tests on the cross samples were found to be unsatisfactory since the homogeneity of the stress state could not be proven	The stress-strain behavior of ETFE films can be divided into a linear elastic region and a plastic range
Yoshino and Kato (2016) [45]	Viscous characteristics of ETFE film sheet (under equal biaxial tensions)	ETFE membrane film structures for applications in construction	Biaxial tensile test; FEM	The behavior under biaxial tension test was expressed sufficiently accurate by the proposed theory; however, for the prediction of the biaxial creep strains for long-term, further improvements of the viscoelastic coefficients used in the proposed	The validity of the proposed constitutive equation was verified

				formulation are needed	
De Focatiis and Gubler (2013) [46]	Thermal and mechanical response	Several commercial grades of ETFE copolymer films	Differential scanning calorimetry; Mechanical testing	The thermal analysis showed that, even if the films have similar degrees of crystallinity and melting temperatures, there are obvious differences in terms of the melting endotherms and crystallisation exotherms	Ways in which biaxial stretching could lead to improvements in terms of the properties across the plane of the film were proposed and discussed in the frame of production of polymer electrolyte membranes for energy applications
Hirschmann et al. (2014) [47]	Thermo-mechanical characterization of fluoropolymer films	Fluoropolymer films with emphasis on applications for solar concentrators	Differential scanning calorimetry, dynamic mechanical analysis and tensile testing	FEP and THV could not fulfil the thermo-mechanical requirements in terms of glass transition temperature and yield strength at application relevant temperatures; As most appropriate materials, ETFE copolymers were recommended even if no ETFE film fulfilled all of the requirements	Five transparent fluoropolymer films were characterized: three different ETFE, one FEP and one THV; The goal of the study was to find an appropriate material for utilization as transparent layer in a pneumatic pre-stressed sun-concentrator made of polymer films
McKeen (2016) [48]	Tribology of fluorocoatings	Several fluorocoatings	ASTM D1894-08 standard test method for static and kinetic coefficients of friction of plastic film and sheeting, etc.	Static coefficient of friction of Chemours Tefzel® HT-2004-25% glass fiber reinforced polyethylene tetrafluoroethylene: 0.31 (static coefficient of friction) for pressure 0.69 MPa	Tribological properties are most often useful when the materials are used in dry lubrication applications but the tribological properties are often considered for other types of applications
Liu et al. (2016) [49]	Solar radiation properties of common membrane roofs	Membrane roof materials (ETFE, PTFE, PVDF, TPO and PE were examined)	Numerical simulations (CFD), specimen tests	ETFE and PE membranes show high solar radiation transmittance (up to 0.8) and this can be modified for example by printing silver dots	The temperature of the steel structures below ETFE and PE membrane roofs was found to be over 61.7°C during summer (at least 27.7°C higher than the ambient air temperature)
Ebnesajjad	Chemical	Fluoropolymers	Several	The hydrolytic	ETFE presents

(2015) [50]	properties of fluoropolymers	methods (exposure to boiling water, etc.)	stability of ETFE is indicated by retention of its physical properties after an extensive exposure to boiling water: Tensile strength and elongation changed little after an exposure of 3000 h of unfilled ETFE to boiling water	excellent resistance to many chemicals: it is somewhat influenced by oxidizers, chlorinated solvents, ketones, and esters (however, it resists acids, alkalis as well as organic solvents)

2.3.2. Issues related with light transmission and insulation

In terms of the impact of longwave transmission on the total heat transfer, in the literature there is a study about energy modelling of ETFE membranes in building applications [10]. A mathematical model was developed, simplified and focusing on the maximum potential effect during a warm summer day. The results showed that the impact of longwave transmission is insignificant for the case of a warm sunny day [10].
With respect to insulating issues, a standard three-layer ETFE cushion presents around 1.95 W/m^2K U-value that is remarkably better than triple glazing when used horizontally. Cushion insulating characteristics can be further improved by the adoption of further layers. In this way, U-values below 0.6 W/m^2K can be achieved. On the other hand, ETFE foil absorbs a big part of infrared light transmitted, a quality which can be used in order to improve the energy consumption of the buildings [42].
Regarding light transmission, the optical characteristics of the transparent ETFE foil offer multiple advantages. ETFE shows high translucency by transmitting up to 94-97% of visible light (380-780 nm) and 83-88% of UV range (300-380 nm). This is an important issue for the well-being of humans and plants [42]. Moreover, the almost natural daylight makes the indoor environment more enjoyable for activities such as shopping (for the case of shopping malls) and swimming (for indoor swimming pools) and for places such as atrium roofs, markets, football stadiums and tennis courts. Another interesting issue is the fact that ETFE cushions can be lit internally with LED lighting in order to make them glow or projected onto externally (e.g. giant cinema screens) [42]. The utilization of ETFE material for roofs of swimming pools has been also examined in the work «Piscine publiques: sobres en énergie (2011)» [51].
Mainini et al. [12] proposed an alternative dynamic solar-gains-mitigation strategy for a double layer, non-cushion, ETFE panel for façades. A water spray system was located in the air-gap between the parallel ETFE foils in order to reduce surface temperatures and solar access. It was mentioned that the results are preliminary; however, it was noted that a reduction of up to 10% in total solar gains could be achieved as well as a reduction of 10°C in surface temperature.

Moreover, Mainini et al. [11] presented a work about measurements and evaluation of soiling effects of spectral light and solar transmittance decay of ETFE membranes (after three and six months of exposure; Milano city outdoor urban conditions; different tilt and orientations). The obtained values where utilized in order to evaluate thermal and solar properties of a multilayer ETFE panel. It was noted that after six months of exposure (urban outdoor conditions), ETFE showed decay in terms of light and solar transmittance performances. It was also mentioned that visible light transmittance is the most influenced performance. Soiling influences light transmission and solar heat gain coefficient of a double-layer ETFE; however, the average percentages of reduction are 4-8%. The maximum soiling was observed after 6 months of exposure, but soiling after three and six months were similar. The maximum performance reduction was found for the surfaces exposed on horizontal and the minimum for the vertical surfaces. The average value that was calculated for the thermal conductance was 5.158 W/m^2K.

In addition, Ahadi et al. [13] proposed an improved transient-plane-source method for measuring the thermal conductivity of thin films. It was noted that the conventional transient-plane-source method cannot accurately evaluate bulk thermal conductivity of thin films and coatings due to the inclusion of thermal contact resistances in the results. A new modified transient-plane-source method was proposed, offering accurate measurement of bulk thermal conductivity of thin films and coatings. The results, based on the proposed method, showed thermal conductivity values of 0.174 ± 0.002 W/mK for ETFE [13].

Lau et al. [52] proposed an experimental approach in order to investigate the luminous environment in lightweight fabric structures. It was concluded that the selective use of transparent and translucent components in the ETFE envelope can offer well balanced, yet dynamic lit scenes. Furthermore, by combining single-skin ETFE foil and double-layer or triple-layer ETFE cushion and by introducing ETFE cushions with different light transmittance to the building envelope, improvement of the overall visual and luminous environment can be achieved [52].

In the literature there is also a study about the experimental assessment and thermal characterization of ETFE foils [53]. The study [53] focused on the evaluation of heat transfer through ETFE membranes as well as on issues such as heat losses and solar gains.

Regarding transmittance, the spectral transmittance of semi-transparent materials appropriate for protective covers of solar concentrators has been measured [54] and the results showed yielding solar-weighted normal transmittance values of 0.913 and 0.946 for100 μm thin films of ETFE and FEP, respectively.

Based on the above mentioned literature studies about light transmission/insulation of ETFE material for building applications, it can be seen that, for example, ETFE cushion insulating characteristics can be further improved by using additional layers.

Concerning light transmission, the optical characteristics of the transparent ETFE foil are very advantageous; however, it should be taken into account that in practice, after several months of exposure, ETFE shows decay in terms of light and solar transmittance performances.

2.3.3. Lifespan

Flüeler and Aller [55] presented a work about long-term expectations and experiences of ETFE membrane constructions and it was noted that ETFE-membranes show an excellent physicochemical long-term performance, exceeding 30 years. During use phase (results based on three buildings) it was observed damage by hail (22 years of use). It was highlighted that such constructions should be protected against hail, impact of sharp objects and against vandalism [55].

In subsection 2.7, more details about ETFE lifespan and other issues which also influence the environmental profile of an ETFE system are presented, based on several literature studies.

2.3.4. ETFE vs. glass

In comparison to glass, ETFE film has lower weight, it transmits more light and it is resilient. Its properties such as self-cleaning (thanks to its nonstick surface) and recyclability at lower cost are superior [42]. For the case of pressurized pillows, it is possible to have control of sunlight transmission and effective insulation. Furthermore, ETFE material does not cause annoying echoes indoor. In addition, unlike glass, ETFE film is shatterproof [42].

Candemir [15] presented a work about an inflatable pillow system, based on ETFE, as a glass substitute for building envelope. The following issues were discussed:

- Regarding light transmittance, it was noted that double-layer ETFE and triple-layer ETFE present lower light transmittance in comparison to single-layer. Nevertheless, both double-layer and triple-layer ETFE pillows show higher values than double-glass glazing. However, it was highlighted that pillow system can interrupt the vision because of its curved nature. Glass and ETFE foil can glare and lose their transparency for high amounts of sunlight [15].

- In terms of thermal transmittance, it was explained based on certain examples, that multi-layer ETFE configurations present better insulation properties than glass [15].

- Concerning acoustical performance, ETFE pillows may influence the internal comfort in a positive or in a negative way, depending on its use and design. The designer should be aware of the acoustical performance of the materials and even if ETFE pillows

sound-reduction index is lower than the one for glass glazing, the use of double-glazing does not mean that double glazing contributes to the acoustical comfort. Furthermore, single-glass glazing presents better sound-reduction index than the one for the same width double-glazing [15].

- With respect to other issues, the advantages of ETFE in comparison to glass are the considerable reduction of the weight, the flexibility of the configurations and the increase of module «productivity» by transmitting the total sunlight spectrum (from UV to IR) to the solar cells (for the cases which combine claddings with ETFE configurations) [15].
- By taking into account building performance (including heating, lighting and mechanical equipment costs) membrane-glazing systems are found to be better than glass. The energy efficiency, along with the durability and the flexibility of the pillows can be adopted for several applications, offering advantages for the building [15].
- In terms of the cost (for the system itself, for the construction and for the maintenance and transportation), membrane configurations offer cost-effective solutions in comparison with conventional structures (based on conventional materials e.g. glass) [15].
- From environmental point of view, ETFE foil presents considerably lower embodied energy per m^2 of surface (in comparison to glass) [15].

In the frame of the comparison ETFE vs. glass, in the work of Kronenburg [18] it was noted that extruded as a film, ETFE is lighter and stronger than glass, and its original architectural application was for replacement of greenhouse glass.
Based on the above mentioned literature studies, it can be noted that ETFE shows many advantages, in comparison with glass, from different points of view (building, environment, etc.): lower weight, flexibility, self-cleaning, recyclability in lower cost, shatter-proofing, good transmission of the sunlight (possibility for combination of ETFE with PVs), cost-effective membranes, etc.

2.4. Acoustics related to structures with ETFE

Acoustics is one of several design issues that should be taken into account in order to assess if a lightweight, tensile fabric is suitable for a building enclosure. Materials such as ETFE and PTFE are widely used, offering multiple advantages (UV resistance, high reflectance, flexibility, waterproofing, light transmittance, etc.). However, further research studies should be conducted, by taking into account the suitability of the materials based on space use and occupancy [20]. Lightweight fabric membranes such as ETFE pillows present interesting acoustic properties because of the inherent thickness, weight and airspace. The benefit of this acoustic transparency is the fact that

the reflected sound can enhance the acoustic energy back into the space. An example of this effect can be found in stadia where the noise from the crowd can enhance the sense of excitement. Nevertheless, a disadvantage is that the reverberation and noise build-up from the middle to high frequencies is difficult to control for speech intelligibility. On the other hand, the noise that it is generated from inside a space enclosed with a membrane skin façade may disturb nearby people and buildings. In addition, environmental noise (for example from aircrafts, cars and railways) may easily be heard inside the space and it may be distracting for the occupants [20]. Moreover, rain noise is another issue for lightweight fabric membranes. The impact from rain falling on a lightweight fabric system can cause a drumming noise inside the space and usually noise mitigation is needed in order to minimize the effect of this impact noise. In this way, manufacturers of ETFE and PTFE materials are aware of this issue and they offer integral acoustic solutions so as to reduce rain noise [20]. For example, there are ETFE roofing systems with rain suppressors [56]. Related with the above mentioned issue, Toyoda and Takahashi [19] investigated rain noise from an air-cushion-membrane structure with ETFE films and it was noted that the results (theoretical and experimental) demonstrate the possibility of attenuating the noise by adding absorptive layers and/or damping materials.

Based on the above mentioned issues, acoustic design evaluations should be conducted at early design stages in order to examine if a lightweight tensile fabric system is appropriate for example for a building enclosure [20]. Some parameters related to this issue are: noise survey (sound measurements of external ambient noise, etc.), mechanical and electrical noise assessment, feasibility of speech intelligibility requirements. Finally, it should be noted that designers should know that different façade membrane products present different acoustic performances related to mass and material [20].

2.5. Shading issues about ETFE configurations

The material is very transparent and ETFE foil can be treated (by means of different ways) in order to manipulate its transparency and radiation transmission characteristics. In the frame of this concept, several strategies can be adopted such as the addition of more layers, tinting, printing, surface treatments and radiation [42]. Moreover, in the frame of «clever shading», it is also possible to control the amount of light that is transmitted to the inside by adopting a combination of one translucent with two printed ETFE films into a three-layer configuration and by moving the middle layer up and down. In this way, maximum shading or reduced shading can be obtained (when it is required). Thereby, it is possible to make a building skin which is reactive to the environment through changes in climate [42]. It should be noted that the middle layer is

programmed to rise and fall (by using the air pressure) in order to increase and decrease the percentage of printed area and thereby, to control the solar gains [42].

Cremers and Marx [22] presented a comparative study of a new IR-absorbing film for the improvement of solar shading and thermal comfort for ETFE structures. It was noted that standard ETFE foils show a very high solar transmission and this can create overheating and thermal discomfort. In this way, a new material infra-red absorbing was proposed by Nowofol (Nowoflon ET 6235 Z-IR). Cremers and Marx [22] presented a comparison between conventional ETFE constructions with clear (transparent) film or with silver printing (65%) and ETFE constructions with of one layer with the new material Nowoflon ET 6235 Z-IR. The new IR-absorbing ETFE film is not fully neutral in terms of the color (its transmission and reflection is slightly blue/greyish). In the study [22], the upper membrane was replaced by the new IR absorbing foil. The meteorological data of Stuttgart (Germany) were adopted. For summer, the thermal comfort showed an improvement of approximately 10% compared to a conventional ETFE construction. The savings in terms of cooling energy were 5-8%. Different climatic zones were examined [22].

With respect to the above mentioned issues, a single layer of NOWOFLON ET 6235 Z-IR-Film offers reduced heat transfer [57]. In addition, the transparency is completely maintained through linear light transmission and there is no color distortion. The annoying reflections can be reduced by more than half. Regarding UV, the transmission of UV-light is reduced to UV-A. Moreover, this ETFE film presents longevity, flame resistance, mechanical strength and it can be printed with a wide variety of designs [57].

In addition, Martin et al. [21] presented a work about the thermal and lighting performance within an ETFE structure. The findings of the field studies revealed that the temperature within an unventilated enclosed ETFE-panel structure can become too high for occupant comfort (during the summer). On the other hand, the enclosure may need heating during winter. The necessity for ventilation and shading in order to extend the time periods of comfort was discussed. The overall brightness within the structure was found to be acceptable but rather high for the occupants during intense insolation. It was noted that plants would prosper under slightly diffused light [21].

2.6. Inspection of transparent construction materials

Hinz et al. [23] presented a work about an image engineering system for the inspection of transparent foils, in particular ETFE foils. The developed bursting test including the photogrammetric recording and image analysis system offers possibilities for the evaluation of transparent materials, such as ETFE foil, in the multi-dimensional viscolelastic range up to the breaking point. It was highlighted [23] that the system can acquire precise 3D and 4D information. It was also noted that the calculated results are adequate to study the strain behavior of the foils quantitatively at early and middle

stages. Moreover, it was mentioned that the point accuracy should be improved in order to evaluate the strains at later stages [23].

2.7. Issues about ETFE from LCA/environmental point of view

In the study of Robinson-Gayle et al. [14] it was noted that ETFE is sold by manufacturers in granules and it is heated to its softening temperature (170^{o}C) in the hopper of an extruder. Then, the extrudate is blow moulded into large sheets and the sheets are heat welded together in order to form the three-layer cushion. Moreover, the pneumatic cushions are suspended in aluminium or steel frames. A critical issue is the very high heat input necessary to cause the raw materials combination. In addition, there are significant gaseous by-products (such as CO_2, SO_x and NO_x) [14]. Furthermore, embodied-energy values of 26.5 GJ/t and 27.0 MJ/m^2 (for ETFE foil) and 20 GJ/t and 300 MJ/m^2 (for glass) were presented [14]. Related with the above mentioned issues, in the work of Candemir [15] it was highlighted that, ETFE foil presents remarkably lower embodied energy per m^2 of surface (comparing to glass). On the other hand, Cremers [16] highlighted that in the literature there are big differences in terms of the proposed values of ETFE embodied energy, ranging from 26.5 MJ/kg [14] to 210 MJ/kg [17].
In the work of Monticelli et al. [17], details about the ETFE embodied energy were presented. The case examined was the embodied energy in order to obtain 1 kg of an extruded ETFE film. The system boundaries were from the retrieval of the raw material to the cushion make up, taking into account the extrusion process. The embodied energy during the cushion manufacturing phase was around 210 MJ/kg:
- 173 MJ are because of the generation of the raw materials; it was noted that (for ETFE) there are gases (ethylene and R22) which are introduced in the polymerization process: the 80% of this amount is due to the production process of the clorodifluoromethane (because of the utilization of natural gas and brow coal during its creation process), which produce TFE (tetrafluoroethylene) by pyrolysis [17].
- 28 MJ are because of the polymerization process and granulation of the raw materials into ETFE pellets (53% is the energy rate from steam, 35% is from electricity and 12% from gas) [17].
- 9 MJ are due to extrude ETFE pellets in thin films [17].
Maywald and Riesser [58] examined (from environmental point of view) the use of glass and the use of ETFE (Texlon® ETFE) in the frame of two projects in Germany (Berlin and Aachen), based on LCA. A lifespan of 30 years was considered for both cases (ETFE and glass). The selected standard foil cushion consists of three layers of NOWOFLON® ET foil. The selected glass includes double-glazing with panes, laminated with a PVB (polyvinyl butyral) film. The method of CML was adopted for the LCA, based on 1 m^2 of roof for both claddings. It was noted that globally, the results of the environmental impact assessment are better for the Texlon® roof than for the

glass roof, except of the impact category of Ozone layer depletion. The production of Texlon® cushions requires much less energy in comparison to glass production, and less structure materials are needed in order to support the whole system (thereby, there is less impact during manufacturing phase). It was highlighted that ETFE foil membranes can be considered as a more ecological solution in comparison to glass [58]. Results about the environmental impact for the production of 1 m^2 of a representative foil cushion (average values from 2012) for NOWFLON®ET foil have been also presented in the report «epd-norge.no» [59], based on «environmental product declaration».

In addition, in the work of Viguier [60] it was highlighted the fact that ETFE is a recyclable material, a characteristic that shows interest (from environmental point of view): for example in the frame of the evaluation of ETFE systems over their lifespan, end-of-life and disposal.

Flexible PV modules (flexcell) from amorphous silicon covered with an ETFE layer of 0.1 mm thickness have been evaluated, based on Ecological Scarcity 2006 method [61]. The findings of the study showed that the supply chain of ETFE has a major contribution to the environmental impact of the Flexcell modules. In the frame of a sensitivity analysis, the effect of a thinner ETFE coating on the environmental performance of the modules was examined. The reduced coatings of 0.05 mm ETFE and of 0.025 mm ETFE respectively, were compared to the standard thickness of 0.1 mm ETFE and the results revealed that by using half thickness, the environmental impacts of a module are reduced by a percentage of 18% [61]. It was noted that the chlorofluorocarbon emissions during the phase of production of the ETFE feedstock (R22) remarkably influence the results of different indicators. Moreover, it was mentioned that the data quality of the ETFE production was medium (because of the lack of production data, the material consumption and certain emissions were modelled theoretically) [61].

In addition, it should be noted that information in terms of life-cycle inventory data about ETFE have been analytically presented (including unit process raw data and the uncertainties for the production of 1 kg ETFE) in the report of Jungbluth et al. [62]. Moreover, Monticelli and Zanelli [63] presented a review about life-cycle design and efficiency principles for membrane architecture, including information about ETFE environmental profile.

In terms of the production of ETFE, ETFE is produced by mixing tetrafluoroethylene and ethylene monomers and the copolymerization of these monomers is very energetic. The copolymers of tetrafluoroethylene and ethylene can be prepared based on aqueous, non-aqueous, or mixed systems [62]. In the work of Jungbluth et al. [62] it was also noted that ETFE can be reinforced by using glass fibres. The operating temperature of

ETFE resins is from around -100°C to (at least) +150°C. ETFE is a good insulating material and ETFE resins are non-flammable in air [62].

In the literature there is also a study about LCA of polymer solar cells [28]. Several scenarios were examined, including encapsulation steel-foil/EVA/ETFE, in analogy to flexible PV modules manufactured on metal substrates [28].

In Table 2 information about ETFE that is related with the environmental profile of an ETFE system over its life-cycle, is presented. From Table 2 (studies conducted from 2001-2016) it can be seen that:

1) Most of the investigations examine embodied energy, showing values ranging from 26.5 to 210 MJ/kg, depending on the assumptions/boundaries adopted for each study.

2) Several types of ETFE appropriate for building applications (foils, cushions, etc.) have been examined.

3) Some studies compare ETFE with glass and the results reveal that, in general, ETFE configurations can be considered as more environmentally friendly than glass-based systems.

4) ETFE material is resistant, with lifespans ranging from 25 to 40 years.

Table 2. Selected literature studies which include LCA/environmental issues about ETFE.

Study/year	Materials	Environmental issues studied	Expected lifespan, durability, etc.	Additional information
Robinson-Gayle et al. (2001) [14]	ETFE foil cushions	Embodied energy: 26.5 GJ/t and 27.0 MJ/m^2	Current tests have run for 25 years; ETFE is very stable and it can resist chemicals and UV; its optical properties are not diminished over time	A comparison with glass was included, showing embodied energy for glass (6-mm float glass) 20 GJ/t and 300 MJ/m^2
Monticelli et al. (2009) [17]	ETFE film	Embodied energy to obtain 1 kg of an extruded ETFE film: 210 MJ/kg	ETFE pillows show outstanding durability, reducing the needs of replacement	The greatest part of the 210 MJ/kg (173 MJ/kg) are due to the generation of the raw materials introduced in the polymerization process
Monticelli (2010) [64]	ETFE cushions	The multi-layer ETFE cushion involves less energy (159.6 MJ/m^2) than	ETFE pillows show remarkable durability (40	ETFE-cushion roof requires less energy (than other roofs) because it is

		other roofing systems	years)	lightweight and it needs less quantities of materials
Maywald and Riesser (2016) [58]	ETFE foil vs. glass	CML method; ETFE foil membranes can be considered as a more ecological solution in comparison to glass	A lifespan of 30 years was considered for both materials (ETFE and glass)	Selected materials: standard foil cushion of three layers of NOWOFLON® ET-foil; Glass: double-glazing with panes, laminated with a PVB film
Jungbluth et al. (2012) [62]	ETFE, at plant	Inputs and products; Energy demand; Water use; Transportation; Infrastructure and land use; Emissions to air; Emissions to water; Solid waste	ETFE: its resistance to chemicals and solvents is excellent (strong acids and bases have no effect on ETFE resins)	Unit process raw data and uncertainties for ETFE copolymers (at plant) were presented
Zeh (2009) [65]	ETFE membranes	Durability, etc.	ETFE: it is supposed to have a guarantee of 30 years	Two structures roofed in PVC-coated polyester and one structure roofed in ETFE were compared

2.8. Applications

2.8.1. Requirements in terms of claddings

Before presenting studies about ETFE façades (and, in general, about ETFE for buildings), it is necessary to present some information about the requirements for the case of claddings. In the work of Paech [24] several critical issues were presented:

- Protection of the interior of the building from the external environmental conditions (rain, temperature, sun, wind, etc.).
- Creation of private interior spaces.
- Withstanding of the outer loads (maintenance loads, temperature, wind, etc.).
- Good thermal performance and good performances with respect to solar radiation and light management and response.
- Good fire behavior of the materials.
- Acoustic performance.
- Durability.
- Aesthetic value and appearance of the surface (in terms of translucency, color, etc.).
- To allow complex architectural geometries (for certain cases).

- Weight of the materials.
- Cost of the materials.
- Installation issues (regarding costs, time, etc.).
- Maintenance requirements.
- Recyclability of the components and sustainability.

Paech [24] noted that since the cladding is the main component of a façade, the materials and their specific requirements should be examined during the initial stage of the design. Given the fact that building projects are very distinctive (in terms of their location, their purpose, etc.) it is impossible to list all the demands for each application with claddings. However, the above mentioned factors present some critical issues.

2.8.2. Studies about ETFE façades, roofs and atria

Paech [24] presented a work about structural membranes used in modern building façades. General demands about façade systems were analyzed. Material and system options, properties, limits of membrane façades, case studies and multiple solutions including typical material combinations (ETFE, glass-PTFE, PVC polyester, glass-PTFE mesh, multi-layer insulated systems) were also discussed.

Robinson-Gayle et al. [14] presented some examples of ETFE foil roofs. It was concluded that ETFE foil is an appropriate technology for specific building applications, especially for the cases where the volume of the space is large and there is a need for high levels of light. In addition, it was highlighted that ETFE foils can improve the environmental performance of a building and they can reduce the overall environmental burden related to the construction process as well as the burden of the building over its lifespan [14].

Afrin et al. [25] presented results based on on-site monitoring of foil surface temperatures and thermal environment within two atria configurations covered with different compositions of ETFE foil cushion roof (1: two-layer, 2: three-layer) and different ventilation regimes. A strong vertical stratification in both atria was found. Moreover, it was demonstrated that the foil surface temperatures respond rapidly to high solar radiation with the internal layer being hotter than both the external layer and the adjacent internal air. Furthermore, it was found that during night the surface temperature of the external foil follows the ambient external temperature closely and the internal layer temperature follows approximately the mean of adjacent internal temperature in the atria and external temperature [25].

Masih et al. [66] presented the results of a field work about the luminous environment of an atrium enclosed by ETFE cushion roof and a test structure constructed with ETFE-encapsulated panels. A theoretical study was also conducted. The goal was to

examine how the typical homogeneous and dull luminous environment can be improved. It was found that the selective use of translucent and opaque components in the frame of ETFE enclosures can offer good lighting conditions [66]. In addition, the selective positioning of these components in different parts of the ETFE structures can enhance the visual perception. Different case studies were examined. One of these case studies is based on the Engineering and Science Learning Centre at the University of Nottingham, including student support office, graduate center, learning and teaching spaces as well as a multi-functional central atrium. The atrium roof consists of three-layer ETFE cushions with extruded aluminum frames connected to the primary steel truss structure. The geometry of the above mentioned building has an arc-shape in plan and the atrium roof offers daylight for all the internal spaces. In addition, a glazed aperture on the top of the south-west façade provides supplementary daylight (Figure 2) [66].

In addition, configurations with ETFE for roofs/atria have been presented in the following works: INRA [67], Tanno [68], Découverte en avant-première du pôle de Commerces et de Loisirs Confluence [69].

Figure 2. The external and internal views of the Engineering and Science Learning Centre at the University of Nottingham (Source: Masih et al. [66]).

2.8.3. Combination of ETFE with PV or PVT

Zhao et al. [70] conducted field experiments and numerical modeling in order to study the temperature of an amorphous-Si PV system which is combined with a three-layer ETFE cushion roof. The experiments were done for four typical weather conditions (winter sunny, winter cloudy, summer sunny and summer cloudy). The results showed that the temperature variation under cloudy condition was more significant than that under sunny condition. Comparisons between experimental and numerical results were presented. For the temperature characteristics, a good agreement between experimental and modeling findings was observed.

Hu et al. [71] presented a work about experimental studies on summer performance and feasibility of a system which combines BIPVT (building-integrated photovoltaic/thermal) with ETFE cushion. The proposed system offers collection of

thermal energy due to enclosed cushions. An experimental mock-up of a three-layer ETFE cushion and amorphous-Si PV modules was developed. Experiments were performed during summer, (especially for sunny and sunny-to-cloudy conditions). The results based on the experiments demonstrated that the system operates smoothly and steadily. One-day and three-day evaluations of the system were done. The findings showed that for energy, the average stored electricity was 61 Wh. In addition, the average temperature difference between the air temperature inside and outside of the cushion was found to be 18.1°C [71]. In this way, system electricity feasibility and potential in solar energy utilization were verified. For cushion structures, the temperatures on structural ETFE membranes used to resist external loads were within the acceptable range and the pressure performance was found to be satisfactory. Thus, the structure feasibility was demonstrated. Hu et al. [71] noted that their study reveals the technical feasibility of ETFE cushion structure integrated with PV and it was mentioned that their study provides a way to extent BIPVT/cushion applications [71]. Furthermore, there is a study [72] which examines the performance of organic PV layers on architectural membranes. It was noted that organic PVs are promising due to their low cost and easy fabrication. Several cases in terms of organic PVs in combination with architectural-membrane materials were discussed [72]. It was highlighted that ETFE printed Ag layer conductance is a little less sensitive than PET (polyethylene terephthalate)-printed one with large strains, which is highly favored for the use of ETFE as a substrate of organic PVs [72].

Additional studies which include ETFE combined with PVs have been presented by Hu et al. [26], Hu et al. [27], Lenzmann et al. [28] as well as in the frame of the ETFE-MFM project [73]. In Fig. 3 the experimental ETFE-PV mock-up (Fig. 3a) and the PV arrangement (Fig. 3b) studied by Hu et al. [26] are illustrated.

a)

b)

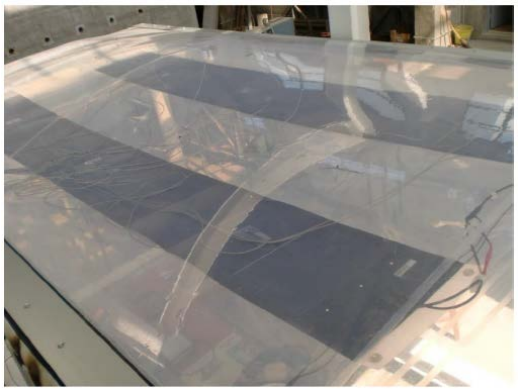

Figure 3. a) Experimental ETFE-PV mock-up and b) PV-arrangement (Source: Hu et al. [26]).

2.8.4. Several configurations which include ETFE

In the frame of the project «Emballage de la Rotonde» [74] for «La Rotonde de Saint-Etienne», in France, several plastic materials were examined (based on different criteria: economic, environmental, mechanic). It was noted that a double ETFE membrane around the construction of «La Rotonde de Saint-Etienne» can provide multiple benefits (e.g. insulating effect by means of a recyclable material) [74].

Within the field of agricultural applications, ETFE material can be also adopted for greenhouses [15, 18, 66, 75]. In the work of Masih et al. [66] a test structure with ETFE-encapsulated panels (two-layer 150 μm ETFE foils) as external skin built at the garden of a detached house (near Grantham, UK) used as an outdoor room and a greenhouse for plants (Fig. 4), was presented. In addition, in the study of Waaijenberg et al. [76] about a highly insulated greenhouse design with an inflated roof system with PVDF (polyvinylidene fluoride) or ETFE membranes, it was noted that new materials such as PVDF and ETFE-membranes offer an opportunity to create a double inflated structure, which has a light transmittance comparable to single glass thanks to the very high initial light transmittance of these films.

Another type of ETFE applications refers to solar thermal collectors. Beikircher et al. [77] presented a work about a flat-plate collector for process heat with full surface aluminium absorber, vacuum super insulation and front foil. It was noted that between the glass cover and the absorber of the collector it is added a transparent ETFE foil for the reduction of the heat loss coefficient. Related with the above mentioned study, Beikircher et al. [78] presented a review about advanced solar flat-plate collectors with full area absorber, front side film and rear side vacuum super insulation.

Other types of applications include ETFE for fuel cells [79-81], ETFE for inflatable tubes [82], ETFE as materials to protect for example reflectors of solar concentrators [54], ETFE for electrical and fiber-optic wiring, liner in pipes, tanks and vessels [43].

Figure 4. The external and internal views of a structure with ETFE encapsulated panels: external skin built at the garden of a detached house used as an outdoor room and a greenhouse for plants (Source: Masih et al. [66]).

2.8.5. Discussion about ETFE applications

Based on the literature it can be seen that ETFE can be adopted in the frame of different applications: for example for roofs, façades, atria as well as in combination with PVs. Except of the building sector, ETFE has also agricultural applications, e.g. for greenhouses. Moreover, ETFE can be used as additional component for the development of solar systems (solar thermal collectors, etc.).

Regarding ETFE-PV combination, it can be noted that ETFE shows interest for example for organic PVs, for flexible amorphous-Si PVs, for BI (building-integrated) applications. ETFE provides a protection (from weather conditions) for the PV cells and specifically for BIPV (building-integrated photovoltaic) systems, configurations with ETFE can offer multiple advantages: enhancement of the use of BIPV systems in constructions, development of innovative façades with different lighting possibilities, etc. [73].

For the specific case of adopting ETFE as cladding, certainly, certain requirements (which are requirements, in general, for cladding materials) should be fulfilled: good thermal performance, durability, high aesthetic value, low weight, good performance in terms of solar radiation and light management and response, etc.

2.9. Case studies

In the present subsection several case studies based on ETFE material, with emphasis on buildings and architectural constructions, are presented (Table 3). From Table 3 it can be seen that:

1) The case studies refer to several countries with different climatic conditions (Spain, UK, France, Germany, etc.).

2) Multiple ETFE configurations have been presented (membranes, inflated cushions, with/without lighting, transparent or printed, etc.).
3) The constructions are for different uses (commercial, sports, etc.).
4) ETFE configurations offer multiple advantages (they can be manufactured to any size and to fit any shape, they can be combined with modern constructions as well as with buildings of historical character, etc.).

In general, the case studies demonstrate that ETFE can play an important role in the building sector, offering multiple configurations. For example, the combination of ETFE with PVs (e.g. AWM Carport [73]) is an interesting solution, taking into account the importance of PVs towards the development of net zero energy buildings [97] which provide advantages from energetic as well as from economic point of view [98]. Another example is the combination of ETFE with different types of lighting, pleasing from aesthetic point of view [73]. In addition, ETFE configurations offer possibilities for ventilation and temperature control [3, 90] as well as natural daylight illumination [3, 89].

Table 3. Selected case studies with constructions which include ETFE material.

Name of the construction and reference	Location	ETFE configuration	Use of the construction	Additional information
Memorial [83]	Madrid, Spain	Glass cupola in combination with ETFE	Memorial	The memorial includes 2 parts, related: the glass cupola and the room underneath it (from the room, the visitors can see the inside part of the cupola)
Millennium Dome [73]	Valladolid, Spain	ETFE in combination with lighting	Multiple activities	ETFE can be combined with different types of lighting
Centre de loisirs Vitam'Parc [84]	Neydens, France	ETFE in combination with a wooden construction	Sports, commercial	The aquatic center has a wave-shaped roof
L'heure tranquille [85]	Tours, France	Inflated ETFE cushions	Commercial center	The construction includes arcs which are combined with ETFE
Grand Stade du Havre [86]	Le Havre, France	Dyed ETFE-membrane, four specially developed shades of blue	Stadium	A stadium forming a uniform and integrated whole
SMAC de Nîmes	Nîmes, France	Façade composed of	Music hall	The north façade

[87]		ETFE cushions		looks like a huge «eye»
Lyon Confluence [88]	Lyon, France	Double-layer ETFE cushions	Shopping and leisure center	There is an enormous illuminated membrane roof
Hampshire Tennis and Health Club [89]	Hampshire, UK	The cladding system over the Tennis Center consists of opaque white Texlon ETFE foils within an exterior tensile structural system	Tennis and health club	The cladding system over the Tennis Center is an elegant and economical solution; The opaque white foil offers diffusion of the natural daylight and natural ambient illumination ideal for sporting events
Chelsea and Westminster Hospital [90]	London, UK	Texlon® ETFE inflated panels	Hospital	A Texlon® ETFE roof needs no external cleaning because it is self-cleansing (under the action of rain), in this way, there are savings in maintenance costs; Texlon® ETFE roof system offers effective ventilation and temperature control, important for a hospital
King's Cross Station [91]	London, UK	Glass, ETFE, polycarbonate	Railway station	The intelligent use of glass and translucent products offers a contemporary railway architecture
Kingsdale School [92]	London, UK	«Variable skin» ETFE roof enclosure	School	An inspiring mixed-use space based on various design interventions is offered
Olympic Swimming Pool, Munich [93]	Munich, Germany	A flexible façade connection includes a pneumatic tube made of ETFE foil	Swimming pool	There is light-flooded appearance of the swimming pool
Festo headquarters [94]	Esslingen, Germany	Texlon® ETFE inflated panels, Texlon® ETFE shading system	Offices	The design includes six finger-like buildings connected by means of a central spine. Three

				of these spaces are covered by Vector Foiltec state-of-the-art Texlon® ETFE variable shading system – Vario® – and in this way, they offer dynamic multi-function atrium spaces
Allianz Arena [73]	Munich, Germany	ETFE in combination with lighting	Football stadium	ETFE can be combined with different types of lighting
AWM Carport [73]	Munich, Germany	ETFE in combination with PVs	Vehicle services	The combination of ETFE with PVs can enhance the use of BIPV
Masoala Rainforest Zoo [95]	Zurich, Switzerland	Membranes of ETFE foil	Zoo, tropical house	The size is 14600 m²
Shopping Mall Dolce Vita Tejo [31]	Amadora, Portugal	Multi-layer ETFE cushion roof	Shopping mall	Innovative building envelope
Commercial center Arena [3]	Valencia, Spain	ETFE double-layer cushions	Commercial center	The cushions include printed and transparent configurations
Malls/Caraba square Islazul [3]	Madrid, Spain	ETFE double-layer cushions	Malls, square	The cushions include printed and transparent configurations
San Mamés New Stadium [3]	Bilbao, Spain	Monolayer ETFE membrane	Stadium	The ETFE membrane is of white color; The façade is composed of more than 2700 membranes
Urban space station, Museum of Modern Art Reina Sofía [3]	Madrid, Spain	Transparent ETFE film	Urban space station, museum	The ETFE membranes can be adapted to any type of project, including new applications
Pavilion (for banquets) in the Restaurant Les Cols [3]	Olot, Spain	Double-layer ETFE	Pavilion in restaurant	The ETFE layer is printed and transparent; There is a space with a special atmosphere thanks to the combination of shadows, light and

				trees above the ETFE cover
Hotel Villa de Laguardia [3]	Laguardia, Spain	Triple-layer ETFE cushions	Hotel	The ETFE layers are printed and transparent; ETFE is used for a semi-circular cover which attenuates the entry of light and solar radiation
Commercial center Vallsur [3]	Valladolid, Spain	Triple-layer ETFE cushions	Commercial center	The solar control system moves the intermediate layer up or down, in this way it changes the passage of light and the solar radiation inside the building
Ancient church of Sant Pere [3]	Corbera d´Ebre, Spain	Monolayer ETFE	Church	The transparent ETFE cover offers a perfect integration with respect to the historical character of the building and it provides a multifunctional space
Commercial center Leclerc Les Portes du Valois [3]	Le Plessis Belleville, France	ETFE: Triple-layer cushions for the building and monolayer for the accesses	Commercial center	At the level of the access to the building the transparent domes are constructed with a monolayer system of ETFE membranes; During the day, natural light floods into the interior space
Allianz Riviera stadium [3]	Nice, France	Monolayer ETFE; Exterior and inner ring	Stadium	The complex structure of wood and steel is visible from the outside through the transparent ETFE enclosure
Le Nuage [96]	Montpellier, France	ETFE cushions for façades and covers	Sport center	Surface: 2200 m^2
School of Health Sciences, University of Aveiro [3]	Aveiro, Portugal	Double-layer ETFE for the building and monolayer ETFE for the footbridges	University	Footbridges: The transparent enclosure allows natural ventilation through openings

Central train station of Luxembourg [3]	Luxembourg	ETFE membranes printed	Train station	ETFE covers show a natural integration with the neo-baroque architecture of this building
Aqualibi water park [3]	Wavre, Belgium	Triple-layer ETFE cushions, transparent	Water park	The ETFE configuration offers conditions close to those of outdoor conditions

3. Conclusions

By taking into account that in the literature there are few review studies about ETFE material, the present article is a critical review about ETFE, with emphasis on building applications.

Selected literature references about ETFE properties (focusing on mechanical properties) are presented and the results show that: 1) the investigations are based on different methods, 2) a considerable part of these investigations is about ETFE foils for claddings/roofs and 3) ETFE material presents resistance to temperature/aging, mechanical strength and chemical resistance.

On the other hand, studies about light transmission/insulation of ETFE material for building applications are included, showing that ETFE cushion insulating characteristics can be further improved by utilizing additional layers. Regarding light transmission, the optical characteristics of the transparent ETFE foil are very advantageous but after several months of exposure, ETFE shows decay in terms of light and solar transmittance performances.

In addition, investigations which compare ETFE with glass are cited, revealing that ETFE offers many advantages, in comparison with glass, from different points of view (building, environment, etc.).

A separate part of the article is based on literature studies about ETFE environmental profile/LCA and the results demonstrate that: 1) most of the investigations evaluate ETFE embodied energy, showing values ranging from 26.5 to 210 MJ/kg, 2) different types of ETFE for building applications (foils, cushions, etc.) have been investigated, 3) certain studies compare ETFE with glass and the comparisons reveal that, in general, ETFE can be considered as more environmentally friendly than glass, 4) ETFE material is resistant, with lifespans ranging from 25 to 40 years.

Concerning ETFE applications, ETFE can be used for different applications: roofs, façades, atria, etc., in combination with PVs (interesting for cases such as BIPV systems and organic PVs), for buildings as well as for greenhouses.

Additional issues (requirements for adopting ETFE as cladding, acoustics, shading, inspection of transparent materials, etc.) are presented and critically discussed. A separate part with case studies is included, along with a discussion.

By considering the fact that ETFE is a promising material for the building sector, with multiple advantages (structures of low-weight, flexible structures with different shapes, etc.), the present article offers useful information about ETFE, based on different points of view.

Acknowledgements

The authors would like to thank "Ministerio de Economía y Competitividad" of Spain for the funding (grant reference ENE2016-81040-R) and Banco Santander UdL-Impuls program.

4. References

[1] BASF, The Chemical Company, Improving the performance of existing commercial buildings: The chemistry of sustainable retrofits.

[2] Robinson LA. Structural Opportunities of ETFE (ethylene tetra fluoro ethylene). MSc thesis, Massachusetts Institute of Technology, 2005.

[3] ETFE l'architecture transparente, IASO, report.

[4] Dunn, Source: http://dunn-lwa.com/etfe/

[5] Teng H. Overview of the Development of the Fluoropolymer Industry. Appl Sci 2012;2:496-512; doi:10.3390/app2020496.

[6] Galliot C, Luchsinger RH. Uniaxial and biaxial mechanical properties of ETFE foils. Polym Test 2011;30:356–365.

[7] Charbonneau L, Polak MA, Penlidis A. Mechanical properties of ETFE foils: Testing and modelling. Constr Build Mater 2014;60:63–72.

[8] Hu J, Chen W, Luo R, Zhao B, Sun R. Uniaxial cyclic tensile mechanical properties of ethylene tetrafluoroethylene (ETFE) foils. Constr Build Mater 2014;63:311–319.

[9] Hu J, Chen W, Zhao B, Wang K. Uniaxial tensile mechanical properties and model parameters determination of ethylene tetrafluoroethylene (ETFE) foils. Constr Build Mater 2015;75:200–207.

[10] Poirazis H, Kragh M, Hogg C. Energy modelling of ETFE membranes in building applications. Eleventh International IBPSA Conference, Glasgow, Scotland, July 27-30, 2009, Building Simulation 2009.

[11] Mainini AG, Poli T, Paolini R, Zinzi M, Vercesi L. Transparent multilayer ETFE panels for building envelope: thermal transmittance evaluation and assessment of optical and solar performance decay due to soiling. Energy Procedia 2014;48:1302-1310.

[12] Mainini AG, Speroni A, Zani A, Poli T. The effect of water spray systems on thermal and solar performance of an ETFE panel for building envelope. Procedia Eng 2016;155:352–360.

[13] Ahadi M, Andisheh-Tadbir M, Tam M, Bahrami M. An improved transient plane source method for measuring thermal conductivity of thin films: Deconvoluting thermal contact resistance. Int J Heat Mass Tran 2016;96:371–380.

[14] Robinson-Gayle S, Kolokotroni M, Cripps A, Tanno S. ETFE foil cushions in roofs and atria. Constr Build Mater 2001;15:323-327.

[15] Candemir KU. Inflatable Pillow System as a Glass Substitute In Terms of Building Envelope, MSc thesis, Izmir Institute of Technology, Turkey, 2003.
[16] Cremers J. Environmental impact of membrane and foil materials and structures – *status quo* and future outlook, Technical transactions, Architecture, 7-A/2014.
[17] Monticelli C, Campioli A, Zanelli A. Environmental load of ETFE cushions and future ways for their self-sufficient performances. Proceedings of the International Association for Shell and Spatial Structures (IASS) Symposium 2009, Valencia, Evolution and Trends in Design, Analysis and Construction of Shell and Spatial Structures, 28 September – 2 October 2009, Universidad Politecnica de Valencia, Spain, Alberto Domingo and Carlos Lazaro (eds.).
[18] Kronenburg R. 1- Introduction: the development of fabric structures in architecture, *In* Fabric Structures in Architecture, A volume in Woodhead Publishing Series in Textiles, Pages 1–21, Elsevier; 2015.
[19] Toyoda M, Takahashi D. Reduction of rain noise from Ethylene/TetraFluoroEthylene membrane structures. Appl Acoust 2013;74:1309–1314.
[20] Chiu S, Noble D, Valmont E. 9- Acoustics in architectural fabric structures: the case of ETFE pillows, *In* Fabric Structures in Architecture, A volume in Woodhead Publishing Series in Textiles, Pages 241–256, Elsevier; 2015.
[21] Martin BAJ, Masih D, Lau B, Beccarelli P, Chilton J. An evaluation of thermal and lighting performance within an ETFE structure, In Gorse, C. and Dastbaz, M. (Eds.) International SEEDS (Sustainable Ecological Engineering Design for Society) Conference, 17–18 September 2015, Leeds Beckett University, UK.
[22] Cremers J, Marx H. Comparative Study of a New IR-Absorbing Film to Improve Solar Shading and Thermal Comfort for ETFE Structures. Procedia Eng 2016;155:113–120.
[23] Hinz S, Stephani M, Schiemann L, Zeller K. An image engineering system for the inspection of transparent construction materials. ISPRS J Photogrammetry Remote Sens 2009;64:297-307.
[24] Paech C. Structural membranes used in modern building facades. Procedia Eng 2016;155:61–70.
[25] Afrin S, Chilton J, Lau B. Evaluation and Comparison of Thermal Environment of Atria Enclosed with ETFE Foil Cushion Envelope. Energy Procedia 2015;78:477–482.
[26] Hu J, Chen W, Cai Q, Gao C, Zhao B, Qiu Z, Qu Y. Structural behavior of the PV–ETFE cushion roof. Thin Wall Struct 2016;101:169–180.
[27] Hu J, Chen W, Qiu Z, Zhao B, Zhou J, Qu Y. Thermal performances of ETFE cushion roof integrated amorphous silicon photovoltaic. Energy Convers Manage 2015;106:1201–1211.
[28] Lenzmann F, Kroon J, Andriessen R, Espinosa N, Garcia-Valverde R, Krebs F. Refined life-cycle assessment of polymer solar cells. 26th European Photovoltaic Solar Energy Conference and Exhibition, 5-9 September 2011, Hamburg, Germany.
[29] Hu J, Chen W, Zhao B, Yang D. Buildings with ETFE foils: A review on material properties, architectural performance and structural behavior. Constr Build Mater 2017; 131:411–422.
[30] Hu Z, Jiang MF. Review on the Production and the Market of Tetrafluoroethylene / Ethylene Copolymer (ETFE). Fine Chem Intermediates 2012-06.
[31] Chilton J. Lightweight envelopes: Ethylene tetra-fluoro-ethylene foil in architecture, Proceedings of Institution of Civil Engineers: Construction Materials, Volume 166, Issue 6, December 2013, Pages 343-357.
[32] Chen X, Yang H, Lu, L. A comprehensive review on passive design approaches in green building rating tools, Renew Sustain Energy Rev 2015;50:1425–1436.

[33] Godfryt JJ, Aldous F. The roof-to-wall interface: designing for optimum performance, BEST 1 Conference, 10-12 June 2008, Minneapolis, MN.
[34] Lee E, Selkowitz S, Bazjanac V, Inkarojrit V, Kohler C. High-Performance Commercial Building Façades, LBNL-50502, Building Technologies Program, Environmental Energy Technologies Division, Ernest Orlando Lawrence Berkeley National Laboratory, University of California, Berkeley, CA 94720, June 2002.
[35] Dyneon: 3MTM DyneonTM Fluoropolymers, Membrane Architecture, Your ideas, our solution, 3M.
[36] Kawaguchi K. 19 Recent developments in architectural fabric structures in Japan, In Fabric Structures in Architecture, Edited by J. Llorens, Pages 687-725, Elsevier; 2015.
[37] Huntington CG. 18 Recent developments in architectural fabric structures in North America, Fabric Structures in Architecture, Edited by J. Llorens, Pages 661-686, Elsevier; 2015.
[38] Zhao B, Chen W, Hu J, Chen J, Qiu Z, Zhou J, et al. Mechanical properties of ETFE foils in form-developing of inflated cushion through flat-patterning. Constr Build Mater 2016;111:580–589.
[39] Toniolo P, Carella S. Halar® High Clarity ECTFE film – an highly transparent film for new buildings structures. Procedia Eng 2016;155:28–37.
[40] Wu M, Wu Y, Kim JY. ETFE foil spring cushion structure and its analytical method. Thin Wall Struct 2011;49:1184–1190.
[41] Attipou K. Étude des Instabilités dans les Membranes Minces sous Chargements Thermomécaniques. Thèse pour l'obtention du grade de Docteur de l'Université de Lorraine, Spécialité: Mécanique des Matériaux, 2015.
[42] ONART, ETFE façades and roofs, Report.
[43] McKeen LW. 11 Fluoropolymers, In Fatigue and Tribological Properties of Plastics and Elastomers (Third Edition), 2016, Pages 291-315, http://dx.doi.org/10.1016/B978-0-323-44201-5.00011-3
[44] Blum R, Bögner-Balz H, Köhnlein J. On the mechanical behaviour of ETFE-films: Elastic range, yielding conditions, break determined by different test methods and the influence of the results on the analysis of ETFE-structures. Procedia Eng 2016;155:496–506.
[45] Yoshino T, Kato S. Viscous characteristics of ETFE film sheet under equal biaxial tensions. Procedia Eng 2016;155:442–451.
[46] De Focatiis DSA, Gubler L. Uniaxial deformation and orientation of ethylene–tetrafluoroethylene films. Polym Test 2013;32:1423–1435.
[47] Hirschmann B, Oreski G, Pinter G. Thermo-mechanical characterization of fluoropolymer films for concentrated solar thermal applications. Sol Energy Mater Sol Cells 2014;130:615–622.
[48] McKeen LW. 15 Introduction to the Tribology of Fluorocoatings. In Fluorinated Coatings and Finishes Handbook, The Definitive User´s Guide, Second Edition, 2016, Elsevier, Pages 277-297.
[49] Liu H, Li B, Chena Z, Zhou T, Zhang Q. Solar radiation properties of common membrane roofs used in building structures. Mater Design 2016;105:268–277.
[50] Ebnesajjad S. 15 Chemical Properties of Fluoropolymers, In Fluoroplastics, Volume 2, Melt Processible Fluoropolymers, The Definitive User´s Guide and Data Book, Second Edition, 2015, Pages 432-474, Elsevier.
[51] Piscine publiques: sobres en énergie, Concevoir la piscine du futur, Technique, CHAUD - FROID - PERFORMANCE - N° 745 - Mai 2011.

[52] Lau B, Masih DAA, Adesoji Ademakinwa A, Woon Low S, Chilton J. Understanding Light in Lightweight Fabric (ETFE Foil) Structures through Field Studies. Procedia Eng 2016;155:479–485.
[53] Dimitriadou EA, Shea A. Experimental Assessment and Thermal Characterization of ETFE Foil, ATINER CONFERENCE PAPER SERIES No: CON2012-0145, 2012.
[54] Good P, Cooper T, Querci M, Wiik N, Ambrosetti G, Steinfeld A. Spectral reflectance, transmittance, and angular scattering of materials for solar concentrators. Sol Energy Mater Sol Cells 2016;144:509–522.
[55] Flüeler P, Aller D. Long-Term Expectations and Experiences of ETFE Membrane Constructions. XII DBMC, 12th International conference on Durability of building materials and components, 12-15 April, 2011, Porto, Portugal.
[56] bre, Rain noise, Rain noise from roof glazing, polycarbonate roofing and ETFE roofing.
[57] The climate-smart architecture film NOWOFLON ET 6235 Z-IR, Source: http://www.nowofol.com/files/nowofol/downloads/Press%20release%20NOWOFLON%20ET%206235%20Z-IR.pdf
[58] Maywald C, Riesser F. Sustainability – the art of modern architecture. Procedia Eng 2016;155:238–248.
[59] epd-norge.no, The Norwegian EPD Foundation, ENVIRONMENTAL PRODUCT DECLARATION, Vector Foiltec GmbH, Nowfol Kunststoffprodukte GmbH & Co. KG, Dyneon GmbH.
[60] Viguier JP. Qu'attend l'architecte, l'urbaniste et l'artiste de la chimie?, Source: http://www.mediachimie.org/sites/default/files/chimie_habitat_13.pdf
[61] Stucki M, Frischknecht R, Flury K. ESU-services Ltd., on behalf of Flexcell (VHF-Technologies SA), Life cycle assessment of Flexcell amorphous silicon modules, report, Uster, July 2012.
[62] Jungbluth N, Stucki M, Flury K, Frischknecht R, Büsser S. ESU-services Ltd., Life Cycle Inventories of Photovoltaics, Version: 2012, On behalf of the Swiss Federal Office of Energy SFOE, Uster, September 2012, Report.
[63] Monticelli C, Zanelli A. Life Cycle Design and efficiency principles for membrane architecture: towards a new set of eco-design strategies. Procedia Eng 2016;155:416–425.
[64] Monticelli C. Environmental assessment of ultralight roof structures built with new materials: the case of the ETFE cushions, Proceedings of IASS WG18 Colloquium, 2010.
[65] Zeh M. Fabric Architecture, Aging of membrane materials. November 17th, 2009, By: IFAI, Continuing Education, Source: http://fabricarchitecturemag.com/2009/11/17/aging-of-membrane-materials/
[66] Masih DAA, Lau B, Chilton J. Daylighting Performance in an Atrium with ETFE Cushion Roof and in an ETFE-Encapsulated Panel Structure. Energy Procedia 2015;78:483–488.
[67] INRA. Construction du laboratoire d'écologie et de génomique forestières du centre de recherches forestières. INRA de Nancy, Site de Champenoux, Le 28 septembre 2009, inddigo, ingénieries du développement durable.
[68] Tanno S. ETFE foil cushions as an alternative to glass for atriums and rooflights. ICBEST'97 International Conference on Building Envelope Systems and Technology, 15-17 April 1997, Bath, UK.
[69] Découverte en avant-première du pôle de Commerces et de Loisirs Confluence (2012). Communiqué de presse, Février 2012.

[70] Zhao B, Chen W, Hu J, Qiu Z, Qu Y, Ge B. A thermal model for amorphous silicon photovoltaic integrated in ETFE cushion roofs. Energy Convers Manage 2015;100:440–448.
[71] Hu J, Chen W, Zhao B, Song H. Experimental studies on summer performance and feasibility of a BIPV/T ethylene tetrafluoroethylene (ETFE) cushion structure system. Energy Build 2014;69:394–406.
[72] Fan Z, De Bastani M, Monticelli C, Zanelli A. Performance investigation of organic photovoltaic layers on architectural membrane. 9th International ENERGY FORUM on Advanced Building Skins, 28-29 October 2014, Bressanone, Italy.
[73] ETFE-MFM Project, Integrating PV into a textile architecture to power façade lighting, European project.
[74] Rapport projet énergétique (2011), Emballage de la Rotonde, Par C. Karayan et M. Nafack Mintsa, Encadré par N. Gondran et J. Villot, 9/12/2011, École Nationale Supérieure des Mines, Saint-Etienne.
[75] Liu X, Gao H, Sun Y, Wu Y, Martin B, Chilton J, et al. Thermal and optical analysis of a passive heat recovery and storage system for greenhouse skin. Procedia Eng 2016;155:472–478.
[76] Waaijenberg D, Hemming S, Campen JB. The Solar Greenhouse: a Highly Insulated Greenhouse Design with an Inflated Roof System with PVDF or ETFE Membranes. Acta Hort. 691, 2005, Pages 561-568.
[77] Beikircher T, Osgyan P, Reuss M, Streib G. Flat plate collector for process heat with full surface aluminium absorber, vacuum super insulation and front foil. Energy Procedia 2014;48:9–17.
[78] Beikircher T, Möckl M, Osgyan P, Streib G. Advanced solar flat plate collectors with full area absorber, front side film and rear side vacuum super insulation. Sol Energy Mater Sol Cells 2015;141:398–406.
[79] Li X, Drache M, Gohs U, Beuermann S. Novel concept of polymer electrolyte membranes for high-temperature fuel cells based on ETFE grafted with neutral acrylic monomers. J Membrane Sci 2015;495:20–28.
[80] Henkensmeier D, Ben youcef H, Wallasch F, Gubler L. Radiation grafted ETFE-*graft*-poly (*α*-methylstyrenesulfonic acid-*co*-methacrylonitrile) membranes for fuel cell applications. J Membrane Sci 2013;447:228–235.
[81] Tran Duy T, Sawada S-i, Hasegawa S, Katsumura Y, Maekawa Y. Poly(ethylene-*co*-tetrafluoroethylene) (ETFE)-based graft-type polymer electrolyte membranes with different ion exchange capacities: Relative humidity dependence for fuel cell applications. J Membrane Sci 2013;447:19–25.
[82] He Y, Chen W. Experiment and Theoretical Analysis Study of ETFE Inflatable Tubes. Hindawi Publishing Corporation, International Journal of Aerospace Engineering, Volume 2014, Article ID 925428, 10 pages, http://dx.doi.org/10.1155/2014/925428
[83] https://divisare.com/projects/341110-fam-arquitectura-y-urbanismo-diego-laurino-atocha-station-memorial
[84] Architecture – Bâtiments de sport, 5.6.7, Les fiches bois de Lignum, Centre de loisirs Vitam'Parc, Neydens (F), Source: http://www.lignum.ch/uploads/media/FB.5.6.7_Neydens.pdf
[85] Dossier immobilier, Jeudi 18 Novembre 2010, Les echos, Architecture, La forme gonflée de L´Heure tranquille à Tours.
[86] publications, Stadium in blue – Construction of "Grand Stade du Havre", LEICHT, Source: http://www.leichtonline.com/en/social/publications/1374579791.pdf
[87] Architecture transparante, 5 technique, 5 façades No 101, février/mars 2013.

[88] seele, Source: http://seele.com/references/lyon-confluence-shopping-leisure-complex/
[89] ArchiEXPO, Source: http://www.archiexpo.com/prod/vector-foiltec/product-68767-1386767.html
[90] vector-foiltec, Source: http://www.vector-foiltec.com/projects/chelsea-westminster-hospital/
[91] adf, architects datafile, Glass & translucent materials, May 2014, Source: http://www.netmagmedia.co.uk/wp-content/uploads/2014/05/ADF-May-2014-Glass-Translucent-Materials-Supp-superlo.pdf
[92] Kingsdale School, London, United Kingdom (England), Source: https://www.oecd.org/edu/innovation-education/centreforeffectivelearningenvironmentscele/36931487.pdf
[93] sbp, Source: http://www.sbp.de/en/project/oympic-swimming-pool-new-suspended-ceiling/
[94] vector-foiltec, Source: http://www.vector-foiltec.com/projects/festo/
[95] NOVUM Membranes, Source: http://novummembranes.de/index.php?option=com_content&view=article&id=88:masoala-regenwald-zoo-zuerich&catid=21&Itemid=91&lang=en
[96] IASO, Source: https://www.iasoglobal.com/fr/projet/le-nuage
[97] Deng S, Wang RZ, Dai YJ. How to evaluate performance of net zero energy building - A literature research. Energy 2014;71:1-16.
[98] Berry S, Davidson K. Improving the economics of building energy code change: A review of the inputs and assumptions of economic models. Renew Sustain Energy Rev 2016;58:157-166.
.

Capítulo 4. Análisis de eficiencia y estabilidad de tecnologías OPV

D. Chemisana, A. Moreno, M. Polo, C. Aranda, A. Riverola, E. Ortega, Chr. Lamnatou, A. Domènech, G. Blanco, A. Cot. Performance and stability of semitransparent OPVs for building integration: A benchmarking analysis, Renewable Energy, Artículo aceptado y publicado

Performance and stability of semitransparent OPVs for building integration: A benchmarking analysis

D. Chemisana [a, *], A. Moreno [a], M. Polo [b], C. Aranda [b], A. Riverola [a], E. Ortega [b], Chr. Lamnatou [a], A. Domènech [a], G. Blanco [b], A. Cot [b]

[a] Applied Physics Section of the Environmental Science Department, University of Lleida, Jaume II 69, 25001 Lleida, Spain
[b] COMSA CORPORACIÓN, Av. Roma, 25-27, 08029 Barcelona, Spain

Abstract

Semitransparent (ST) organic photovoltaics (OPVs) are demonstrating great potential for building integration applications, especially in windows. For that purpose, ST-OPVs should achieve adequate transparency and performance stability. In this regard, the present research deals with the experimental performance of three different building-integrated ST-OPV technologies (technology A: developed in the frame of the present study; technologies B and C: commercial modules). More specifically, spectral transmittance and electrical measurements have been conducted in order to determine the characteristics of the modules for building integration and electricity generation purposes. Results regarding the transmittance reveal that technology A outperforms technologies B and C. The stability analysis of the modules verifies that module C is the most stable one with almost no decrease (3.6%) in the power conversion efficiency (PCE). Furthermore, the PCE of technology B is slightly higher than in the case of technology C, which experiences a PCE degradation of about 10-15% over the whole time period. Finally, technology A presents a 20% reduction in PCE at around 500 hours.

Keywords: Semitransparent organic photovoltaics (OPVs); Building-integrated systems; Spectral transmittance; Electrical measurements; Stability.

List of symbols and abbreviations

Ag	Silver
AgNW	Silver nanowire
AVT	Average visual transmittance [%]
BIPV	Building-integrated photovoltaic
DAQs	Data acquisition systems

* Corresponding author. E-mail address: daniel.chemisana@macs.udl.cat

D_λ	Spectral distribution [-]
Dir	Direct irradiance [W/m^2]
FF	Fill factor [%]
Glob	Global irradiance [W/m^2]
I_{out}	Current of the OPV modules [A]
I_{sc}	Short-circuit current [A]
ISOS	International Summit on OPV Stability
ITO	Indium tin oxide
I-V	Intensity-voltage
J_{sc}	Short-circuit current density [A/cm^2]
MoO_3	Molybdenum trioxide
MPPT	Maximum power point tracker
OPV	Organic photovoltaic
PBTZT-stat--BDTT-8	Polymer donor from Merck
$PC_{71}BM$	[6,6]-phenyl-C71-butyric acid methyl ester
PCBM	[6,6]-phenyl-C61-butyric acid methyl ester
PCE	Power conversion efficiency [%]
PEDOT	Poly(3,4-ethylenedioxythiophene)
PET	Polyethylene terephthalate
PSS	Poly(styrenesulfonate)
PTBT	Poly(4,8-bis[(2-ethylhexyl)oxy]benzo[1,2-b:4,5-b′]dithiophene-2,6-diyl-alt-3-fluoro-2-[(2-ethylhexyl)carbonyl] thieno[3,4-b]thiophene-4,6-diyl)
PWM	Pulse Width Modulation
R.H.	Relative humidity
ST	Semitransparent
T	Module temperature [^{o}C] or thermal cycling

TiO_2	Titanium dioxide
UV	Ultraviolet
V(λ)	Photopic vision efficiency [-]
V_{cell}	Potential of the OPV modules [V]
V_{oc}	Open-circuit potential [V]
WO_x	Tungsten oxide
ZnMgO	Zinc magnesium oxide

Greek symbols

λ	Wavelength [nm]
τ	Transmittance [-]
τ_V	Visible transmittance in agreement with EN 410:2011 [-]

1. Introduction

In conventional photovoltaic installations, where the modules are based on crystalline silicone, the solar cells are responsible for the highest cost, not only from an economic point of view but also from an environmental perspective. Due to the issues mentioned above (economic and environmental), during the last years there is an increasing interest for organic photovoltaic (OPV) systems. OPVs are considered as a cost-effective technology [1] with reduced environmental impact. Resources and processes involved in OPV manufacturing phase and recycling are expected to demand less energy inputs and therefore, OPVs are expected to be more eco-friendly in comparison with other types of photovoltaic systems which include solar cells with high environmental impact [2]. An additional advantage of the OPVs is the fact that they can be fabricated as thin films, lightweight, semitransparent, free form and flexible, widening the possible applications in comparison to conventional silicon-based photovoltaic panels.

With respect to the electrical performance, in the literature remarkable advances by utilizing bulk heterojunction organic devices that combine donor and acceptor substances in the blend have been reported [3]. Also, molecular optimization to tune the optoelectronic properties of photovoltaic materials by chemical modulation is an effective strategy to enhance efficiency. More specifically, the present efficiency record of 13.1% has been obtained for a cell where the small molecule acceptor was synthesized via fluorination [4]. This impressive value of 13.1%, even to be very high in terms of OPV cells, is quite far from the percentages obtained by silicone cells (values

above 20%). Although the efficiency trend is quite optimistic, stability and large-scale production issues are not as advanced as the efficiencies [5]. Currently, an important research effort focuses on stability and degradation of OPV cells [6, 7]. Concerning degradation, degradation mechanisms can be influenced by several factors such as oxidation or hydration/hydrolysis that affect the active layer and electrodes, the diffusion of the electrode materials towards the active layer, etc. Usually the combination and interrelation between those factors arises difficulties in understanding the degradation process [8]. However, despite the drawbacks mentioned above, a recent study demonstrates that OPVs with short lifespans of 3 years and efficiencies of around 2% are competitive against conventional photovoltaic technologies and producing electricity at about 0.19 €/kWh [9].

Regarding Building-Integrated Photovoltaic (BIPV) elements, since OPVs can be printed, the size of the module may perfectly match the desired dimensions where the BIPV element should be installed, independently of the shape. Roll-to-roll printing processes are compatible for manufacturing OPV modules, leading to low manufacturing costs. In addition, OPV color range and transparency are easily tunable by simply changing the light-absorbing organic semiconducting small molecule, the polymer type or the thickness [10], additionally to utilizing transparent electrodes. Among OPVs, semitransparent (ST) modules are those bringing the widest variety of possibilities to position them as a perfect candidate for BIPV applications, e.g. in the frame of window-integrated configurations [11]. Figure 1 shows two different semitransparent modules where the grade of transparency and color variability can be appreciated. Figure 1 (a) illustrates a glass laminated red-like color module (Source: [12]) and Figure 1 (b) presents a photograph of a green-like module (Source: [13]).

a) **b)**

Figure 1. a) Red-like (Source: Yan et al. [12]) and b) Green-like (Source: Lucera et al. [13]) semitransparent modules.

In the literature, several investigations about the development of improved ST organic devices, mainly based on utilizing new acceptors (*i.e.* non-fullerene acceptors), light-trapping architectures to gain extra photons and new transparent top electrodes (*i.e.* transparent conductive oxide, silver nanowire, carbon nanotube, etc.) can be found. Nonetheless, although the stability of nontransparent organic cells has been investigated, very little attention has been paid to ST-OPVs [11]. Most of the stability investigations about OPVs, in general, are performed under controlled laboratory conditions; however, the most relevant and challenging tests are those under outdoor exposure (where the OPVs will eventually be operating) [14].

In order to fill the gap of the lack of stability studies about ST-OPVs and specially to analyze their performance under outdoor conditions, the present study focuses on the experimental outdoor performance monitoring of three types of ST-OPV modules, two commercially available modules and a module developed in the SOLPROCEL European project [15].

2. Experimental set-up

In the frame of outdoor stability testing procedures for building integrated OPV modules, there is no regulation to establish the conditions of the experiments. The closest approach is the International Summit on OPV Stability (ISOS) procedure, where several categories of test protocols are defined: dark (D), outdoor (O), simulated light and stress testing (L) and thermal cycling (T). Among them, the ISOS-O, regarding the exigence in the measurements to be conducted, presents three different levels (1: Basic; 2: Intermediate; 3: Advanced). In Table 1, the main characteristics of ISOS-O setup requirements are summed up [16].

Table 1. ISOS-O test setup and testing protocol [16]

		ISOS-O-1	ISOS-O-2	ISOS-O-3
Test setup	Light source	Direct sunlight, no shadows		
	Mounting	Static: facing south and tilted at latitude angle. Tracking: 2-axis		
	Load	MPP tracking (preferred) or Open circuit		MPP tracking or MPP passive (resistor)
	Temperature	Ambient		
	Relative humidity (R.H.)	Ambient		
	Characterization light source	Inside, simulated light	Outside under sunlight	Outside regularly and inside at certain periods
Testing protocol	Temp. / R.H.	Monitor ambient values	Monitor nominal operating cell temperature (NOCT) and ambient R.H.	
	Solar irradiance and irradiation	Monitor irradiance and calculate accumulated irradiation		
	Current (I) - voltage (V) characterization	Measure short-circuit current and open-circuit potential	Measure IV curves	Refer to IEC 60904-1 [17]. Measure IV curves at irradiances close to 1000 W/m^2.
	Min. measurement intervals	Daily to weekly	1/15 min - 1/1 h	Outside: 1/15 min - 1/1 h Inside: weekly or monthly
	Characterization temp.	Monitor specimen temperature on backside		
	Charact. irriadiance	Monitor irradiance		
	Wind monitoring	Optional		Monitor wind speed down to 0.25 m/s
	Incident-photon-to-	Optional		Measure

	electron conversion efficiency			
	Note data taken in ranges	Optional	Ambient temperature outside of range 20±15 ºC. Irradiance below 400 W/m^2	Ambient temperature outside of range 20±15 ºC. Irradiance below 400 W/m^2. Wind speed outside of range 1±0.75 m/s. For 10 min following wind speeds exceeding 4 m/s Wind direction within ±20º east or west.

Moreover, in the indicated protocol, there are some recommendations for the data reported. For instance, degradation curves of normalized photocurrent and power conversion efficiency (PCE) should be presented from data collected only under irradiances in the range of 800-1000 W/m^2 (to avoid non-linear effects) [16].

The items described above state a proper frame for comparisons between different OPV technologies, independently of the location. Nevertheless, in the case of building-integrated devices some of the requirements are not appropriate or hardly achievable (*i.e.* irradiances above 800 W/m^2, or module inclination at latitude angle / tracking, etc.). ISOS-O statements are considered as baseline and they are adapted to the present application of OPV for building façade integration.

The ST-OPV modules were monitored at the Applied Energy Research Centre (CREA) of the University of Lleida (in Spain) which is located in Lleida, at latitude 41.36°N and longitude 0.37°E. Experiments were carried out from the end of July to the beginning of December. Figure 2 illustrates the daily average (line), maximum and minimum (dots) ambient temperatures, R.H. and wind speed (at 2 meters height) jointly with the hourly mean irradiance for the monitored period. It can be noted that ambient temperatures show a big variation from the summer to the end of autumn, ranging from around 30ºC to 2ºC (with considerable thermal amplitude). R.H. registers an important increase from values near to 50% to values almost 100% from the end of October on. This is due to the typical foggy periods reported in Lleida around November. On the contrary, wind speed was very low during the whole time period. Global horizontal irradiance experiences logical trend due to the solar declination evolution with a particular affectation during foggy days.

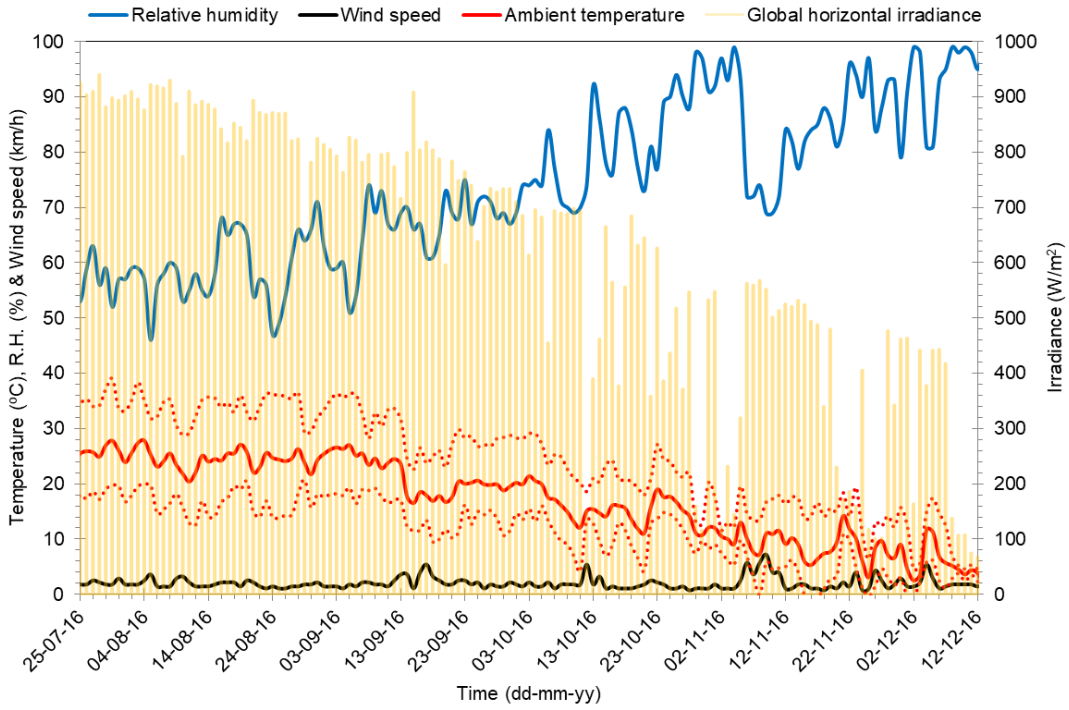

Figure 2. Ambient conditions during the monitoring period (location: Lleida, Spain).

The modules were installed facing south at the outdoor testing unit (Fig. 3). It should be noted that the OPVs are enclosed in a double-glass structure in order to better emulate the real building integration and to keep them flat. Spectral and electrical measurements were performed in order to determine the PCE, transparency and stability of such technologies operating under real building-integrated conditions.

The modules were plugged into a specially designed and manufactured maximum power point tracker (MPPT). There are no available commercial MPP trackers for the ranges of currents and potentials of the assessed modules. Electric outputs, at MPP conditions, have been continuously monitored jointly with daily measurements of the intensity-voltage (I-V) curve and spectral-transmittance measurements throughout the experimental campaign. I-V curves were measured outdoors daily once or twice, while for the transmittance measurements the modules were moved to the laboratory, after the sunset, and then they were installed back to the monitoring set-up 5 times during the experimental campaign.

As it can be seen in Fig. 3, a pyranometer (Kipp&Zonen CMP6) has been placed in the middle of the modules in order to register the proper global irradiance received. Furthermore, each module has attached a T-type thermocouple at its rear surface. In addition, in the interior space of the testing unit, the MPPTs jointly with the Data Acquisition Systems DAQs (Campbell Sci. CR3000) and the I-V tracer (Keithley 2460) have been placed.

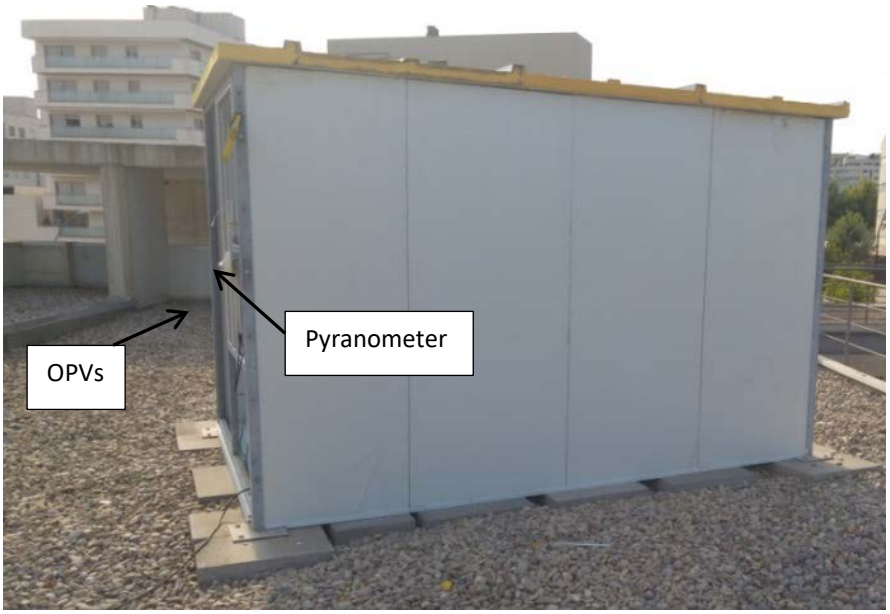

Figure 3. The outdoor testing unit (University of Lleida, Lleida, Spain).

The electronics were controlled by an Arduino Mega board, which commands a bipolar junction transistor by utilizing the PWM (Pulse Width Modulation) output based on the PWM value at which the maximum power of the module is delivered. For that purpose, I-V curves were acquired at maximum velocity at different instants from which the maximum power was derived and the PWM frequency was fixed to commute the transistor. In Fig. 4, all the details of the designed circuit are indicated. From Fig. 4 it can be noted that apart of the previously mentioned elements, other important components have also been included (operational amplifier, different filters, diode, etc.). In addition, an important issue is the incorporation of an external battery of 5V in order to ensure signal stability since the 5V output which the board offers presented fluctuations that affected the accuracy of the system. In the same way, the current (I_{out}) and the potential (V_{cell}) of the OPV modules were monitored with the datalogger for two reasons: 1) because of the simplicity of sampling of all the variables in the same element and 2) due to the fact that Arduino analogical outputs are not sensitive to low values.

Also, the built general circuit allows acquiring data at any time interval and it offers high flexibility, for example, it automatically switches to I-V curve measuring.

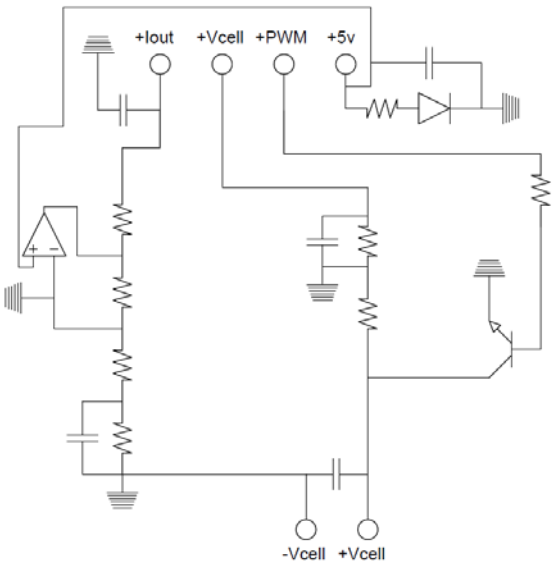

Figure 4. Schematic of the maximum power point tracking electronic circuit.

3. Characterization of the OPV modules

As it was previously indicated, the characterization of the organic modules consists of two types of tests: 1) the spectral transmission which determines the lighting abilities of the technologies and 2) the evaluation of the electrical performances which leads to reliability and suitability features as generation system. The tests were conducted for three ST-OPV technologies. The modules developed during the project are named as Technology A (2 modules tested: A1, A2), and the commercial ones as Technology B (2 modules tested: B1, B2) and Technology C (1 module tested: C).

Technology A modules have been fabricated with inverted structure and were processed on flexible ITO-Metal-ITO sputtered PET substrates with the layer sequence ZnO nanoparticles / PBTZT-stat-BDTT-8:PCBM / PEDOT:PSS / AgNW. The manufacturing process utilized allows obtaining large area modules with minimum losses with respect to the device at cell level. All the stack layers were processed in ambient conditions via slot-die coating with a heatable head [15]. This represents an important advantage with respect to other manufacturing processes that rely on vacuum and /or present difficulties to print large surfaces.

3.1 Spectral transmission

In the field of ST-OPVs, researchers use to refer to the visible region (370-740 nm) based on the Average Visible Transmittance (AVT) parameter [18]. However, for the evaluation of the spectral transmission of the ST-OPVs for building integration applications, it is important to introduce the European Standard EN 410:2011: “Glass in

building — Determination of luminous and solar characteristics of glazing" [19]. The standard states how to determine the visible luminous transmittance (τ_V), Eq.(1), considering the relative spectral distribution of illuminant D65 (D_λ) and the spectral luminous efficiency for photopic vision, $V(\lambda)$ (which ranges from 400 to 700 nm with its peak at 555 nm). The bandwidth defined in the standard comprises the interval where the transmission of the ST-OPV should be enhanced in order to allow a proper vision in the interior spaces.

$$\tau_V = \frac{\sum_{\lambda=380\ nm}^{780\ nm} D_\lambda \tau(\lambda) V(\lambda) \Delta\lambda}{\sum_{\lambda=380\ nm}^{780\ nm} D_\lambda V(\lambda) \Delta\lambda} \quad (1)$$

For the spectral transmission characterization, an Ocean Optics spectrometer has been used, measuring the spectrum transmitted at 5 different points distributed along the module surface (in order to determine the homogeneity of the organic blend). It should be noted that the transmitted light percentage measured does not consider the scattered fraction. Figure 5 illustrates the transmittance spectra measured for the three technologies (A: Fig. 5(a); B: Fig. 5(b); C: Fig. 5(c)) at the five sampling points, indicating that the commercially available modules present slightly less dispersion between the different parts of the module (in comparison to the spectra measured for technology A). In addition, it can be noted that C presents the most uniform behavior, almost overlapping the transmittances for all the sampling points. Moreover, the most important reflected part in all of them was around the blue to green bandwidth; therefore, all the modules appearance is aesthetically similar.

a)

b)

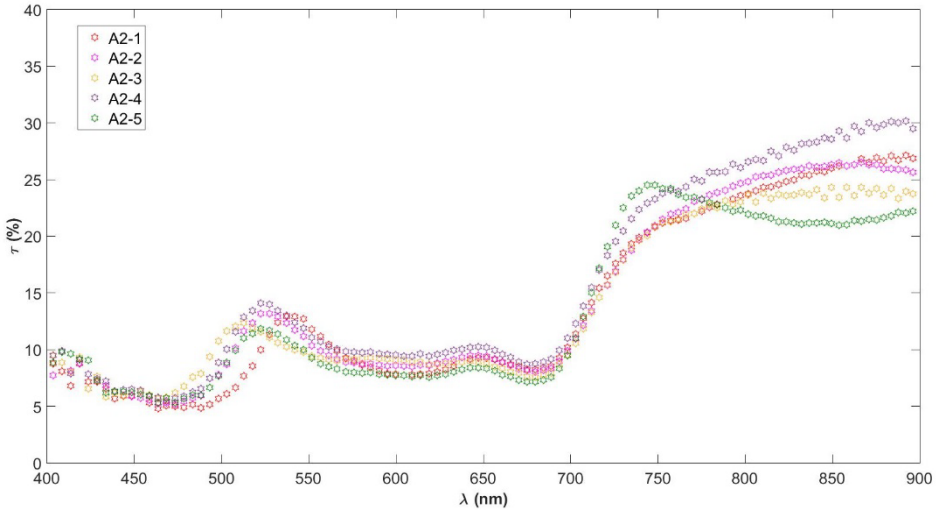

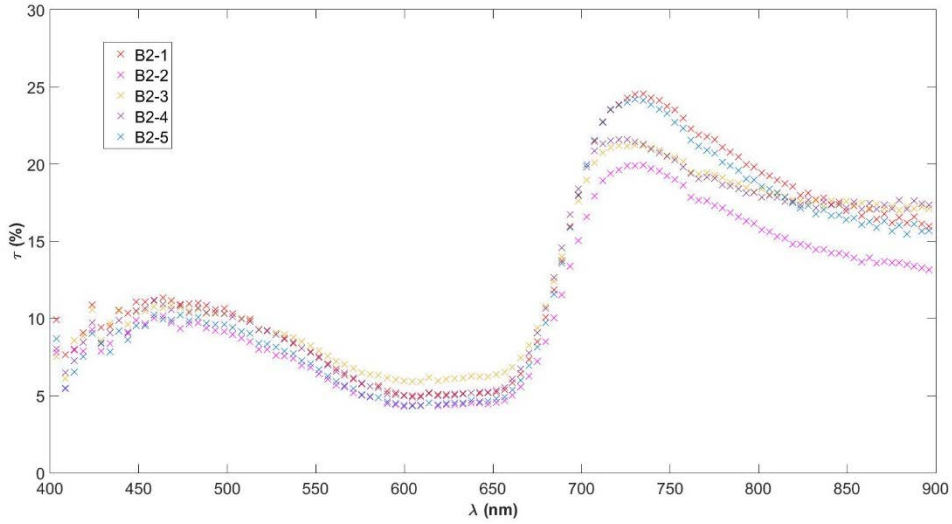

c)

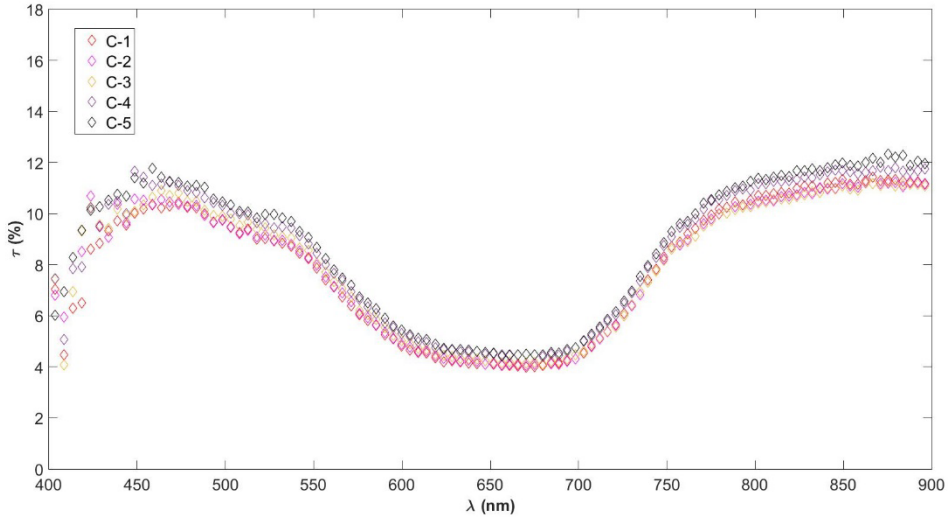

Figure 5. The transmittance spectra measured for the three technologies (a: A2; b: B2; c:C) at the five sampling points.

As it was previously highlighted, due to the high flexibility of the photovoltaic elements and in order to better emulate the building-integration conditions, the modules were encapsulated in an extra clear double-glass sandwich to keep them flat and also to perform the function as structural element. In order to more precisely estimate the transmission of the OPV units, the double glass transmission that supports therein each type of technology has been measured. The obtained mean transmittance value for the double glasses was 85.4% for the interval [380-780] nm.

Figure 6 shows the 5-sampling points mean spectral transmittance (corrected with the double-glass transmittance, τ') for each module technology, measured at the end of the characterization. Also, the curve resulting from the product of the illuminant relative spectral distribution (D_λ) and the photopic vision efficiency, V(λ), is depicted.

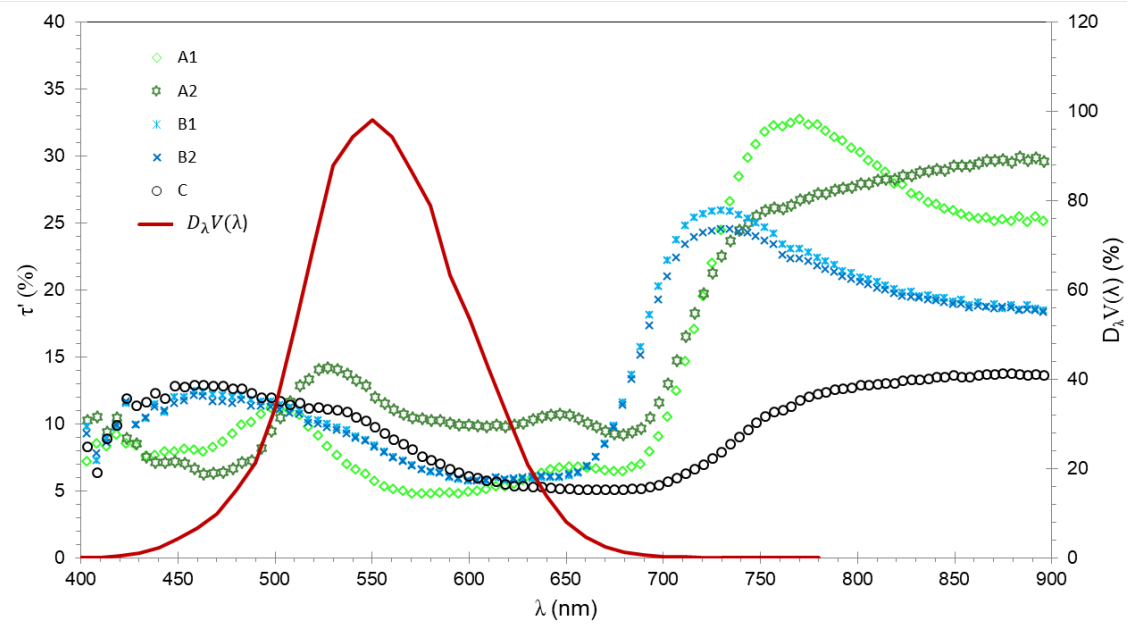

Figure 6. Mean spectral transmittances of the modules at the end of the monitoring period and the $D_\lambda V(\lambda)$ curve.

As it can be seen in Fig. 6, the product $D_\lambda V(\lambda)$ is 0 for wavelengths below 400 nm and above 700 nm since $V(\lambda)$ is 0 as well. Consequently, the effective bandwidth where the ST-OPVs should better transmit is limited to the interval [400-700] nm. Under the bandwidth 400-700 nm, the performance of all the technologies is quite stable and lower than that observed from 700 nm on. Conversely, for module C the spectrum presents a quite flat shape for the whole range. Module A2 presents the highest transmittance (11.3%), followed by modules C (9%) and B (8.25% on average). On the other hand, the other module of technology A, A1, registers the lowest transmittance (6.7 %). This fact confirms the previously indicated necessity of improving repeatability in the manufacturing process to obtain more homogenous blends (Table 2).

Table 2. Visible luminous transmittance.

Tech.	τ_v'(%)
A1	6.7
A2	11.3
B1	8.3
B2	8.2
C	9.0

In general, for the measured spectra, small changes (regarding the spectral content transmitted) have been observed. Specifically for the photopic range, the shape of the spectral transmission between the initial and final measurements appears to be very

similar and the variations seem to be negligible. Table 3 includes the mean transmittances of all the modules A, B and C at the maximum relative luminous efficiency wavelength (555 nm). Concerning the transmittances, these are reported correcting the effect of the double glazing ($\bar{\tau}'$). Also the subscripts *i* and *f* denote the values measured at the beginning and at the end of the experiments, respectively. From the data, it can be pointed out that small variations in spectral transmittance have been registered over the monitoring and technology A (module A2) presents the highest transmittance.

Table 3. Spectral transmission values.

Tech.	$\bar{\tau}_i'_{555}$ (%)	$\bar{\tau}_f'_{555}$ (%)	|Difference| (%)
A1	3.8	5.3	1.5
A2	10.6	11.5	0.9
B1	6.3	5.5	0.8
B2	5.9	5.3	0.6
C	9.5	8.6	0.9

3.2 Electrical performance

3.2.1 Initial electrical characterization

In the present subsection, the electrical characteristic parameters of the modules at the beginning of the monitoring period are analyzed. The modules were placed on a two-axis tracker in order to determine their electrical parameters under stable solar irradiance conditions. Before the monitoring, modules of technologies B and C were stored in dark room environment about three months and modules of technology A were stored one week before the experimental measurements. In the case of the devices developed in the frame of the project (Technology A), two determinations have been included to discern between (1) the behavior after continuous sunlight exposure of ten minutes (in the following notation, this case is indicated as +10 min) and (2) the values measured at the initial time of the exposure (light soaking effects). In Table 4, the measurement conditions, including global irradiance (Glob), direct irradiance (Dir) and module temperature (*T*), along with a summary of the main electrical parameters determined (J_{sc}: short-circuit current density, V_{oc}: open-circuit potential, *FF*: fill factor and *PCE*: power conversion efficiency) are presented.

Table 4. Summary of the main electrical parameters and boundary conditions.

Technology	T (ºC)	Glob (W/m^2)	Dir (W/m^2)	J_{sc} (mA/cm^2)	V_{oc} (V)	FF (%)	PCE(%)
A1	23.22	810	682	0.37	8.75	54.67	2.18
A1(+10min)	24.54	834	705	0.38	8.75	54.82	2.19
A2	21.21	783	672	0.34	8.84	52.92	2.03
A2(+10min)	23.81	802	675	0.35	8.90	52.99	2.06
B1	29.08	1007	875	0.99	8.12	59.19	4.72
B2	29.11	1007	874	1.00	7.59	57.57	4.34
C	30.93	1012	889	0.19	39.28	44.32	3.27

Technology A has advantageous aspects regarding manufacturing and scalable efficiencies from cell to module level; however, as it can be noticed in Table 4, the PCE values achieved are half of the values of the commercial technology B. The main reason which leads to this lower efficiency is the fact that the organic tandem photogenerates half of the short circuit current density produced by B modules (it should be considered that the outdoor irradiance is 25% higher for technology B; thereby, by assuming a direct proportionality between irradiance and short circuit current, the values for A modules should be close to near 0.45 mA/cm^2 with the same irradiance). Nevertheless, the commercial technology C outperforms technology A due to the high potential achieved (since both short-circuit current density and fill factor are lower than for technologies A and B).

3.2.2 Stability analysis

Once the modules were initially characterized, they were installed in the façade-like outdoor experimental testing unit (described in section 2) in order to start the continuous daily monitoring for sunny days. During cloudy days, weekends and on holidays (2 weeks in August) the modules were kept under open-circuit conditions. Leaving the OPVs at open-circuit conditions is a circumstance that a building integrated system may often experience (either the regulator opens the circuit in a configuration with batteries or the inverter opens the circuit in a direct consumption scheme when there are no loads). In addition, the ISOS-O protocol considers open-circuit conditions for its levels 1 and 2 (Table 1). Fig. 7 plots the global irradiance evolution throughout the monitoring and it can be noticed the increase in the irradiance due to the seasonal-lower-solar-altitude effect approaching the winter solstice. On the other hand, it can be pointed out that the ISOS recommended selection of data in the interval [800-1000] W/m^2 for the degradation curves of normalized photocurrent and PCE [16] is hardly achievable for building façade integrated systems (only data from the end of October onwards are above 800 W/m^2).

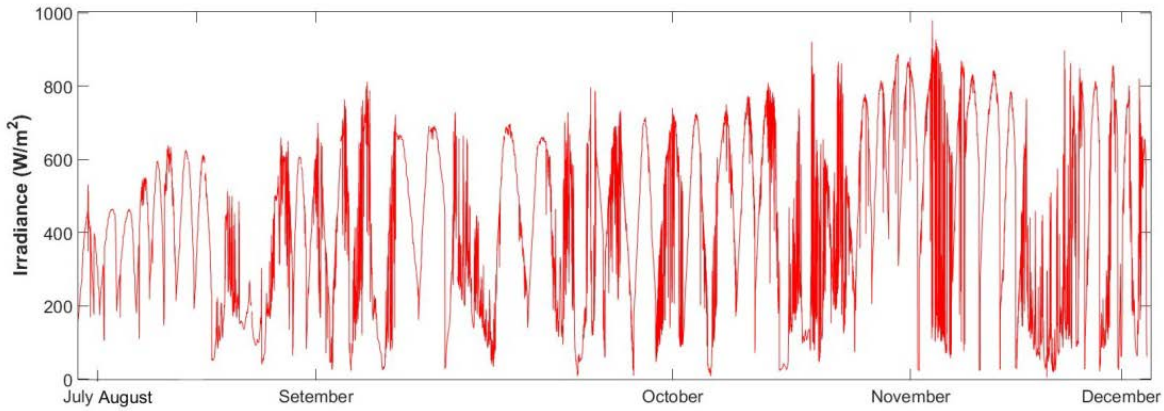

Figure 7. Global irradiance profile at the plane of the modules.

In the following graphs, some representative results which illustrate how the modules perform are presented.

The first result reported is the short circuit current sensitivity against solar irradiance. This indicates the photogeneration proportionality with the solar radiation which should reflect a linear tendency. All the modules presented the expected performance, exhibiting a very good fit with correlation coefficients above 0.9. Figure 8 illustrates the average short circuit currents for each type of technology.

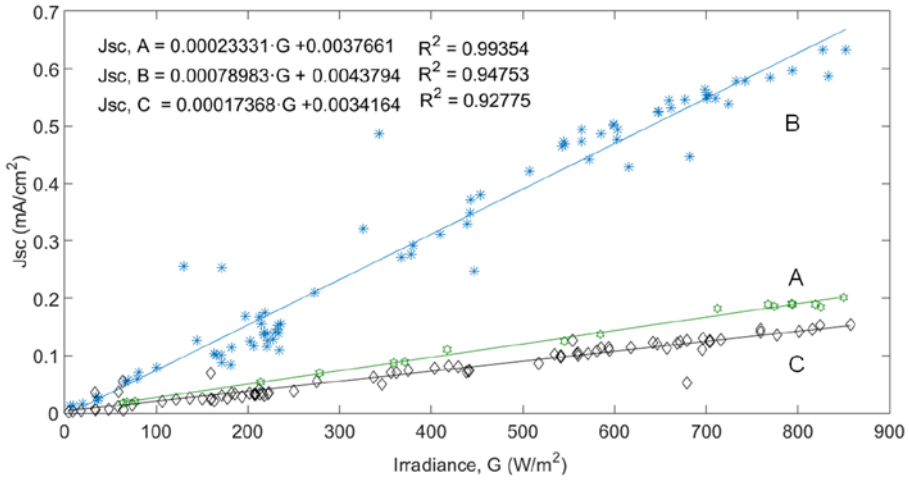

Figure 8. The average short circuit currents for each type of technology (A, B and C) vs. irradiance.

The correlation equations (Fig. 8) show the mean short circuit current density of the modules for an irradiance range registered during the monitoring period (slope) which is representative of the average spectral response that should be expected for a real ST-OPV for building integration applications. The slope value has to be corrected by a factor of 10^4 to homogenize the surface units between irradiance and short-circuit current. Therefore, the modules A and C present average spectral response values of 2.33 $mA \cdot W^{-1}$ and 1.74 $mA \cdot W^{-1}$ (respectively) whilst B modules achieve a mean value

more than three times higher than those of modules A and C (7.90 $mA \cdot W^{-1}$).

On the other hand, in Fig. 9 the maximum power output for the modules A is illustrated. Fig. 9(a) refers to the module A1 and Fig. 9(b) refers to the module A2. From Fig. 9 it can be seen that both modules present similar tendency, decreasing the power output quite sharply at the first half of the monitoring and stabilizing the reduction at the second half. This remark is supported by the efficiency evolution which is depicted in Fig. 10.

a) b)

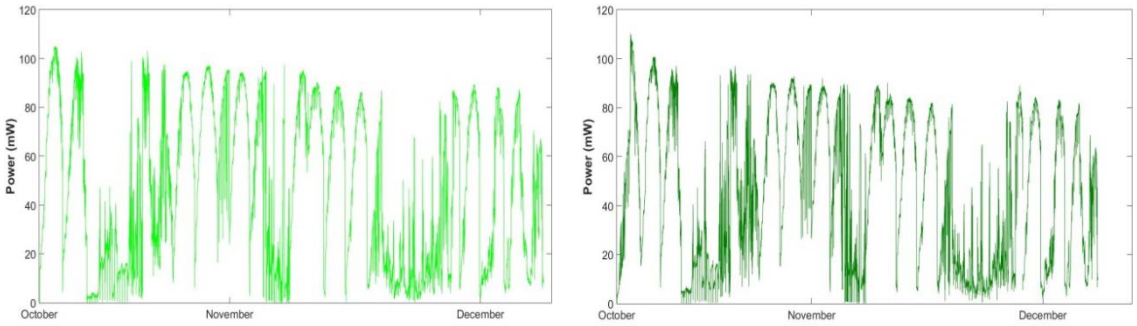

Figure 9. The maximum power output for modules A1 (a) and A2 (b).

Fig. 10(a) demonstrates the efficiency evolution observed for module A2 (for module A1 analogous results were obtained). The efficiency values plotted, measured with the I-V tracer, were previously filtered eliminating all with irradiance values lower than 450 W/m^2 in order to facilitate comprehension and due to the fact that those points registered more noise. A quadratic polynomial fitting is applied denoting that, as it has been indicated above, the efficiency reduction considerably decelerates for the second half of the monitoring. It should be noted that this effect was expected by the SOLPROCEL-project partners.

For technology B, the efficiency reduction over the time period is more linear than in the case of A modules. In Fig. 10(b), the efficiency evolution of module B1 is illustrated. The points included, as in the case of Fig. 10(a), were measured by means of the I-V tracer and a post-processing was applied for selecting values with incident irradiances equal or higher than 450 W/m^2.

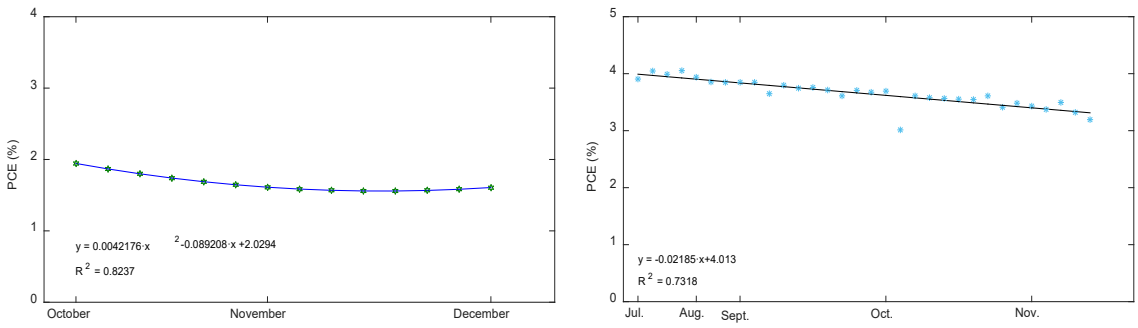

a) b)

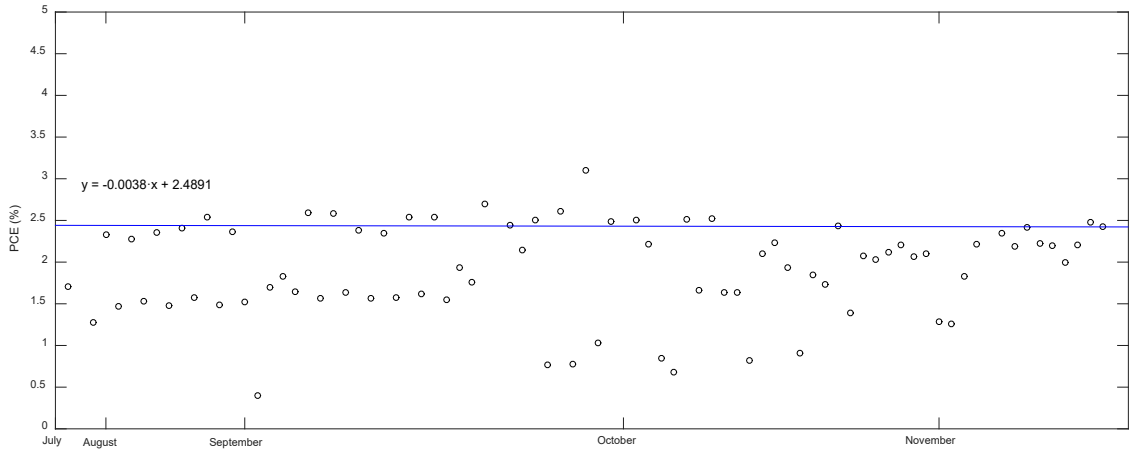

c)

Figure 10. The efficiency evolution for modules A2 (a),B1 (b) and C (c).

Finally, Fig. 10 (c) shows the efficiency evolution for module C, but in this case all the measurements conducted with the I-V tracer are included and the fitting is applied only to those obtained with irradiances equal or higher than 450 W/m^2. It should be noted that technology C is the one achieving the lower efficiency reduction with an almost flat tendency. The correlation coefficient is not included in order to avoid confusion since the cloud of points is wider and the fitting is conducted regarding to the above mentioned irradiance restriction.

In Table 5, the electrical efficiencies at the beginning (indicated with *i*) and at the end (indicated with *f*) of the experimental campaign are summarized. From Table 5, it can be seen that the highest efficiency reduction is presented by technology A, although this reduction shows a much lower rate of reduction at the second half of the monitoring. In addition, the calculated differences are not far from those reported for modules of technology B. Module C is the one achieving the lowest efficiency reduction.

Table 5. Summary of the electrical efficiencies.

	A1	**A2**	**B1**	**B2**	**C**
$\boldsymbol{PCE_i}$ **(%)**	2.083	1.944	3.991	3.722	2.569
$\boldsymbol{PCE_f}$ **(%)**	1.712	1.607	3.396	3.289	2.477
Relative difference (%)	-17.81	-17.33	-14.90	-11.63	-3.581

In the next paragraphs, the I-V curve measurements are expressed normalized in order to compare the differential dynamics of the three technologies on a common basis. For this purpose, the results of the short-circuit current and maximum power have been linearly adjusted to the standard irradiance level of 1000 W/m^2. The parameters have been normalized with respect to the initial values measured. Irradiance values range

from 520 W/m^2 to 825 W/m^2 and temperatures are in the interval [25-55] ºC. The hottest temperatures correspond to the summer period and the coldest ones to the end of November-beginning of December.

Figure 11 demonstrates the stability curves of V_{oc}, J_{sc}, *FF* and *PCE*. In the case of the open-circuit potential, it remains quite stable for the technologies A and C. However, for modules B the potential increases slightly. This performance is attributed to the fact that technology B is more sensitive to the temperature than modules A and C. In this way, since the temperature decreases during the experiment the open-circuit potential gradually increases. FF values in all the modules present the same similar dynamic, showing almost no change during the monitoring. On the contrary, short-circuit current and PCE behave similarly, showing three different decay tendencies. The first one regards to the module C, which even presenting more variability in the point cloud, is the most stable (as it is indicated in Table 5) with almost no decrease in the PCE. The second one corresponds to technology B, which decreases slightly more than technology C. Concerning the PCE, a degradation of about 10-15 % is observed over the whole period. Finally, the third one is associated to technology A, which at around 500 hours decays 20% of the PCE. Nonetheless, it seems that A modules experience a certain recovery afterwards, finishing the experiment with a PCE decrease of about 18%.

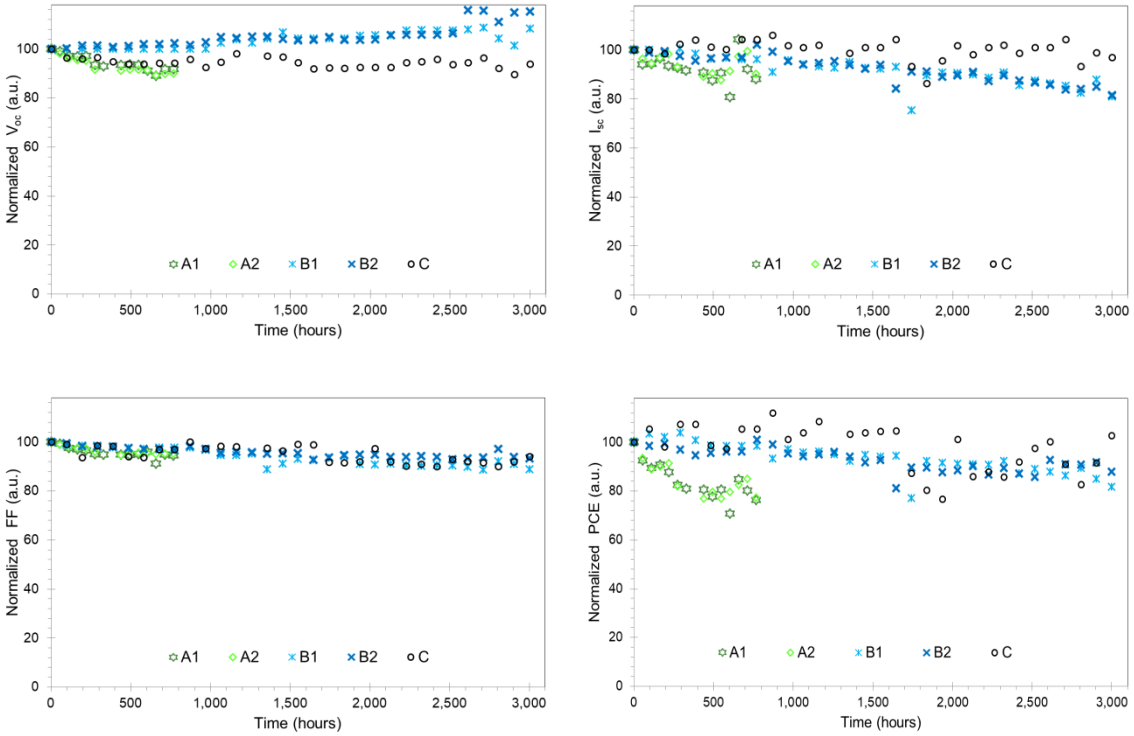

Figure 11. Stability curves of short-circuit current, open-circuit potential, fill factor and power conversion efficiency of the 5 OPV modules that have been studied. The parameters are normalized to the initial values registered.

4. Comparison with other OPV stability studies

The comparison between ST-OPVs modules is an important aspect to frame and identify the state-of -the-art evolution of a promising but highly changeable technology. This comparison becomes even more essential when one of the main applications of such technology is for building integration. In that case, the customers and installers need to know contrasted results in order to gain confidence in this type of devices. In this regard, it should be highlighted again the necessity of conducting more studies under real outdoor operating condition to demonstrate how ST-OPVs perform.

4.1 Light transmission

In the frame of light transmittance, to the authors' knowledge there is no study analyzing the outdoors stability of ST-OPVs in terms of optical parameters. In addition, the ISOS protocol does not refer to this type of characterization [16]. In spite of this fact, some references concerning the transparency tendency of OPVs have been cited. It is indicated that AVT values equal or higher than 25% should be achieved for ST-OPVs applications in windows [20]. In this line, representative results report quite high AVT values (> 50%) and acceptable PCEs over 2% [21-23]. However, efficiency and transmittance performances are confronted since the higher the transmittance the lower the PCE. As a compromise between both parameters a combination of 31% AVT and 10.2% PCE has been recently presented by Jia et al. (2018) [18]. It should be noted that the values reported in the literature are at laboratory scale and at cell level (module PCEs and AVT could be expected to be lower). This makes particularly difficult the comparison with the present study. Also, the results described in section 3.1 refer to the direct transmittance, but in the values found in the literature is difficult to discern if direct or hemispherical transmittances are indicated, and the differences between them may be significant. Moreover, even if the most generalized AVT interval is [370-740] nm depending on the study, the AVT bandwidth is differently defined, for instance in reference [24] the range considered is from 380 nm to 780 nm whilst in study [25] the range includes wavelengths from 400 nm to 700 nm. Based on this argument, it can be seen the necessity of following uniform criteria for the definition of the transparency, for instance the aforementioned EN 410:2011 [19] could be adopted.

4.2 Electrical performance

As it has been indicated in the introduction, in the literature very few studies about the stability of ST-OPVs [11] can be found, and there are no investigations regarding outdoor test conditions. A stability laboratory study following the ISOS-L-1 protocol [16] was conducted for a ST-OPV cell utilizing a transparent electrode made of two different transparent PEDOT:PSS Clevios® PH1000 and a combination of PH1000 with WO_x. The 8-hours stability tests revealed that the device without WO_x exhibited almost

77.91% degradation of PCE while the device with the introduction of WO_x only suffered a decay of 46.94% from the initial PCE [26]. Romero et al. [27] studied the stability, according to ISOS-L-3 [16], of five different bulk heterojunction configurations made of the copolymer based on PTB7 donor blended with $PC_{71}BM$ acceptor. They pointed out that such types of ST-OPVs (when properly isolated from external agents) show potential to become stable devices. Among ST cells, inverted architectures with isolation and 5-layer deposition demonstrated close to 8 times the lifetime of the same inverted cells without the isolation stack and 400 times longer lifetime than standard ST-OPVs. The time at which the efficiency is 80% of the initial value was found to be at 250 hours for the inverted ST-OPV cell and 1900 hours for the optimum one (inverted with multilayer isolation) [27]. Voroshazi *et al*. [28] conducted light stability tests of ITO-free ST-OPV devices. The transparent electrodes tested, based on MoO_3/Ag/TiO_2, excluding UV light, degraded similarly to a cell with ITO electrode, demonstrating the feasibility of the proposed transparent electrode. The tests were developed in agreement with ISOS-L-2 protocol, and the devices lost 20% of their initial PCE in less than 50 hours. Finally, Yin et al. [29], studied the stability, according to ISOS-D-1 protocol, of a ST-OPV cell using a ZnMgO-modified cathode combined with a thin MoO_3/Ag anode. After 2 months of storage, ST-OPVs demonstrated long lifetime stability retaining over 90% of the initial PCE. Also, good stability was observed after 2 years of storage, maintaining a PCE value of 7.02% and stablishing the high efficiency record for long lifetime ST-OPVs.

It can be appreciated that the described studies regard ST-OPV cells and not modules and, in all the cases, the ISOS protocol is followed either at the laboratory under simulated sunlight or under dark storage. From the results indicated, a wide variation between decay time-periods, ranging from few hours to two years, is observed depending on the experiments that were carried out. In addition, all the cited references present potentiality from several points of view: low-cost transparent electrodes, better isolation structures, etc. The investigations presented are promising, however, they are not mature enough and need more reliability in order to be available on the market.

In the present study, the values obtained are difficult to be compared with those mentioned above since degradations obtained are lower, in general, but the frame is different since in the present work outdoor characterization has been performed.

5. Conclusions

In the present study, a comparison between three different ST-OPV technologies (the technology developed in the frame of the SOLPROCEL project and two commercial ones) in order to analyze and compare their efficiency, transparency and stability in an outdoor building-façade environment, has been conducted.

Regarding visible transmittance, a lack of homogeneity in the presentation of results,

with the different bandwidths utilized, has been detected. Since one of the potential applications of ST-OPVs is building integration, the adoption of a common protocol for determining transmittances following the European Standard EN 410:2011: "Glass in building- Determination of luminous and solar characteristics of glazing" is suggested.

Measured transmittances over the experimental campaign, for all the photovoltaic modules that have been studied, presented small variations of less than 2% (at 555 nm) between the beginning and the end of the experiments. Technology A showed higher transmittances than the commercial technologies B and C. More specifically, the module A2 presented the highest transmittance (11.3%), followed by modules C (9%) and B (8.25% on average). On the other hand, the other module of technology A (module A1) showed the lowest transmittance (6.7 %).

Concerning the determination of the uniformity of the transmittance along module surface, 5 different points (distributed along module surface) have been measured. The results indicated that the commercially available modules present slightly less dispersion between the different parts of the module than spectra measured for technology A. Between technologies B and C, it can be noted that technology C presents the most uniform behavior (almost overlapping transmittances for all the sampling points).

An important gap regarding stability studies for ST-OPVs, especially in terms of analyzing their performance under outdoor conditions, has been identified. This may be attributed to the fact that this technology is still emerging and it is difficult to scale it up to module level adequate for realistic pre-market studies. In the frame of outdoor stability testing procedures for building integrated OPV modules, there is no regulation to establish the conditions of the experiments. The closest approach is the International Summit on OPV Stability (ISOS) procedure, with its outdoor protocol. Nevertheless, this should be adapted to the specific conditions of building integrated photovoltaics since some requirements and recommendations do not match well for this specific application: inclination of the module, irradiances achieved, etc.

Form the initial electrical characterization, it can be observed that the PCE values obtained by technology A are half of the values achieved by the commercial technology B. The main factor which leads to this lower PCE is the fact that the organic blend generates less than half of the short-circuit current density of the B modules. The commercial technology C outperforms technology A because of the high potential achieved since both the short-circuit current density and the fill factor are lower than for technologies A and B. More specifically, during the monitored period, the mean spectral responses achieved for technologies A and C are 2.33 $mA \cdot W^{-1}$ and 1.74 $mA \cdot W^{-1}$ respectively whilst B modules achieve a mean value more than three times higher.

With respect to stability, module C is the most stable one with almost no decrease in the PCE (3.6%). PCE of technology B decays slightly more than for technology C,

experiencing a PCE degradation of about 10-15 % over the whole period. Finally, technology A presents a reduction of 20% in PCE in 500 hours. Nonetheless, it seems that A modules experience certain recovery afterwards, finishing the experiment with a PCE decrease of about 18%.

A comparison between the present findings and other ST-OPVs studies indicates: 1) on the one hand, the necessity of homogenizing results to ease comparisons and 2) on the other hand, a big variability between stability results is denoted, with some modules important PCE decays in few hours and others performing well after 2 year period.

Acknowledgments: The authors would like to acknowledge financial support from European Commission 7th Framework Programme (FP7-NMP-2013-SMALL-7).

6. References

[1] J. Yu, Y. Zheng, J. Huang, Towards high performance organic photovoltaic cells: A review of recent development in organic photovoltaics, Polymers 6(9) (2014) 2473–2509.

[2] Hengevoss, D., Baumgartner, C., Nisato, G. & Hugi, C. 2016, "Life Cycle Assessment and eco-efficiency of prospective, flexible, tandem organic photovoltaic module", Solar Energy, vol. 137, pp. 317-327.

[3] N. Bristow, J. Kettle, Outdoor performance of organic photovoltaics: Diurnal analysis, dependence on temperature, irradiance, and degradation, J. Renew. Sustain. Energy 7(1) (2015) .

[4] Zhao, W., Li, S., Yao, H., Zhang, S., Zhang, Y., Yang, B. & Hou, J. 2017, "Molecular Optimization Enables over 13% Efficiency in Organic Solar Cells", Journal of the American Chemical Society, vol. 139, no. 21, pp. 7148-7151.

[5] Y. Wang, W. Wei, X. Liu, Y. Gu, Research progress on polymer heterojunction solar cells, Solar Energy Mat. Solar Cell. 98 (2012) 129-145.

[6] Z. Ding, J. Kettle, M. Horie, S.W. Chang, G.C. Smith, A.I. Shames, et al. Efficient solar cells are more stable: The impact of polymer molecular weight on performance of organic photovoltaics, J. Mater. Chem. A 4 (2016)7274-7280.

[7] R. Hansson, C. Lindqvist, L.K.E. Ericsson, A. Opitz, E. Wang, E. Moons, Photo-degradation in air of the active layer components in a thiophene-quinoxaline copolymer: fullerene solar cell, Phys. Chem. Chem. Phys. 18 (2016) 11132-11138.

[8] N. Grossiord, J.M. Kroon, R. Andriessen, P.W.M. Blom, Degradation mechanisms in organic photovoltaic devices, Org. Electronics 13(3) (2012) 432-456.

[9] Mulligan C.J., Wilson M., Bryant G.,Vaughan B., Zhou X., Belcher W.J., Dastoor P.C., A projection of commercial-scale organic photovoltaic module costs, Solar Energy Mater. Solar Cell. 120 (Part A) (2014) 9-17.

[10] B.v. der Wiel, H.J. Egelhaaf, H. Issa, M. Roos, N. Henze, Market readiness of organic photovoltaics for building integration, Materials Research Society Symposium Proceedings. Volume 1639, 2014 2013 MRS Fall Meeting; Boston, MA; United States; 1 December 2013 through 6 December 2013.

[11] Tai, Q. & Yan, F. 2017, "Emerging Semitransparent Solar Cells: Materials and Device Design", Advanced Materials, vol. 29, no. 34.

[12] F. Yan, J. Noble, J. Peltola, S. Wicks, S. Balasubramanian, Semitransparent OPV modules pass environmental chamber test requirements, Solar Energy Mater. Solar Cell. 114 (2013) 214-218.

[13] L. Lucera, F. Machui, H.D. Schmidt, T. Ahmad, P. Kubis, S. Strohm, et al., Printed semi-transparent large area organic photovoltaic modules with power conversion efficiencies of close to 5 %, Organ. Electronics 45 (2017) 209-214.
[14] Gevorgyan, S.A., Madsen, M.V., Dam, H.F., Jørgensen, M., Fell, C.J., Anderson, K.F., Duck, B.C., et al. 2013, "Interlaboratory outdoor stability studies of flexible roll-to-roll coated organic photovoltaic modules: Stability over 10,000 h", Solar Energy Materials and Solar Cells, vol. 116, pp. 187-196.
[15] Solprocel (2016),www.solprocel.eu
[16] Reese, M.O., Gevorgyan, S.A., Jørgensen, M., Bundgaard, E., Kurtz, S.R., Ginley, et al. 2011, "Consensus stability testing protocols for organic photovoltaic materials and devices", Solar Energy Materials and Solar Cells, vol. 95, no. 5, pp. 1253-1267.
[17] IEC 60904, Photovoltaic devices – Part 1: Measurement of photovoltaic current-voltage characteristics. Ed. 2006.
[18] Jia, B., Dai, S., Ke, Z., Yan, C., Ma, W. & Zhan, X. 2018, "Breaking 10% Efficiency in Semitransparent Solar Cells with Fused-Undecacyclic Electron Acceptor", Chemistry of Materials, vol. 30, no. 1, pp. 239-245.
[19] European Standards EN 410:2011, “Glass in building — Determination of luminous and solar characteristics of glazing”, Ed. 2011.
[20] Chen K-S, Salinas J-F, Yip H-L, et al. Semi-transparent polymer solar cells with 6% PCE, 25% average visible transmittance and a color rendering index close to 100 for power generating window applications. Energy Environ Sci. 2012;5:9551–9557.
[21] Chen C-C, Dou L, Zhu R, et al. Visibly transparent polymer solar cells produced by solution processing. ACS Nano. 2012;6:7185–7190.
[22] Chen C-C, Dou L, Gao J, et al. High-performance semi-transparent polymer solar cells possessing tandem structures. Energy Environ Sci. 2013;6:2714–2720.
[23] Xiao X, Lee K, Forrest SR. Inverted, semitransparent small molecule photovoltaic cells. Appl Phys Lett. 2015;107:033901.
[24] Yu, W., Jia, X., Long, Y., Shen, L., Liu, Y., Guo, W. & Ruan, S. 2015, "Highly efficient semitransparent polymer solar cells with color rendering index approaching 100 using one-dimensional photonic crystal", ACS Applied Materials and Interfaces, vol. 7, no. 18, pp. 9920-9928.
[25] Huan, F., Yip, H-L, Cao, Y. 2015, “ Polymer Photovoltaics: Materials, Physics, and Device Engineering”, Polymer Chemistry Series, The Royal Society of Chemistry.
[26] Kim, H.P., Lee, H.J., Mohd Yusoff, A.R.B. & Jang, J. 2013, "Semi-transparent organic inverted photovoltaic cells with solution processed top electrode", Solar Energy Materials and Solar Cells, vol. 108, pp. 38-43.
[27] Romero-Gomez, P., Betancur, R., Martinez-Otero, A., Elias, X., Mariano, M., Romero, B., Arredondo, B., Vergaz, R. & Martorell, J. 2015, "Enhanced stability in semi-transparent PTB7/PC71BM photovoltaic cells", Solar Energy Materials and Solar Cells, vol. 137, pp. 44-49.
[28] Voroshazi, E., Yaala, M.B., Uytterhoeven, G., Tait, J.G., Andriessen, R.H.A.J.M., Galagan, Y. & Cheyns, D. 2015, "Light stability of ITO-free semi-transparent and opaque organic photovoltaic devices", 2015 IEEE 42nd Photovoltaic Specialist Conference, PVSC 2015.
[29] Yin, Z., Wei, J., Chen, S.-., Cai, D., Ma, Y., Wang, M. & Zheng, Q. 2017, "Long lifetime stable and efficient semitransparent organic solar cells using a ZnMgO-modified cathode combined with a thin MoO3/Ag anode", Journal of Materials Chemistry A, vol. 5, no. 8, pp. 3888-3899.

Capítulo 5. Eficiencia energética y lumínica de envolventes de ETFE/OPV

A. Moreno, D. Chemisana, R. Vaillon, A. Riverola y A. Solans. Energy and Luminous Performance Investigation of an OPV/ETFE Glazing Element for Building Integration, Energies, artículo aceptado y publicado

Energy and Luminous Performance Investigation of an OPV/ETFE Glazing Element for Building Integration

A. Moreno[1], D. Chemisana[1,*], R. Vaillon[2], A. Riverola[1], A. Solans[1]

[1]Applied Physics Section of the Environmental Science Dept., University of Lleida, 25001 Lleida, Spain

[2]IES, Univ. Montpellier, CNRS, F-34000, Montpellier, France

Abstract

The combination of architectural membranes such as Ethylene tetrafluoroethylene (ETFE) foils and organic photovoltaic (OPV) cells offers a wide range of possibilities for building integration applications. This is due to their flexibility, free-shape, variable color and semitransparency, light weight, cost-effectivity and low environmental impact. In addition, electrical generation is provided. Four configurations of ETFE foils designed to be integrated onto a south façade glazing element were studied for two representative European locations with different climatic conditions: Barcelona and Paris. These configurations comprise a reference one based on a double ETFE foil with a 10 mm air gap in between, and the other three incorporate on the inner ETFE foil either an OPV cells covering 50% or 100% of its surface or a shading pattern printed on it covering 50% of its surface. Results show that, in terms of energy, the configuration with higher OPV coverage area is the one achieving the lowest net energy consumption in both locations. However, when looking at the illumination comfort this option results in insufficient illumination levels. Therefore, a tradeoff strategy balancing energy performance and illumination comfort conditions is necessary. Based on that, the best solution found for both cities is the configuration integrating OPV cells covering 50% of the glazing area and for a window to wall ratio of 0.45.

Keywords: Ethylene tetrafluoroethylene (ETFE), Organic photovoltaics (OPV), Daylighting, Thermal performance, Energetic simulation, Building integrated photovoltaics (BIPV).

1. Introduction

It is widely known that the building sector is the largest energy consumer in the world. In the European Union (EU), buildings are responsible for approximately 40% of energy consumption and 36% of carbon dioxide emissions. These figures are explained by the simple fact that 75% of the buildings in Europe are energy inefficient [1]. In

addition, energy demand in buildings keeps on rising because of an improved access to energy in developing countries, a more intense use of energy-consuming devices, and a rapid growth in floor area in buildings (around 3% per year) [2].

With the aim of alleviating and then reversing this trend, the European Union defined a series of policies. The last Directive of the European Parliament is the 2018/844, which amends Directive 2010/31/EU on the energy performance of buildings and Directive 2012/27/EU on energy efficiency. This new Directive extends the so-called "20-20-20" goals (20% increase in energy efficiency, 20% reduction of CO2 emissions from 1990 levels, and 20% of energy production from renewables) to be reached by 2020, to more demanding ones to be fulfilled by 2030. The new targets set that energy efficiency should be improved by 32.5%, greenhouse gas emissions should be decreased by 40%, and 32% of energy production should be from renewables [3].

In order to meet these requirements for buildings, a smart solution is to integrate photovoltaic systems into buildings. Using a combination of insulating and glazing elements for shading control, building integrated photovoltaics (BIPV) not only provides electrical power, but also fulfills an architectural function. With the functions that add to electrical power generation, BIPV is a promising and strategic technology which is able to address simultaneously the requirements of higher renewable energy share and better energy efficiency. In recent years, different approaches have been used for developing BIPV. The most common approach is to use glass-based structures [4]. Nonetheless, a growing percentage of architectural designs makes use of lighter transparent structures which offer a larger flexibility in shapes and functionalities in comparison to the glass-based structures [5]. Polymeric foils and membranes have emerged as a potential candidate to properly cover those characteristics of flexibility and lightness. Among the available polymer materials, ethylene tetrafluoroethylene (ETFE) is one of the most accepted since it possesses the highly adequate characteristics for being integrated into buildings: light, flexible, transparent, self-cleaning, mechanically adequate, stable, thermally insulating and environmentally friendly [6]. In particular, several articles point out that the environmental impact of ETFE is less than that of glass [6,7].

Concerning the photovoltaic technologies that are best suited for integration into buildings, organic photovoltaic (OPV) cells are attractive thanks to several characteristics: light, semitransparent, free-form, flexible, cost-effective, performant under low-light and diffuse light illuminations, and one of the most eco-friendly photovoltaic (PV) technology [8,9]. A drawback of OPV is degradation of performances over time, which seems to be still an issue to be fully solved. However, the commercial OPV cells manufactured by Heliatek are sold with a 5-year product warranty and a 20-year performance warranty, with an efficiency of 6% for 30% transparency cells [10].

Based on the positive features described above for both ETFE and OPV, combining for BIPV seems to be a logical step forward. In recent years, a few articles report on ETFE foils combined with thin film PV modules, mostly made with amorphous silicon [11,12]. Similarly to OPV, PV cells made of amorphous silicon have low efficiency and stability issues. However, amorphous silicon PV technology suffers from significantly higher greenhouse gas emissions and energy payback times than OPV [9,13,14]. Nevertheless, since the technologies involved are relatively recent, very limited research investigating configurations combining ETFE with OPV for integration into buildings is reported in the literature. In 2018, a pioneering work analyzed the feasibility of printing OPV on ETFE [15]. Another article analyzed the mechanical robustness linked to the electrical performance of an OPV structure printed on Polyethylene terephthalate (PET, the most conventional substrate) and ETFE [16].

The study focused on analyzing the mechanical-electrical effects on the printed electrode layers made of Ag and Ag/poly(3,4-ethylenedioxythiophene) -PEDOT-, depending on whether they are printed on PET or ETFE. The mechanical analysis is crucial since most of the ETFE configurations are built as multilayer inflated cushions. The results revealed that ETFE-printed electrodes are less brittle and sensitive to tensile strain and that the use of Ag/PEDOT layering can double the tensile strain threshold. Finally, it was stated that further research is needed to investigate the properties of direct-printed full OPV on ETFE. In spite of the fact that more research is needed, in a previous publication the authors indicate that although OPV can be integrated in ETFE membranes either by lamination or mechanical fixing, research on OPV directly printed onto architectural membranes such as ETFE is imperative since this configuration is the one achieving the most promising market prospect due to: high through output, low production cost and high applicability in modern architectural context [17]. In the same direction, Hu et al. [18] assessed the electrical-thermal-mechanical properties of OPV/ETFE foils. They observed that under normal operating conditions electrical properties are relatively not affected by thermal and mechanical changes. However, a direct relation between mechanical and thermal properties (stress curves at different temperatures) is observed. It should be noted that specimens analyzed are mechanically fixed onto ETFE and not printed. Menéndez et al. [4] designed, fabricated and tested a novel planar multifunctional ETFE module comprising LEDs, OPVs and flexible electronics. OPV cells, manufactured by OPVIUS GmbH, are integrated into the ETFE foils by lamination. Performance was monitored for different pressure and temperature conditions. Based on the results, an optimized lamination process was stated to ensure proper performance. Almost one year outdoor monitoring was conducted with positive feedback, that lead to a step forward for developing the final demonstrator (1.5 m by 6 m façade screen).

It can be noticed that there are a limited number of studies describing performances of OPV combined with ETFE. Among them, only one study conducts experiments outdoors but in a free-rack module. Therefore, bearing in mind that OPV/ETFE is mainly developed for building integration applications, more research is needed for analyzing the behavior of the OPV/ETFE glazing in a building integrated environment. In order to fill in this gap, the present research deals with the full modelling of a planar OPV/ETFE system integrated in a south façade (northern hemisphere), determining the effect on the illumination of the interior space, the thermal demands and electrical power generation. These performances are analyzed for different configurations defined as a function of the percentage of OPV cells in the glazing and the coverage area of the glazing in the façade. As a result, the paper aims at demonstrating the suitability of such a configuration for building integration.

The contents of the paper are organized as follows. In section 2 the methods utilized for the different characterizations are described. Spectral transmittance and reflectance values were measured in the laboratory whilst OPVs electrical performance was monitored outdoors. Section 3 explains the model and the main parameters and assumptions involved. The model, fed with the experimental results, is utilized to simulate the performance of the OPV/ETFE system integrated in an office building and to conduct a sensitivity analysis. Once the model is introduced, the main results are discussed in section 4 and the main conclusions of the study are provided.

2 Characterization of ETFE foils and OPV cells

Three different ETFE foils were analyzed in this study: two ETFE clear foils with different thicknesses (150 and 250 μm) and the same 250 μm-thick ETFE clear foil but with silver prints resulting in 28% opacity. Printing allows reducing light transmission and provides an effective shading element.

Commercially available OPV cells were selected for this study. They are considered to be representative of the wide variety of organic technologies.

2.1 Optical properties

The spectral transmittance and reflectance of the ETFE foils and the OPV cells were determined from 0.35 to 50 μm with a Fourier-transform spectrometer Bruker Optics - IFS 66v/S equipped with an integrating sphere. This spectral range covers both the solar range and almost the full range of thermal emission (>96% for 25 ºC) in the mid-infrared for common operational temperatures. Using Kirchhoff's law, the absorptance can be derived from the experimental measurements as follows:

$$\tau + \rho + \alpha = 1 \quad (1)$$

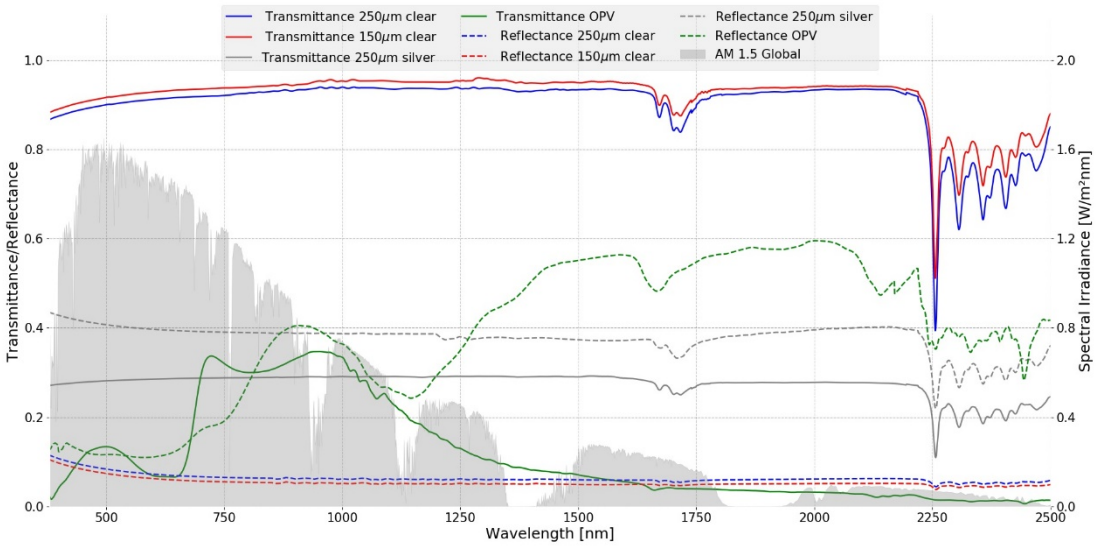

Figure 1. Experimental transmittance and reflectance of the three ETFE foils and the OPV cells

The ETFE clear foils behave similarly regardless of their thickness with high transmittances over the solar range (~90%) whereas the printed ETFE reflects 30% of the incoming solar light and transmits only ~40% of it. In the IR, ETFE foils start to absorb more with some transmission peaks that can reach values higher than 50%.

2.2 Luminous and solar characteristics

The methods to determine luminous and solar characteristics of glazing in buildings from spectral reflectance and transmittance measurements are detailed in EN 410:2011 [19]. These properties are taken as inputs to evaluate performances in terms of lighting conditions, and heating and cooling demands. In addition, a comparison between different foils can be performed based on their performances.

The main parameters derived from the spectral measurements are the solar transmittance (τ_e), the solar reflectance (ρ_e), the visible transmittance (τ_v), the visible reflectance (ρ_v), the transmission factor of solar energy (g) and the shading coefficient (SC). Other parameters that can be obtained from experimental measurements are the correlated color temperature (CCT) that is defined as the absolute temperature of a blackbody whose chromaticity most nearly resembles that of the light source. This parameter is key for interior spaces since it is related to human perception. It was calculated using McCamy's equation [20]:

$$CCT = 449\ n^3 + 3525\ n^2 + 6823.3\ n + 5520.33 \quad (2)$$

where n is calculated using the x, y coordinates from CIE 1931 [12] as:

$$n = \frac{(x - 0.3320)}{(0.1858 - y)} \tag{3}$$

Another useful parameter is the color rendering index (CRI), also known as general index of color reproduction (Ra) (UNE-EN 410). A summary of the values obtained for all the studied foils is provided in Table 1.

Table 1. Summary of luminous and solar characteristics

	τ_e	ρ_e	τ_v	ρ_v	**g**	**SC**	**CRI** [%]	**CCT** [K]
ETFE 250µm	0.910	0.074	0.907	0.77	0.917	1.051	99.09	6377.4
ETFE 150µm	0.926	0.064	0.923	0.067	0.932	1.068	99.09	6377.4
ETFE-Silver 250µm	0.283	0.396	0.284	0.401	0.350	0.437	99.09	6377.4
OPV	0.165	0.232	0.100	0.114	0.296	0.405	76.36	9083.9

2.3 Thermal characteristics

In order to assess the performances of the ETFE window integrated into a building, its thermal properties have to be determined. The level of insulation is given by the thermal transmittance (U-value) which is obtained by computing the heat flow through the element for a known temperature difference between its two faces.

In the EU and associated countries, the procedure to calculate the U-value is reported in the UNE-EN 673 [22]. The algorithm was substantially simplified compared to the ISO 15099 [23] algorithm, which is used in North America to predict the thermal and optical performances of windows. The thermal properties of glazing systems are calculated based on a comprehensive heat transfer model, analyzing conductive, convective and radiative heat transfer.

The thermal conductivity, the specific heat and the density of ETFE were obtained from the manufacturer data sheet (Table 2) and allowed to compute conductive and convective calculations [24]:

Table 2. Summary of thermal characteristics

	Value	**Units**
$\lambda_{ETFE\ 20°C}$	0.24	W/mK
$Cp_{ETFE\ 20°C}$	1172	J/Kg·K
$\rho_{ETFE\ 20°C}$	1700	Kg/m^3

The normal emissivity (ε_n) is crucial to calculate the radiative heat flux and therefore the U-value. Antretter et al. evaluated the heat flux through an EFTE cushion and concluded that 30% of it was due to convection and 70% due to radiation, thus stressing the importance of an appropriate radiative modeling [25]. The normal emissivity can be calculated following the procedure reported in the UNE-EN 12898 [26]. This standard uses as an input the optical measurements previously provided. In the next table (Table 3), the resulting values are provided:

Table 3. Summary of normal emissivity

	ε_n
ETFE 250µm	0.894
ETFE 150µm	0.897
ETFE-Silver 250µm	0.774
OPV	0.712

2.4 OPV cells characterization

The OPV power density output was characterized over a period of five months (July-November) under real conditions. The OPVs were placed vertically on a south-oriented testing unit at 1.5 m height to avoid albedo effects. The irradiance was measured using a pyranometer (CMP6) located at the same position as the OPVs. Temperatures were monitored using T-type thermocouples attached at the rear part of the OPV cells, which were connected to a Maximum Power Point Tracker (MPPT). Figure 2 shows the power density as a function of irradiance for the entire time period. The average, minimum and maximum module back temperatures together with the standard deviation can be seen in Table 4.

The power density dependence with temperature is very week. Therefore, a linear regression relating power and irradiance obtained from the experimental campaign was applied while neglecting the temperature dependence.

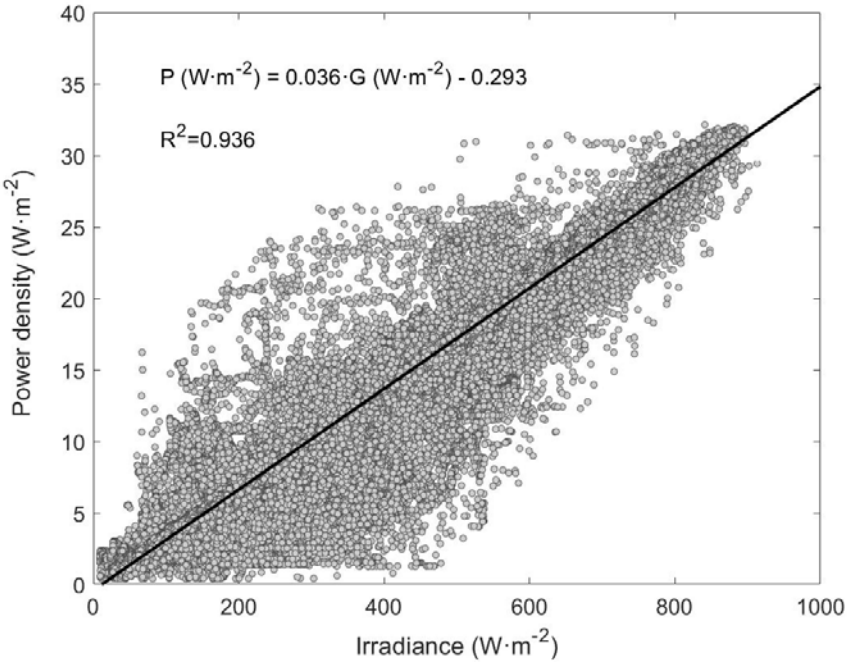

Figure 2. Experimental OPV power density as a function of irradiance

Table 4. Summary of thermal characteristics

T_{mean} (°C)	Standard deviation (°C)	T_{min} (°C)	T_{max} (°C)
31.36	8.79	4.8	48.9

3. Model description

3.1 Studied configurations

ETFE foils may be configured in different ways depending on the application in which they are expected to be used and its associated requirements (illumination control, high thermal insulation, etc.). Four different configurations were analyzed in this study, all of them composed of two flat films and an intermediate layer of air (10 mm). Figure 3 shows the selected configurations: a) a panel composed of two clear 250µm-thick ETFE layers, b) a panel comprised of a clear 250 µm-thick EFTE layer and OPV cells attached onto a clear 150 µm-thick ETFE layer and covering 100% of its area, c) a panel composed of a clear 250 µm-thick EFTE layer and OPV cells attached onto a clear 150 µm-thick ETFE layer and covering 50% of its area, d) a panel comprising a clear 250 µm-thick EFTE layer and another clear 250 µm-thick EFTE layer with 50% of its area silver printed. The studied configurations are plotted in Figure 3 and are identified using the nomenclature introduced in Table 5.

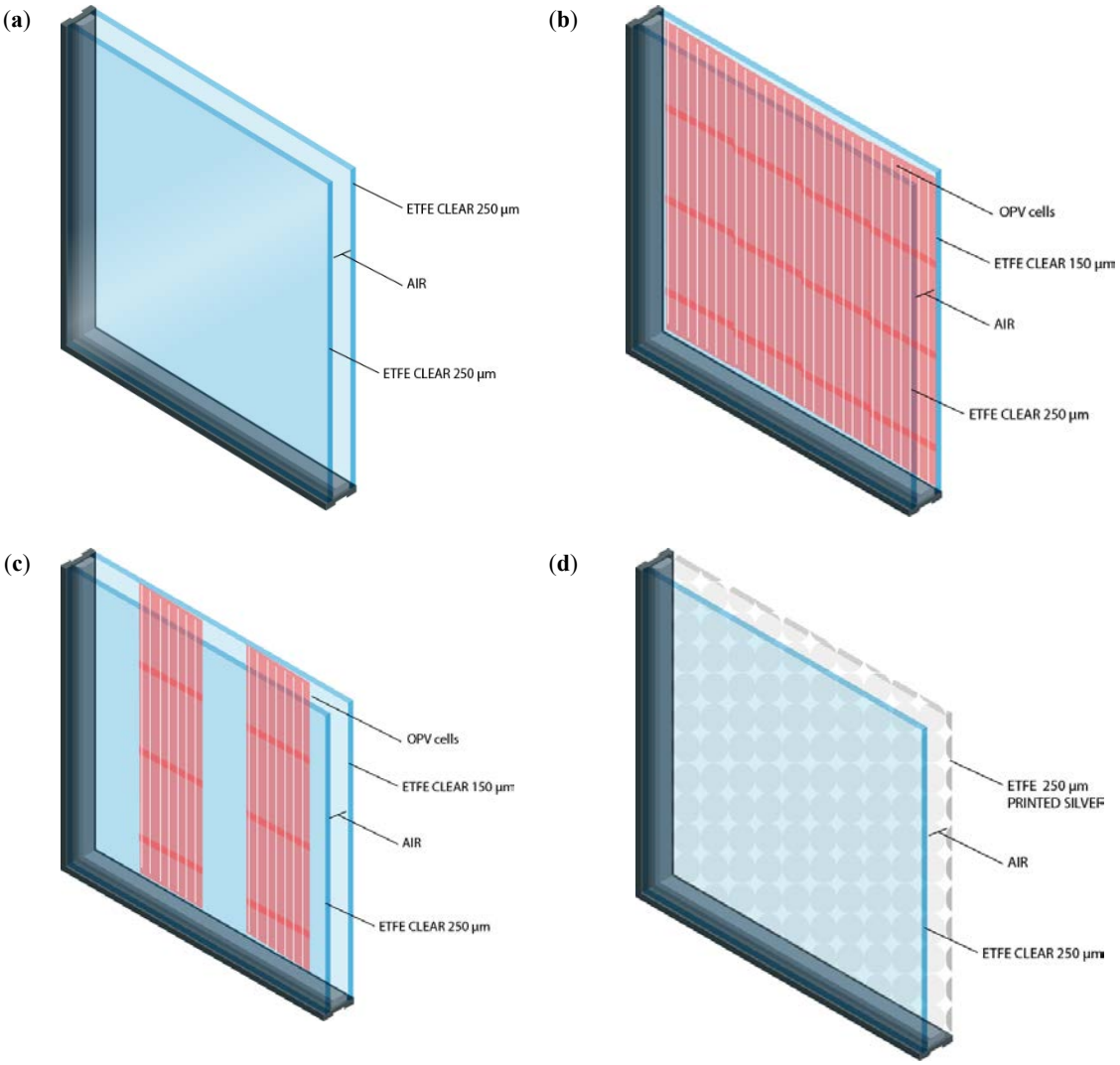

Figure 3. Studied configurations. (**a**) ETFE+ETFE; (**b**) ETFE + OPV/ETFE; (**c**) ETFE + OPV(50%)/ETFE, (**d**) ETFE + ETFE-SILVER(50%)

Table 5. ID of configurations

ID	Configuration
REF	ETFE 250µm /air gap/ ETFE 250µm
C1	ETFE 250µm /air gap/ OPV (100%)/ETFE 150µm
C2	ETFE 250µm /air gap/ OPV (50%)/ETFE 150µm
C3	ETFE 250µm /air gap/ ETFE-SILVER (50%) 250µm

The luminous, solar and thermal characteristics of every configuration are provided in Table 6. It can be appreciated that the reference configuration is the one achieving the highest transmittance and solar factor, but as a consequence the higher shading coefficient and thermal transmittance values. The U-value was calculated following the simplified UNE procedure and the ISO one, noticing that those calculated by UNE exceed the ISO ones. The configuration 1, C1, results in the lower transmittance and solar factor values by far with respect to the other configurations. However, regarding the U-values, a small variation can be observed. Differences in the two standard calculations for the U-value are noticeable for this case since for the U-value referred to ISO, C1 gets a value slightly higher than C3, but referring to UNE C1 has the lowest U-value. In the case of configurations C3 and C4, similar values are reported for the tabulated parameters.

Table 6. Summary of luminous, solar and thermal characteristics of the configurations

ID	τ_e	ρ_e	τ_v	ρ_v	g	SC	U_{ISO} [W/m^{2}K]	$U_{UNE\text{-}EN}$ [W/m^{2}K]
REF	0.834	0.135	0.827	0.151	0.84	0.97	2.81	2.91
C1	0.147	0.306	0.065	0.21	0.27	0.593	2.68	2.78
C2	0.474	0.238	0.435	0.197	0.57	0.756	2.75	2.85
C3	0.554	0.272	0.550	0.277	0.60	0.746	2.64	2.81

3.2 Building model parameters and assumptions

A 3D model of an office building was created in SketchUp and imported from Trnsys [27]. The building has a floor area of 25 m^2 (5 m x 5 m) with a height of 3 m, resulting in a total volume of 75 m^3. The different ETFE window configurations proposed in this study were integrated in the south façade (selected locations are in the northern hemisphere) with different window wall ratios (WWR) ranging from 25% to 95% in 10% steps. Window wall ratio is defined as the percentage of glazed area with respect to the total wall area where the glazing is placed. The simulations allowed evaluating the lighting conditions, and the thermal and electrical behaviors.

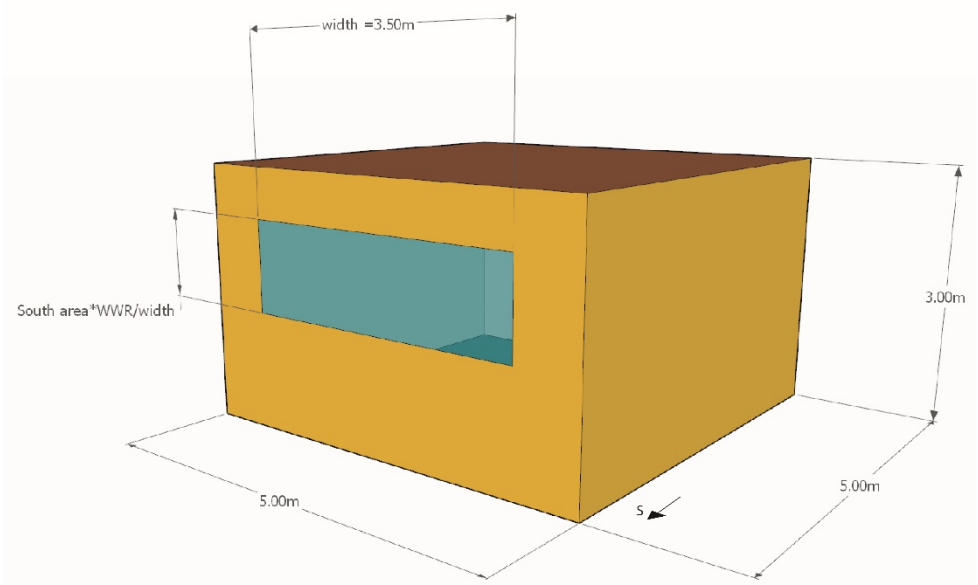

Figure 4. Building model description

The thermal characteristics under standard conditions (20 ºC and 1 atm) of the selected building are selected based on the minimum required values of each country regulations [28,29] given in Table 7.

Table 7. Envelope thermal characteristics

Elements	**U-value** [W/m^{2}K]	
	Barcelona	**Paris**
Walls	0.75	0.36
Roof	0.5	0.20
Ground Floor	0.75	0.20

Nonetheless, the thermal transmittance depends on the different temperatures across the system and also some of the parameters involved are angle dependent. Therefore, the U-value is calculated at each time step considering the specific conditions by means of the LBL Window Program [30], which generates a DOE-2 file format that is subsequently read by Trnsys.

Glazing temperatures are calculated considering the transmittance, reflectance and absorptance of each specific system to incoming direct and diffuse solar radiations and also to diffuse short-wavelength radiation reflected through the multilayered system.

Also, convective, conductive and long-wave radiative heat transfer calculations are performed between individual layers and inner and outer environments.

The internal heat gains generated by occupancy, lighting and appliances have been considered and calculated according to standard EN16798-1[31]. This norm also indicates the values for ventilation rates including infiltration, which for the present case takes a value of 0.8 l s^{-1} m^{-2} (office building with normal level of expectation). The space heating and cooling demands are calculated to maintain an interior temperature of 20 ºC in winter and 26 ºC in summer (latent control not applied). The heating season is considered to start on October, 16th and to finish on May, 15th and the cooling season from May, 16th to October, 15th.

The heating demand is covered by a reversible heat pump with a coefficient of performance (COP) of 3.38 for heating and an energy efficiency ratio (EER) of 3.35 for cooling. These values were set according to the requirements established by the European Commission in the rule nº206/2012 and by the standard UNE-EN 14511-1[32]. The heat pump operation time was set to 11 hours per day (7:00 h - 18:00 h) from Monday to Friday.

The main parameters and assumptions for these calculations are summed up in Table 8.

Table 8. Assumptions

Description	Value	Units
Set point in heating period	20	°C
Set point in cooling period	26	°C
Occupation rate [31]	10	m^2/per.
Heat gains per person (sensible) [31]	5	W/m^2
Heat gains per person (latent) [31]	3.3	W/m^2
Ventilation including infiltration [31]	0.8	l·s^{-1}·m^{-2}
Light heat gains	Daylighting in Trnsys model	W
Appliances heat gain [31]	12	W/m^2
Lighting, illuminance in working areas [31]	500	lux

3.3 Climate conditions

The ETFE windows performance was assessed in Barcelona (Spain, Latitude: 41.4º, Longitude: 2.15º) and Paris (France, Latitude: 48.4º, Longitude: 2.3º). In this study,

typical meteorological year weather data from the Meteonorm Trnsys database were used. This data is hourly based and represents long-term statistical trends and patterns.

Figure 5 shows the monthly cumulated global horizontal irradiance (GHI) and the average ambient temperatures. The annual cumulated GHI in Barcelona is 1536 kWh/m^2 and the annual average temperature is 15.3 °C whereas in Paris the GHI is 1044 kWh/m^2 and the annual average temperature is 9.83 °C. Regarding the global vertical irradiance over the south façade, Barcelona receives 1102 kWh/m^2 and Paris 811 kWh/m^2.

Figure 5. Monthly irradiances and mean temperatures for Barcelona and Paris.

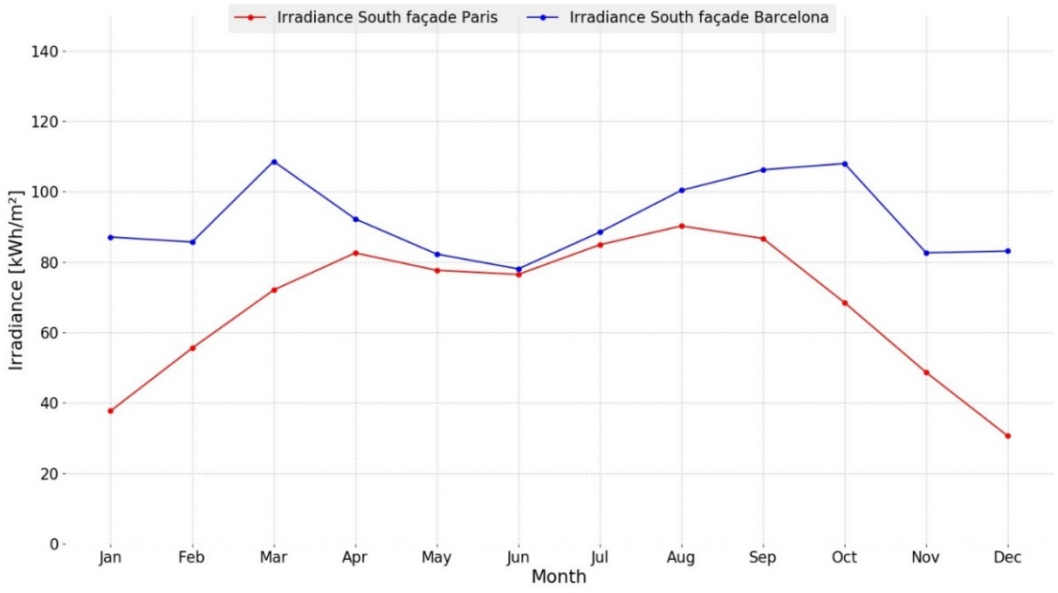

Figure 6. Monthly irradiances at the south façade for Barcelona and Paris.

3.4 Simulation criteria

The purpose of this document is to analyze the thermal, electrical and lighting behaviors when incorporating the different systems as a substitute for conventional windows. Concerning lighting, daylight availability describes the light transmitted through a window system to an indoor space. It can be defined by dynamic/climate-based metrics such as Daylight Autonomy (DA), Useful Daylight Illuminance (UDI) or Annual Light/Sunlight Exposure [33].

Daylight autonomy (DAx lux) is a climate-based metric defined as the percentage of occupied hours in a year when a minimum illuminance threshold (x lux) can be met by daylight alone. Illuminances of 300 lux (DA300 lux) and 500 lux (DA500 lux) are the most common target thresholds for offices, classrooms and libraries. For any given point in a building, daylight is considered sufficient if the daylight autonomy exceeds 50% of the occupied hours of the year (ie. DA300 lux or 500 lux > 50%) [33].

Useful Daylight Illuminance (UDI) is a modification of Daylight Autonomy conceived by [13]. In contrast to measures of daylight autonomy, the UDI paradigm gives significance to those daylight illuminances below a design threshold or between two values. The UDI range is further subdivided into three ranges. The range UDI<100 Lux indicates a low level of illumination in which artificial lighting will be necessary, the range UDI 100-2000 indicates levels of comfort lighting in which the majority of activities can be carried out, and the range UDI> 2000 indicates that the lighting levels create a discomfort situation due to the high level of illumination. Normally this last case happens in south orientations where the solar radiation directly impacts the interior of the building.

In addition to the luminous performance, an analysis of the energetic demands for the different configurations is conducted. The annual global consumption of energy ($Q_{overall}$) is determined by subtracting the annual energy produced by the OPV cells ($-E_{PV}$) (if installed) to the annual energy consumed by the air conditioning equipment ($Q_{heating} + Q_{cooling}$).

$$Q_{overall} = Q_{cooling} + Q_{heating} - E_{PV} \quad (4)$$

Thus, small values of $Q_{overall}$ indicate less energy demand in the building and more energy savings.

4. Results

The annual energetic performance of the four system configurations integrated onto the south façade with several WWR was evaluated for Barcelona and Paris. The space

heating and cooling demands, as well as the electrical production for the cases where OPV cells are used, were calculated.

The impact of the WWR is clearly illustrated in Fig. 7. Increasing WWR brings higher cooling demands and less heating demands due to the enhanced solar gain. Although the heat flux increases with bigger windows (higher losses especially during the night), the demands are not impacted to a great extent mainly due to the diurnal occupation for an office case-study. The criterion followed to establish the WWR range is that the maximum WWR considered in the interval is the one where the overall energy demand in both configurations including OPVs (50% and 100%) is the minimum. Figure 7 includes also the subsequent WWR to illustrate that overall energy demands change in slope and start to increase.

(a)

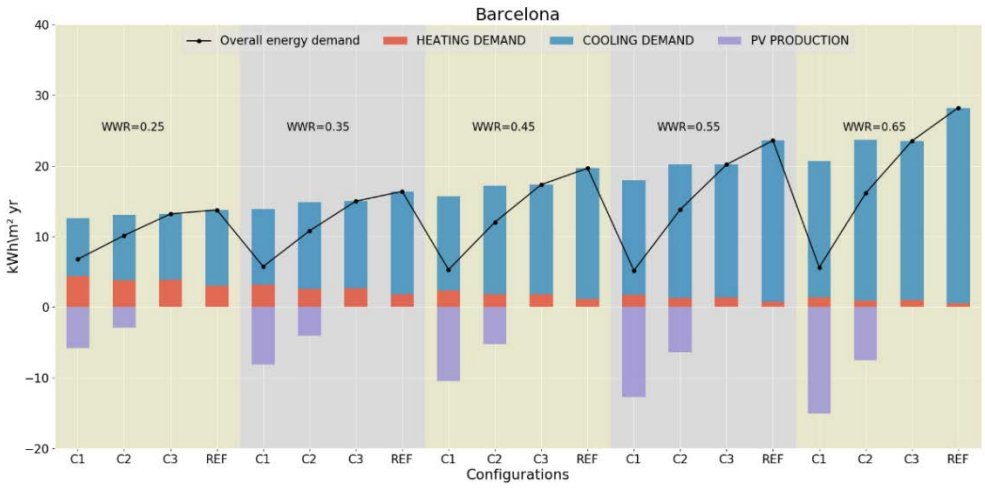

(b)

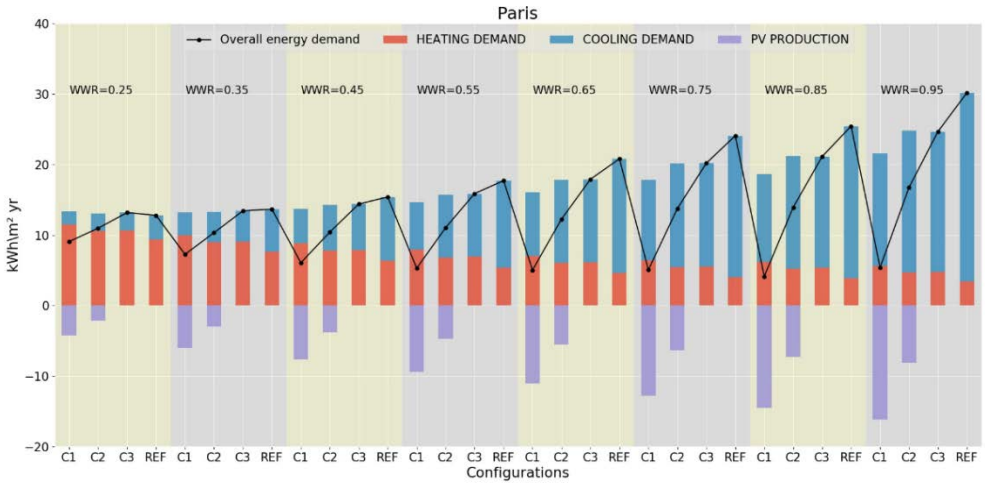

Figure 7. Annual consumption of different configurations: (**a**) Barcelona; (**b**) Paris.

In Barcelona, the impact of increasing the size of the windows can be directly related to a higher cooling demand due to its hot and sunny summers and mild winter Mediterranean climate (Csa) [35]. WWRs vary from 25% to 65% since under the last WWR the net/overall energy demands for the configurations including OPVs grow with respect to the previous WWR (55%). WWR of 55% is set as the upper limit of the WWR interval. It is observed that configurations ETFE+OPV(100%)/ETFE (C1), ETFE+OPV(50%)/ETFE (C2) and ETFE+ETFE-SILVER(50%) (C3) bring energetic savings with respect to the reference case ETFE+ETFE (REF) since they act as shading elements. On the other hand, Paris has an oceanic semi-continental climate (Cfb) [35]. As a consequence, increasing the WWR reduces the overall energy demand and equalizes the space heating and cooling demands. Configurations with higher shading increase the heating demands due to the colder climate in Paris. Due to this fact, the maximum WWR value considered is 85%. Under 95% WWR the overall energy demand values increase.

In general, configurations C1 and C2 produce electrical energy and, as a consequence, reduce the overall energy demand. An exception is configuration C1 in Paris when WWR is 0.25, where the net energy does not improve since the small fraction of glazing in the south wall reduces solar gains. Thus in the end the heating demand has become larger than the savings achieved due to the smaller cooling demand in summer.

In Barcelona, configuration C1 brings a heating demand reduction spanning from 8.69% (WWR=0.25) to 24.04% (WWR=0.55) compared to the reference case. In addition, a fraction ranging from 46.00% to 71.05% of the consumption is covered by PV production. In Paris, also for C1, the heating demand is increased (4.22%) for a WWR of 0.25. However, with higher WWR (0.35, 0.45, 0.55, 0.65, 0.75 and 0.85) the heating demand drops (3.30%, 10.84%, 17.25%, 22.64%, 25.98% and 26.85% respectively). Interestingly, for WWR 0.35-0.85 the PV production is able to cover from 31.93% to 77.79% of the total consumption.

Configuration C2 in Barcelona reduces the heating demand from 5.22% (WWR=0.25) to 14.45% (WWR=0.55) and the PV production covers from 22.16% (WWR=0.25) to 31.54% (WWR=0.55) of the energy consumption. Differently in Paris, the same system increases the heating demand for WWR=0.25 (2.31%). However a larger WWR comes with a drop in heating demand, from 2.77% (WWR=0.35) to 16.83% (WWR=0.85) and the PV production covers from 16.27% (WWR=0.25) to 34.21% (WWR=0.85) of the total energy consumption. All the values reported above are compared to the reference case.

Configuration C3 only acts as a shading element (there is no PV production) and its thermal performance is similar to configuration C2. Nonetheless, configuration C2 reduces the heating demand globally more than 2% compared to configuration C3.

In the end, in Barcelona, configuration C1 is the less energy consuming option, with the same level independently of the WWR (up to 0.55). It is worth noticing that when WWR is the largest, PV production is fortunately larger to compensate for the cooling needs. In Paris, large window areas with the maximum coverage of OPV cells (configuration C1) is optimum for net energy consumption. Thus luminous performance will be required for finding the optimum WWR in Barcelona and for checking if configuration C1 remains attractive in both locations.

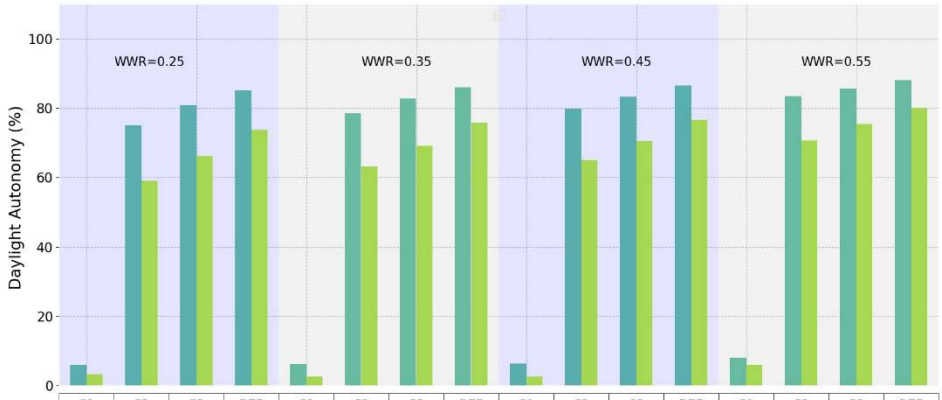

	C1	C2	C3	REF	C1	C2	C3	REF	C1	C2	C3	REF	C1	C2	C3	REF
DA300 Barcelona	6.0	75.1	80.8	85.1	6.2	78.5	82.6	86.0	6.3	79.9	83.3	86.5	8.1	83.3	85.6	88.1
DA300 Paris	3.2	59.0	66.2	73.7	2.5	63.1	69.1	75.6	2.6	64.9	70.4	76.6	5.9	70.6	75.3	79.9

Figure 8. Daylight Autonomy (300 lux) for the different configurations in Barcelona and Paris.

Regarding the luminous performance, DA and UDI were evaluated (Figure 8). The WWR doesn't impact on the DA at 300 lux (DA300). Therefore a WWR of 0.25 would be sufficient for all configurations except C1 (ETFE+OPV(100%)/ETFE). This configuration has a limited transmissivity of solar light and therefore artificial illumination would be necessary during the vast majority of the day. Higher WWRs than 0.55 are not included for the case of Paris since DA at 300 lux is not influenced.

The UDI of interest is from 100 to 2000 lux since it comprises the range 100-300 lux where only additional illumination would be required and the 300-2000 lux range where luminous comfort is achieved without having recourse to artificial light. For increasing values of WWR and considering the reference case, UDI 100-2000 lux gets reduced by increasing UDI>2000 lux. But this high level of illumination causes discomfort. Figure 9 shows that the results are similar in both Barcelona and Paris. Based on this indicator, for the case of Barcelona the best configuration is found to be a WWR of 0.45 and the configuration C2, achieving an illumination level from 100 lux to 2000 lux during 82.2% of the annual hours. For the rest of the WWR analyzed, configuration C2 always performs the best, except for a WWR of 0.25 where the glazing including the silver

printed pattern (configuration C3) slightly outperforms configuration C2. In the case of Paris, the best performances are when WWR is equal to 0.35 for configuration C2. Based on this result, larger WWRs than 55% are not included in Figure 9. Similarly to the results obtained for Barcelona, with a WWR of 0.25 the combination including a silver printed ETFE foil (C3) provides a better illumination than configuration C2.

On the other hand, configurations with shading elements (either an OPV/ETFE or a silver printed ETFE layer) achieve DA values around 80% in Barcelona and 70% in Paris (4% lower than the reference case for both cities). The UDI indicator in the range 100-2000 lux is increased with higher WWR except for large values (>0.5) where it starts to decay.

(**a**)

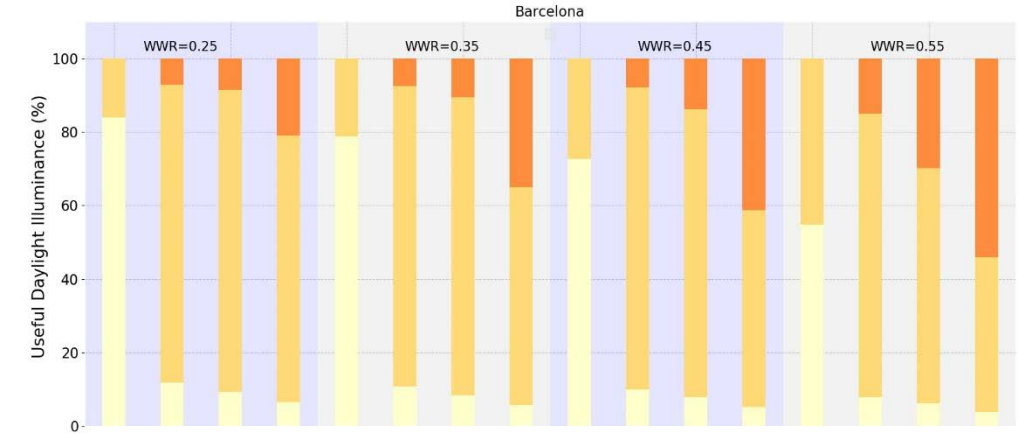

	C1	C2	C3	REF	C1	C2	C3	REF	C1	C2	C3	REF	C1	C2	C3	REF
<100	83.9	11.9	9.3	6.5	78.8	10.8	8.4	5.6	72.6	9.9	7.9	5.2	54.7	7.9	6.1	3.9
100-2000	16.1	80.9	82.1	72.4	21.2	81.6	81.0	59.4	27.4	82.2	78.2	53.4	45.3	77.1	64.0	42.0
>2000	0.0	7.3	8.6	21.1	0.0	7.6	10.6	35.0	0.0	7.9	13.9	41.4	0.0	15.1	29.9	54.1

(**b**)

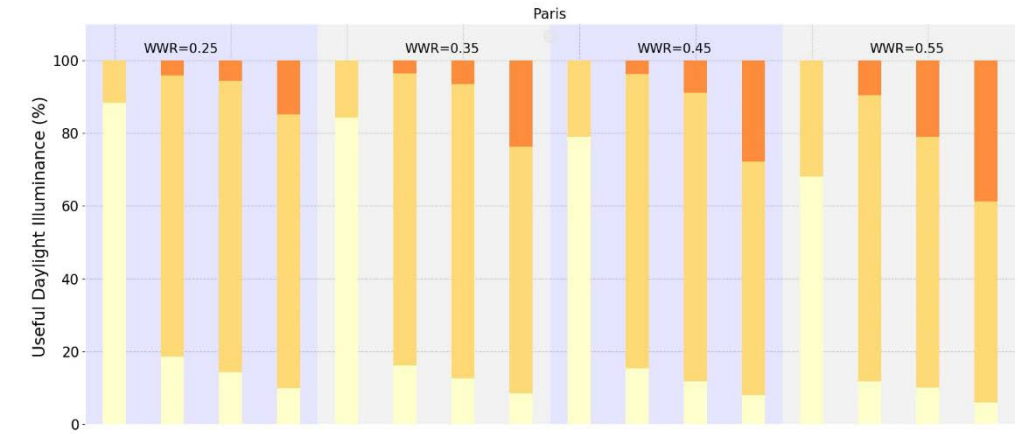

	C1	C2	C3	REF	C1	C2	C3	REF	C1	C2	C3	REF	C1	C2	C3	REF
<100	88.3	18.6	14.4	9.9	84.2	16.3	12.6	8.6	78.9	15.4	11.8	8.0	68.1	11.8	10.2	6.0
100-2000	11.7	77.3	79.9	75.1	15.8	80.1	80.8	67.7	21.1	80.8	79.3	64.2	31.9	78.6	68.7	55.2
>2000	0.0	4.1	5.7	14.9	0.0	3.6	6.6	23.7	0.0	3.9	8.9	27.8	0.0	9.6	21.1	38.7

Figure 9. Useful Daylight Illuminance: (**a**) Barcelona (**b**) Paris.

When combining the analyses on energy consumption and illumination performances, conclusions can be drawn about optimum strategies for integrating OPV/ETFE windows in buildings as a function of the local climate

5. Conclusions

OPV/ETFE building integrated windows are a promising alternative to conventional glass windows. They have advantageous characteristics such as low environmental impact, flexibility, light weight, color variability, free-shape and more generally customization options. Transmittance and reflectance spectral measurements of three different EFTE foils and a commercial OPV have been performed. The main optical, thermal and luminous properties have been calculated from this experimental characterization to perform a dynamic simulation in Trnsys for a model office building. The luminous and energetic performances have been evaluated for 4 different window configurations, different WWRs and 2 locations (Barcelona and Paris). The four configurations comprise a reference case (REF) which does not have any shading element, a case where a tinted layer is added (C3), and two cases where OPV cells are added with area coverages of 50% (C2) and 100% (C1). Energy produced by the OPV cells partly covers electrical demands of the reversible heat pump.

The main conclusions that can be drawn from this study are the following. Firstly, ETFE foils with OPVs are able to provide reasonable shares of the total heating and cooling demands. Values higher than 22% for Barcelona and 16% for Paris can be attained (WWR of 25%). The configuration that best performs in terms of energy fraction covered, in both locations, is found to be C1 since it has the higher PV area to generate electricity. On the other hand, configuration C1 in combination with the various WWRs is different for the two locations. In the case of Barcelona, the net energy is almost the same for WWR from 0.25 to 0.45. For a WWR of 0.55 the cooling demand increases in a bigger proportion than the rise in electricity produced thanks to a larger area coverage, resulting in a net energy consumption slightly smaller than for lower WWRs. In Paris the most effective WWR is 0.85 because the heating demand is predominant and the higher the glazing area the higher the energy flux entering the interior space.

Secondly, a solar control system should be added to the reference system since high percentages over the yearly daytime hours with levels of illumination higher than 2000 lux are registered, with the associated discomfort.

Thirdly, configurations C1, C2 and C3, which have shading elements, are key to create luminous comfort for climates and latitudes such as Barcelona. The cooling needs are reduced, and when increasing WWR, the luminous comfort characterized by the UDI 100-2000 lux is enhanced. On the other hand, adding shading elements in places like Paris increases the heating demands whilst improving the luminous comfort. In both

locations, configuration C2 under a WWR of 0.45 is the combination providing the best UDI percentages of about 80% (80% of the daytime yearly hours are under illumination comfort).

Finally, OPV cells in windows transform a passive system into an active one able to provide a fraction of the total energy demands. In addition, OPV cells act as shading elements and therefore change the thermal and luminous performances. The area of the window covered by the OPV cells is key to achieve a satisfactory tradeoff between all the targets. High OPV coverage area in windows could be a possibility for places like Barcelona characterized by hot temperatures during long periods over the year. However, for places with colder climates such as Paris OPV cells can have more detrimental impacts. Higher OPV coverage of the total area reduces the luminous comfort (UDI) and the useful daylight (DA300) in both cities. Even though high OPV areas provide high coverage of building demands, the luminous discomfort associated may lead to discarding this option.

Acknowledgements

This research was supported by the "Generalitat de Catalunya" (grants 2018FI_B1_00136, 2017 SGR 1276 and ICREA Academia) and "Ministerio de Economía y Competitividad" of Spain (grant reference ENE2016-81040-R). The authors would like to acknowledge the collaboration with the company IASO SA.

5. References

[1] The energy performance of buildings directive factsheet (2019), Available online: ec.europa.eu/energy/sites/ener/files/documents/buildings_performance_factsheet.pdf (accessed on Apr 10, 2019).

[2] International Energy Agency (2019). Available online: https://www.iea.org/topics/energyefficiency/buildings/ (accessed on Apr 10, 2019).

[3] EU Directive (EU) 2018/844 of the European Parliament and of the Council of 30 May 2018 amending Directive 2010/31/EU on the energy performance of buildings and Directive 2012/27/EU on energy efficiency. 2018.

[4] Menéndez, A.; Martínez, A.; Santos, A.; Ruiz, B.; Moritz, K.; Klein, I.; Díaz, J.; Lagunas, A.R.; Sauermann, T.; Gómez, D. A multifunctional ETFE module for sustainable façade lighting: Design, manufacturing and monitoring. Energy Build. 2018, 161, 10–21.

[5] Robinson-Gayle, S.; Kolokotroni, M.; Cripps, A.; Tanno, S. ETFE foil cushions in roofs and atria. Constr. Build. Mater. 2001, 15, 323–327.

[6] Lamnatou, C.; Moreno, A.; Chemisana, D.; Reitsma, F.; Clariá, F. Ethylene tetrafluoroethylene (ETFE) material: Critical issues and applications with emphasis on buildings. Renew. Sustain. Energy Rev. 2018, 82, 2186–2201.

[7] Maywald, C.; Riesser, F. Sustainability - The Art of Modern Architecture. Procedia Eng. 2016, 155, 238–248.

[8] Yu, J.; Zheng, Y.; Huang, J. Towards high performance organic photovoltaic cells: A review of recent development in organic photovoltaics. Polymers (Basel). 2014, 6, 2473–2509.

[9] Hengevoss, D.; Baumgartner, C.; Nisato, G.; Hugi, C. Life Cycle Assessment and eco-efficiency of prospective, flexible, tandem organic photovoltaic module. Sol. Energy 2016, 137, 317–327.
[10] Heliatek – The future is light Available online: https://www.heliatek.com/en/ (accessed on Apr 10, 2019).
[11] Hu, J.; Chen, W.; Qiu, Z.; Zhao, B.; Zhou, J.; Qu, Y. Thermal performances of ETFE cushion roof integrated amorphous silicon photovoltaic. Energy Convers. Manag. 2015, 106, 1201–1211.
[12] Hu, J.; Chen, W.; Liu, Y.; Zhao, B.; Yang, D.; Ge, B. Two-layer ETFE cushions integrated flexible photovoltaics: Prototype development and thermal performance assessment. Energy Build. 2017, 141, 238–246.
[13] Jean, J.; Brown, P.R.; Jaffe, R.L.; Buonassisi, T.; Bulović, V. Pathways for solar photovoltaics. Energy Environ. Sci. 2015, 8, 1200–1219.
[14] Lizin, S.; Van Passel, S.; De Schepper, E.; Maes, W.; Lutsen, L.; Manca, J.; Vanderzande, D. Life cycle analyses of organic photovoltaics: A review. Energy Environ. Sci. 2013, 6, 3136–3149.
[15] Zanelli, A.; Beccarelli, P.; Monticelli, C.; Ibrahim, H.M. Technical and Manufacturing Aspects in order to create a smart façade system with OPV integrated into ETFE foils. 2012, 2.
[16] Fan, Z.; De Bastiani, M.; Garbugli, M.; Monticelli, C.; Zanelli, A.; Caironi, M. Experimental investigation of the mechanical robustness of a commercial module and membrane-printed functional layers for flexible organic solar cells. Compos. Part B Eng. 2018, 147, 69–75.
[17] Fan, Z.; Bastiani, M. De; Monticelli, C.; Caironi, M.; Zanelli, A. Performance investigation of organic photovoltaic layers on architectural membrane. 9th Energy forum 2015, 1255–1269.
[18] Hu, J.; Chen, W.; Yin, Y.; Li, Y.; Yang, D.; Wang, H.; Zhang, X. Electrical-thermal-mechanical properties of multifunctional OPV-ETFE foils for large-span transparent membrane buildings. Polym. Test. 2018, 66, 394–402.
[19] Aenor Español La. UNE-EN ISO 79632006. Ensayos no Destr. por Ultrason. Especificaciones para el bloque calibración No2. 2011, 1–16.
[20] McCamy, C.S. Correlated color temperature as an explicit function of chromaticity coordinates. Color Res. Appl. 1992, 17, 142–144.
[21] Smith, Thomas; Guild, J. The C.I.E. colorimetric standards and their use". Transactions of the Optical Society. 33 (3): 73–134. 1931.
[22] En, N.E. 673 673. Glass in building - Determination of thermal transmittance (U value) - Calculation method. 2011.
[23] ISO 15099. Thermal performance of windows, doors and shading devices -- Detailed calculations 2003.
[24] The Chemours Company Tefzel TM ETFE Fluoropolymer Film; 2017;.
[25] Antretter, F.; Dr. Haupt, W.; Dr. Holm, A. Thermal Transfer through Membrane Cushions Analyzed by Computational Fluid Dynamics. 2008.
[26] EN 12898. GLASS IN BUILDING. DETERMINATION OF THE EMISSIVITY. 2001.
[27] Klein, S.; Beckman, W. TRNSYS 18: A transient system simulation program: mathematical reference 2017.
[28] Código Técnico de la Edificación (CTE) Documento Básico de Ahorro de Energía (DB-HE). 2017.
[29] Legifrance Arrêté du 28 décembre 2012 relatif aux caractéristiques thermiques et aux exigences de performance énergétique des bâtiments nouveaux et des parties

nouvelles de bâtiments autres que ceux concernés par l'article 2 du décret du 26 octobre 2010 relatif aux. 2013, 97.
[30] Berkeley, L. WINDOW 7 User Manual. 2019.
[31] CEN prEN 16798-1: Energy performance of buildings - Part 1: Indoor environmental input parameters for design and assessment of energy performance of buildings addressing indoor air quality, thermal environment, lighting and acoustics - Module M1-6. 2015, 44.
[32] En, N.E. Norma Española bombas de calor para la calefacción y la refrigeración de locales y enfriadoras de proceso con compresores accionados eléctricamente Parte 1 : Términos y definiciones. 2019.
[33] Sun, Y.; Wu, Y.; Wilson, R. A review of thermal and optical characterisation of complex window systems and their building performance prediction. Appl. Energy 2018, 222, 729–747.
[34] Nabil, A.; Mardaljevic, J. Useful daylight illuminance: A new paradigm for assessing daylight in buildings. Light. Res. Technol. 2005, 37, 41–59.
[35] Kottek, M.; Grieser, J.; Beck, C.; Rudolf, B.; Rubel, F. World Map of the Köppen-Geiger climate classification updated. eschweizerbartxxx Meteorol. Zeitschrift 2006, 15, 259–263.

Capítulo 6. Análisis óptico y térmico de membranas ETFE/OPV en forma de cojín

A. Moreno, A. Riverola, D. Chemisana, R. Vaillon. Design and modelling of an OPV-ETFE cushion for semi-transparent glazing, 15th Conference on Sustainable Development of Energy, Water and Environment Systems (SDEWES), resumen aceptado y artículo para libro de actas enviado.

Design and modelling of an OPV-ETFE cushion for semi-transparent glazing

A. Moreno[1], A. Riverola[1], D. Chemisana[1,*], R. Vaillon[2], A. Solans[1]

[1] Applied Physics Section of the Environmental Science Department, University of Lleida, 25001 Lleida, Spain;

[2] IES, Univ Montpellier, CNRS, Montpellier, France

Abstract

Architectural glazing presents several advantages in terms of aesthetics and user well-being perspectives. However, they can have large impacts on heating and cooling demands and artificial lighting requirements. Ethylene tetrafluoroethylene (ETFE) cushion systems present adequate insulating and transparency characteristics, and, combined with organic photovoltaic (OPV) modules, become a glazing element leading towards energy efficient buildings. The present manuscript presents a detailed optical, thermal and electrical analysis of a 3-layer ETFE/OPV cushion that may support these glazing-type systems by providing a better performance understanding. Spectrophotometric optical measurements up to 50 μm offer a complete view of the individual layer behavior. These measurements feed the optical and thermal models that aim at determining the influence of the OPV module depending on the position in the cushion. In addition, based on the OPV spectral response, electricity production is estimated. Results reveal that the best configuration is the one placing the OPV module in the inner layer, since it represents a trade-off solution between thermal control and electricity potential production.

1. Introduction

Buildings are the most energy intensive sector, weighting 40 % of the overall energy consumption in the case of the European Union (EU). In addition, 75% of the EU's buildings are energy inefficient [1]. Although a better insulation could lead to building energy savings, architectural concepts tend to increase the glazing fraction of the building envelope. Glazing elements need to be carefully tackled since they present a large impact on building energy demands, including space heating and cooling, and artificial lighting requirements. From a positive perspective, glazing has an influence on sustaining human health and well-being [2]. Even though there has been technological progress in developing more efficient glazing systems, they still act as a thermal weak point, provoking higher cooling demands in summer and higher heating demands in winter [3].

On the other hand, a Directive of the European Parliament (2018/844) specifically addresses the above indicated issues by defining the objectives to be fulfilled in buildings by 2030: energy efficiency should be improved by 32.5%, greenhouse gas emissions should be reduced by 40%, and 32% of energy production should come from renewable energy [4]. These EU Directive goals should be met by integrating renewable energies and by incorporating energy efficient materials in the building envelope, especially those involved in architectural glazing.

Among renewable energies, solar energy stands as the one with the greatest potential since the solar resource is the most extended. Specifically, photovoltaic (PV) modules represent one of the most efficient and practical ways to convert solar energy into electricity [5]. Within PVs, organic photovoltaic (OPV) technologies present interesting features that position them as a great candidate for building integration applications, such as lightness, semitransparency, free-form, flexibility, cost-effectiveness, performance under low-irradiance and diffuse light illuminations, and one of the most eco-friendly [6]–[8].

Regarding architectural glazing, traditional glass-based systems are being gradually replaced by polymeric foils and membranes, especially in building applications like transparent atriums, sport stadiums double skins, commercial centers, etc. [9]–[13]. One of the most used polymers is ethylene tetrafluoroethylene (ETFE) due to its adequate properties for being an architectural material (mechanical resistance, stability, transparency, self-cleaning, reduced environmental impact, etc.). A deep analysis of the ETFE characteristics is reported in [14].

Based on the aforementioned characteristics of both OPV modules and ETFE foils or membranes, it seems logic to integrate both in a PV glazing system. In fact, several authors conducted research developing this type of technology in the last decade. The last study found in the literature analyzing an OPV/ETFE glazing deals with the dynamic energetic simulation and luminous performance of a building façade system [15]. The system consists of a plane 2-layer window, where the OPVs are placed in the internal ETFE layer. Different window-to-wall ratios and configurations were assessed for two different locations, Barcelona and Paris, and the influence on the heating and cooling demands and on the illumination indicators, with respect to a reference glazing case, was analyzed. The simulated results did show improvement, to a greater or lesser extent depending on the configuration, in all the indicators analyzed. Previous studies dealt with similar configurations, either for plane or curved (cushion) geometries, stating the potential uses of ETFE-OPV for building integration [16]–[19].

In light of the investigations mentioned above, there is no study analyzing the spectral performance of ETFE-OPV architectural membranes from the ultraviolet to the large

infrared. The largest wavelength considered is usually 2500 nm;. However, operating temperatures of building glazing elements are usually in the range 10-50 ºC. This means that thermal exchange occurs at wavelengths much longer than 2500 nm. In order to fill this important gap, the present research deals with the optical and thermal modelling of ETFE-OPV membranes in the spectral range 0.35-50 µm based on spectral measurements of the layers involved. In addition, the electrical output of the OPVs is included in the model.

2. Methodology

2.1 Optical measurements

The spectral transmittance ($T(\lambda)$) and reflectance ($R(\lambda)$) of ETFE foils (150 and 200 µm thick) and commercially available OPVs fabricated by InfinityPV [20] were determined from 0.35 to 50 µm with a FTIR (Fourier-transform infrared) spectrometer Bruker Optics—IFS 66 v/S equipped with an integrating sphere. This spectral range covers both the solar range and almost the full range of thermal emission (> 99% for 25 °C) in the mid to far infrared for common operational temperatures. The measurements were carried out at room temperature and considered to be valid over the operating range [21]. Using Kirchhoff's law, the spectral absorptance (emittance) can be derived from the experimental measurements as follows:

$$E(\lambda) = A\,(\lambda) = 1 - R(\lambda) - T(\lambda) \tag{1}$$

The optical characteristics of the ETFE foils and the OPV cells are depicted in Figures 1 and 2.

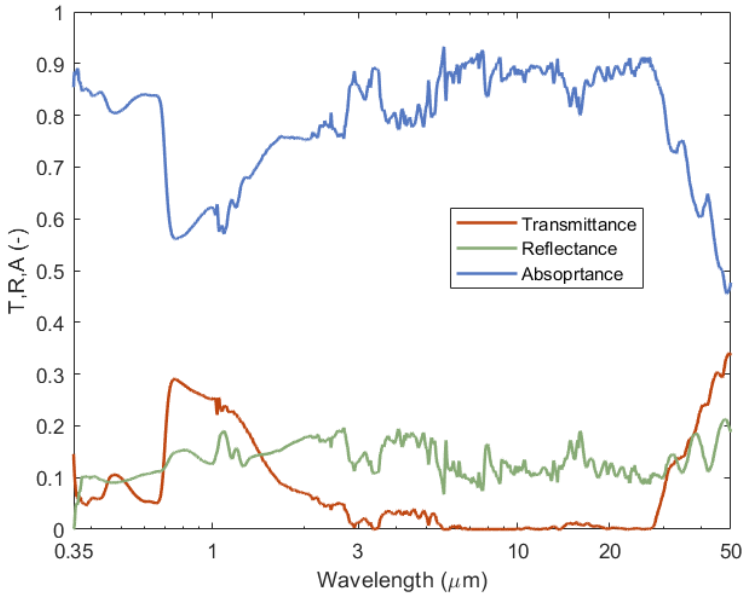

Figure 1. OPV optical properties under normal incidence

Figure 1 shows the spectral characteristics of the OPV under normal incidence. As expected from an organic PV cell, OPVs are highly absorptive from the ultraviolet up to 0.65 μm (the range where photovoltaic conversion takes place). At around 0.65 μm, there is a sharp decrease in absorptance from 0.84 to 0.57. From 0.65 μm to almost 30 μm, the absorptance grows from 0.57 to 0.9 just before decreasing again. The reflectance has some fluctuations over the measured bandwidth but around an average value of 13%.

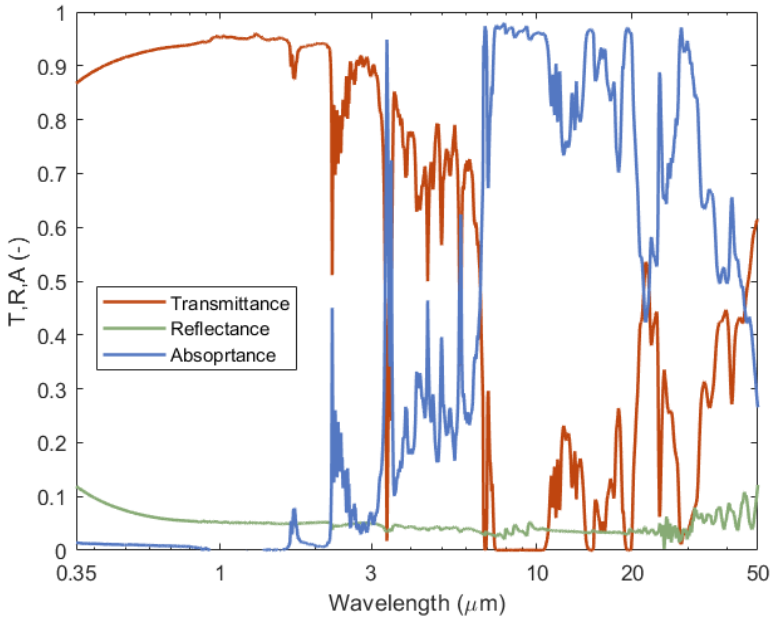

Figure 2. ETFE optical properties (150 μm-thick) under normal incidence

The spectral characteristics of the 150 μm-thick ETFE foil are shown in Figure 2. ETFE barely absorbs photons for wavelengths below 2 μm. From 2 μm up to 6.5 μm, the absorptance grows steadily from almost 0 to 0.4. Then, it increases up to 30 μm except with a dip at 23 μm. Finally, the absorptance decreases from 0.9 to 0.5 between 30 and 50 μm.

The reflectance is almost constant at 0.06 from the ultraviolet to the far-infrared and, therefore, the transmittance follows a trend which is opposite to that of the absorptance. Nonetheless, ETFE is highly transmissive from the ultraviolet up to 6.5 μm allowing the solar fraction to pass through almost unaltered.

In addition, since two ETFE foils with different thicknesses were measured, the complex refractive index ($\bar{n} = n + \hat{\imath}k$) of ETFE was calculated so that it can be used for the ray-tracing algorithm following the method described in [22].

ETFE layers and OPVs are very well suited for use as semi-transparent solar envelopes. The ETFE high transmittance over the solar range combined with its high emissivity over the atmospheric main transparency window (8 - 13 μm) are key properties for

glazing elements. On the other hand, both ETFE and OPV are great absorbers in the mid infrared region. Figure 3 shows the ETFE and OPV emissivity together with the atmospheric transmittance and the AM1.5G solar spectrum [23].

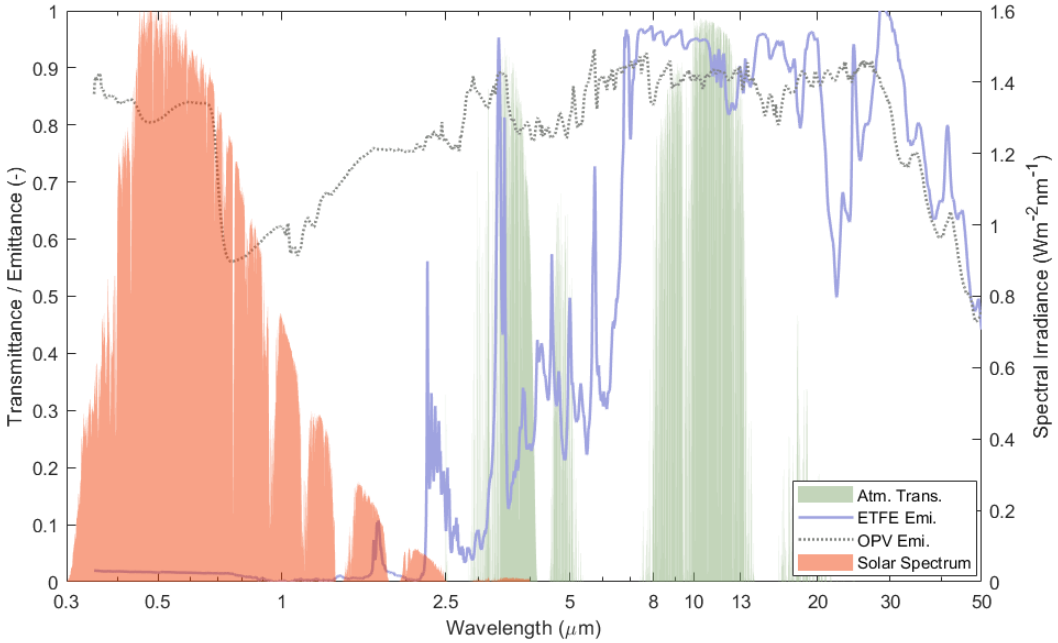

Figure 3. Spectral emittance of the ETFE foil (150 μm-thick) and the OPV module.

2.2 Emittance modelling

The spectral directional absorptance/emittance of the ETFE/OPV cushions was modelled over solar and thermal ranges (0.35 μm – 50 μm) using a 3D ray tracing algorithm programmed in Matlab. The code is formulated to consider all photonic interactions within the cushions.

The exact 3D geometry of commercially available ETFE cushions was modelled as depicted in Figure 4 [24]. The square cushions are 1 meter wide and have a height of 0.16 meters. The cushions are comprised of three layers where two of them act as shellelements (envelope, superior and inferior) adopting the shape of Figure 4 when inflated. The third layer splits the inner chamber into two air chambers.

Four different cushion configurations with ETFE and OPVs acting as layers have been studied as described in Table 1:

Table 1. Set of studied cushion configurations.

Configuration	Top	Middle	Bottom
C0	ETFE	ETFE	ETFE
C1	OPV	ETFE	ETFE
C2	ETFE	OPV	ETFE
C3	ETFE	ETFE	OPV

Configuration C0 stands for a cushion where the three layers are considered to be 250 μm-thick ETFE foils. This configuration is already commercially available and installed in several building worldwide, hence stressing the importance of the present work which considers properly its optical and thermal properties. Configuration C1 substitutes the EFTE outer layer by a continuous array of OPVs facing the sun directly. C2 configuration includes OPVs in its inner layer keeping the cushion envelopes with ETFE foils. Finally, configuration C3 substitutes the inner layer (the one facing the building interior) with the OPVs array.

These configurations have been selected in order to properly assess how incorporating OPV in semi-transparent envelopes impacts its performance (optical, thermal and electrical output) and to determine the best position for the OPV module within the cushion. The electrical and thermal productions are closely related and depend on how the module is illuminated as a function of its position within the cushions.

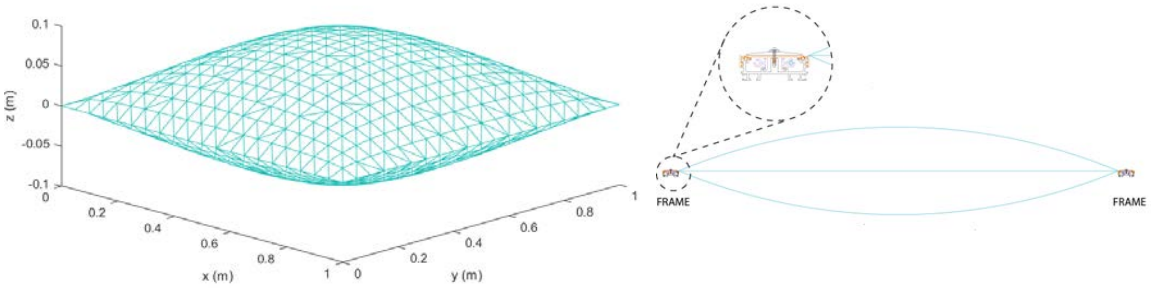

Figure 4. 3D exterior geometry of the cushion with the triangularization and cross-sectional view with a detail of the fixing frame.

A triangularization of the curved cushions was performed to compute the ray-tracing algorithm while considering the exact geometry. Consequently, surfaces were split into a set of small triangles that all together replicate the exact geometry.

The ray-tracing code considers the optical constants derived from the experimental measurements to determine the total emittance of the cushion and the emittance of each individual layer. It computes the absorption at different layers as a function of point above the cushion where the ray is launched and the incidence direction (zenith and azimuth). Different launching points were considered to properly assess radiative interactions between different layers in the thermal model. A sufficient number of rays was traced following a Monte-Carlo approach to ensure the results were not dependent on this number.

2.3 Thermal model

A computational fluid dynamics (CFD) model was built in Comsol Multiphysics to simulate the cushion configuration. First, a two-layer ETFE cushion was modelled and

experimentally validated. Later, the model was extended to a three-layer system including the OPV module in the inner one (see Fig. 4).

An experiment with a two-layer ETFE cushion was assembled in the laboratory. The experimental setup had only 2 layers of ETFE instead of 3, because it was not possible to maintain the pressure adequately with 3 layers. Heat flux (Hukseflux®) and several temperature (T-type thermocouples) sensors were installed to measure the flux passing through the walls (*Qw*) and the ETFE layers, and interior (*Ti*) and exterior (*Te*) temperatures. The cubicle where the ETFE was installed at the top had a 0.15 m-thick insulated walls and 1x1x1 m^3 dimensions. Figure 5 shows a schematic of the experiment and a picture. In the picture, the blowing unit to keep the air pressure inside the cushion and the data acquisition system (DAQ) system are visible. From the experiment, the thermal transmittance (*U*) can be obtained by calculating the heat flux passing through the cushion as the difference between the heat flux of the electric resistor and the heat flux passing through the walls:

$$U = \frac{Qh - Qw}{(Ti - Te)A} \quad (1)$$

where *A* is the aperture area of the cushion.

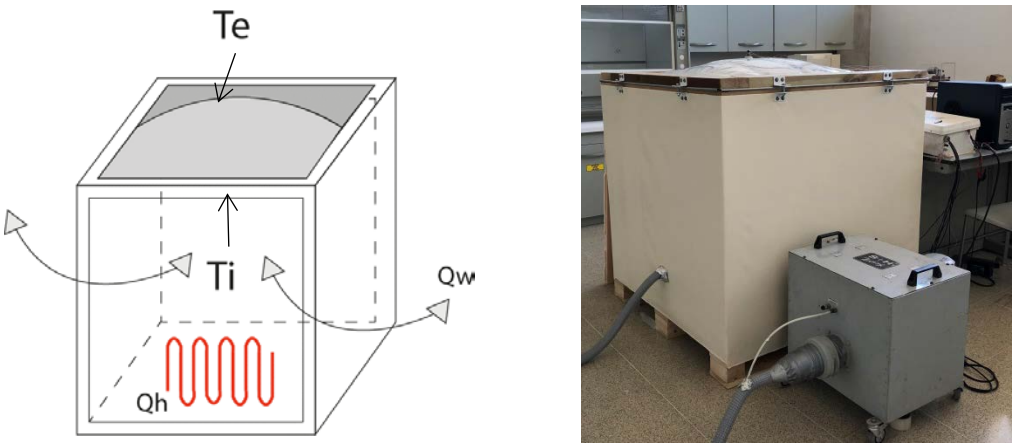

Figure 5. Schematic and photograph of the experimental unit.

3. Results

3.1 Optical performance

In this subsection, the optical performance of the four selected configurations is assessed. It should be noted that, as previously remarked, the absorptance and the emittance are named indistinctly.

The first results shown in Fig. 6 are about the reference configuration consisting of three ETFE layers. Since all the layers are ETFE foils, the configuration is highly

transmissive over the solar range with an average value of 0.8. On the other hand, C0 is highly absorptive over the mid- to far-infrared above 7 μm, and in particular over the atmospheric transparency window (8-13 μm). These two characteristics are key for radiative cooling purposes while bringing a very good transparency over the solar range for lighting.

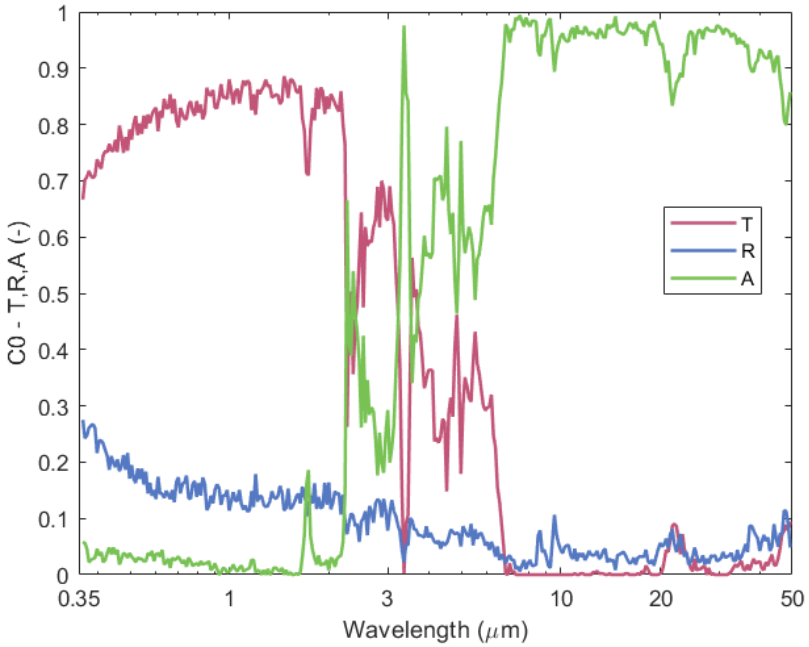

Figure 6. Optical characteristics for configuration C0.

Figure 7 charts the reflectance, absorptance and transmittance of configurations C1, C2 and C3. Several differences with Figure 6 can be spotted. Cushions including OPVs (regardless of its position) become much more absorptive in the solar range. The three configurations (C1, C2 and C3) show similar overall reflectance, absorptance and transmittance with minor differences. These cushions are transmissive from 0.7 to 1 μm with peaks of transmittance not larger than 0.35.

On the other hand, there are some differences between C1, C2 and C3 when looking at the absorptance of the OPV. As expected, the configuration where the module is placed at the outer layer (C1) is where the OPV absorbs more solar irradiation and thermal radiation. In C2, the OPV still absorbs most of the solar irradiance due to the high ETFE transmittance (0.08 less than in C1) while most of the thermal mid-infrared radiation coming from the atmosphere is absorbed by the outer layer. Finally, configuration C3 follows the same trend but, since solar irradiance has to cross two ETFE layers before impacting the module, the amount of solar radiation absorbed is reduced considerably compared to C1 and C2. In addition, the amount of infrared thermal radiation reaching the module is very low.

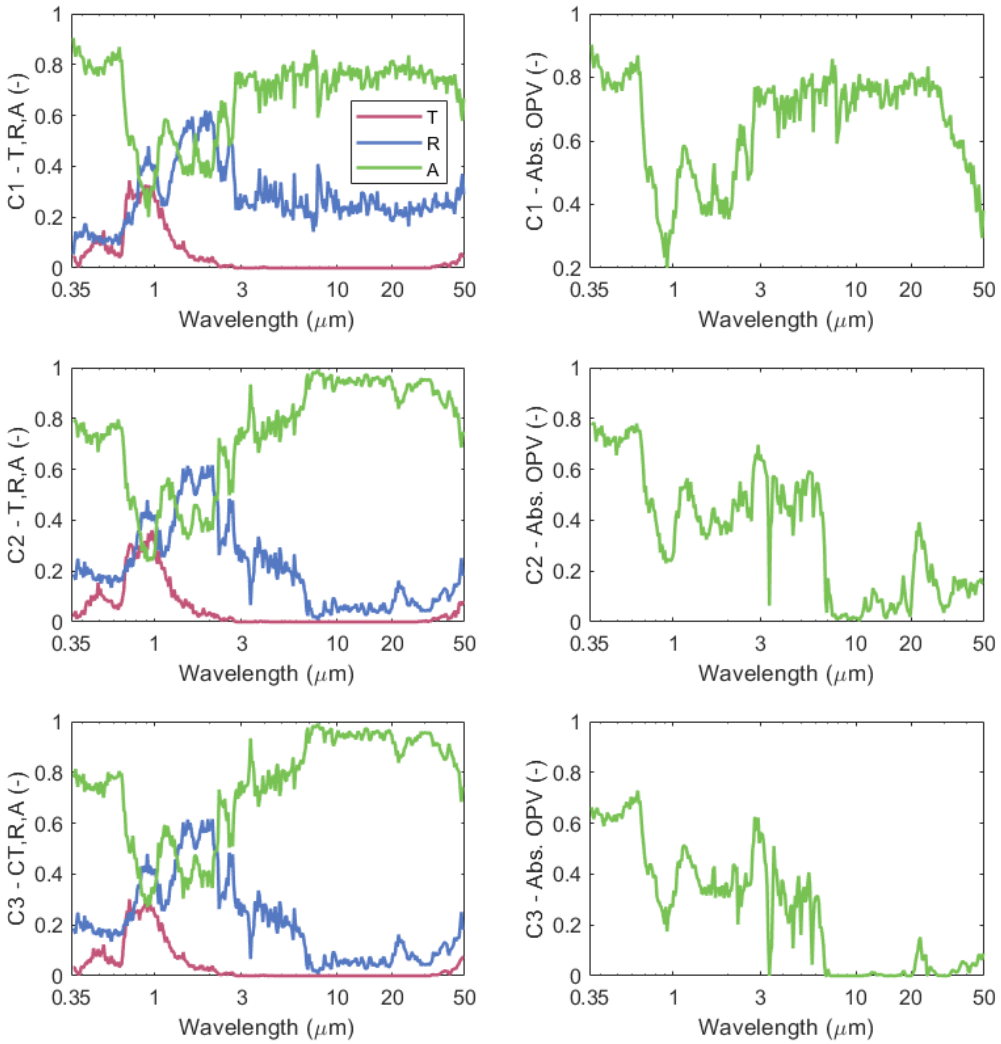

Figure 7. Optical characteristics of configurations C1, C2 and C3 together with the OPV absorptance in each configuration.

3.2 Thermal performance

Figure 8 displays the temperature contours and the velocity streamlines of air enclosed between foils. The simulation was conducted following the UNE regulation for glazing elements [27], that for the present case set the interior temperature at 20 ºC, the exterior at 0 ºC and the interior and exterior heat exchange coefficients to 7.7 W/(m^{2}K) and 25 W/(m^{2}K) respectively. The cavity, with the hotter temperature at the bottom, experiences natural Rayleigh-Bénard convection and in the velocity streamlines graph the Bénard cells can be clearly identified.

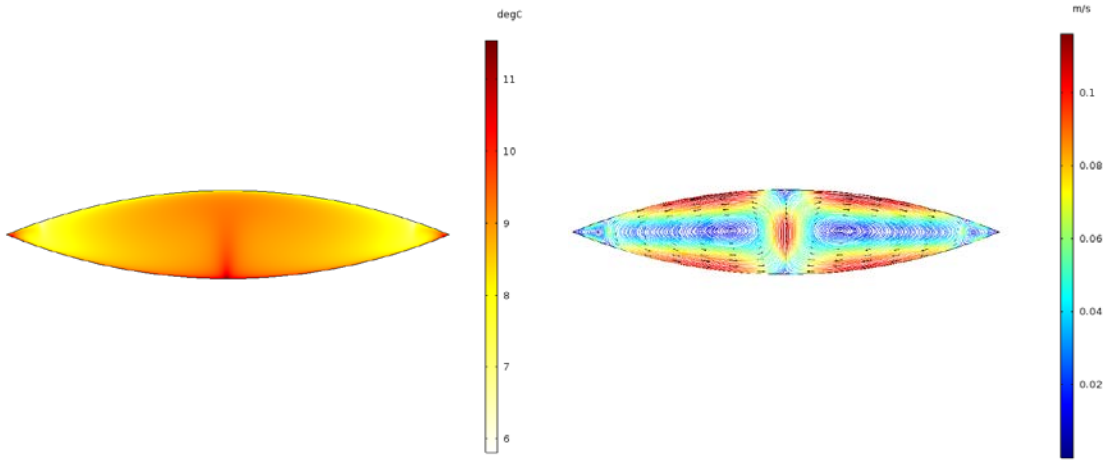

Figure 8. 2-layer cushion air temperature contours and velocity streamlines.

With these results, the mean thermal transmittance coefficient for a 2-layer cushion placed horizontally was found to be U = 2.65 W/ m^{2}K. This result was experimentally validated with the experimental setup described in the previous section 2. Figure 9 (left) illustrates the monitored temperatures of the interior and exterior ETFE layers. The interior temperature, when the electrical resistor is on, experiences a linear increase. However, the exterior temperature follows a periodical trend. It increases up to certain point when suddenly it decreases before starting the same cycle again. This behavior was due to the pump blowing air to keep the pressure constant. When the pressure sensor detected a decrease in pressure, fresh air from outside was blown in, thus provoking the observed effect. The heat flux was calculated for several cycles, getting the tendency included in Fig. 9 (right).

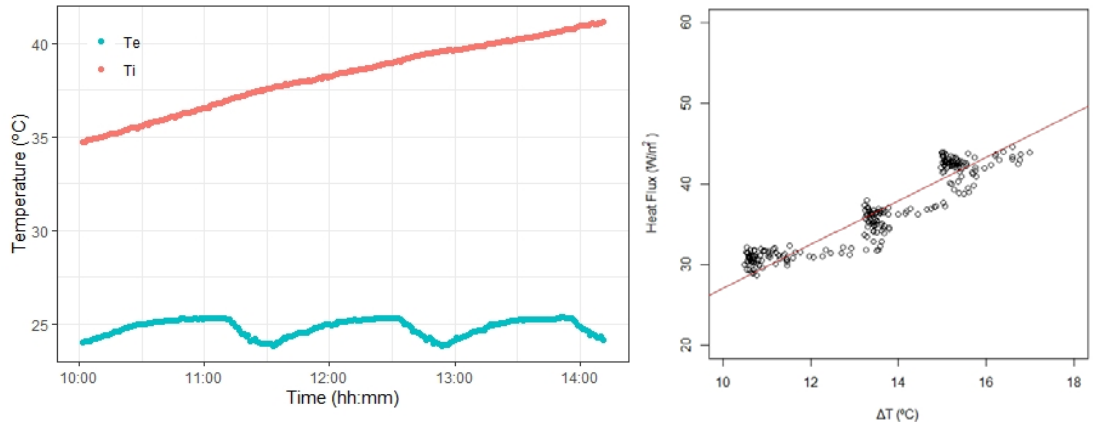

Figure 9. Left: Interior and exterior temperatures in the test unit; Right: heat flux crossing the cushion as a function of the interior and exterior temperatures difference.

The slope of the heat flux vs. temperature difference curve is the mean thermal transmittance, which is 2.70 W/ m^{2}K. This value, compared with the CFD result (2.65

W/ m^2K), means a relative difference of less than 2%, thus showing a very good agreement.

The next results, after considering that the CFD model is validated, deal with the temperatures for the 3-layer configuration. The boundary conditions are the same as for the 2-layer case, as indicated by the norm [27].

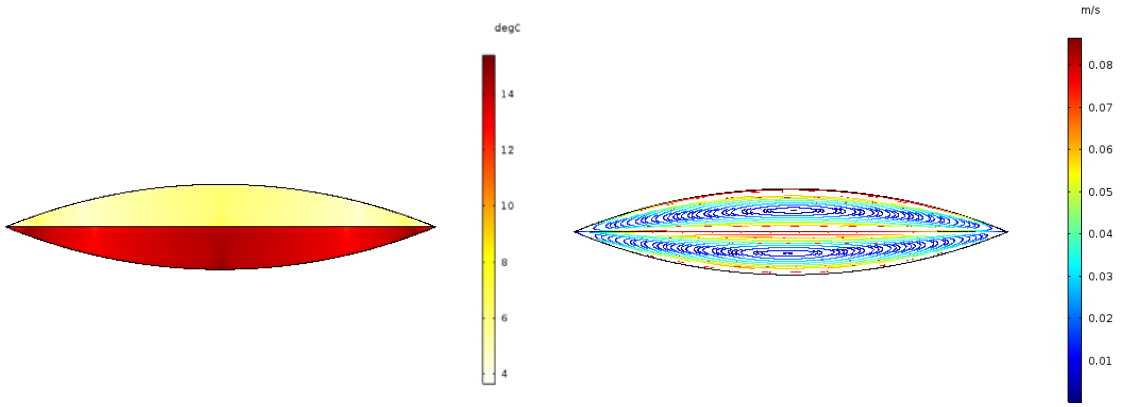

Figure 10. 3-layer cushion air temperature contours and velocity streamlines.

Temperature contours and velocity streamlines considerably change with respect to the previous configuration since the middle layer creates two different temperature zones and breaks the two Bénard cells to one per cavity. For this configuration the thermal transmittance decreased to 1.58 W/ m^2K. This value is similar to that of very high quality double glass windows with air cavities between 6 mm glass panes of about 16 mm. However, in the case of the ETFE cushions, the foil thickness is 250 μm compared to the 6 mm and, in addition, the density of ETFE is half of the glass. Moreover, using ETFE allows manufacturing glazing elements up to about 6 m by 3 m per framing structure and, since the energy required for fabrication and recycling is much less than that for the glass, the associated environmental costs are lower [14].

The mean temperatures of the layers are 4.5 ºC for the external layer, 9.3 ºC for the middle layer and 14.1 ºC for the internal layer. It should be remarked that, following the European regulation [27], simulations neither consider the solar spectrum nor thermal radiation effects (internal heat sources within the foils due to radiation exchange) and therefore, since the calculations deal with temperatures only in the range [0-20]ºC, no differences regarding the position of the OPV layer in the sandwich are found out.

3.3 Electrical performance

Figure 11 shows the solar irradiance absorbed by the OPV with the spectral range where photogeneration takes place. Ideally, high irradiance is desirable over this range and radiation absorbed out of it will just heat up the module.

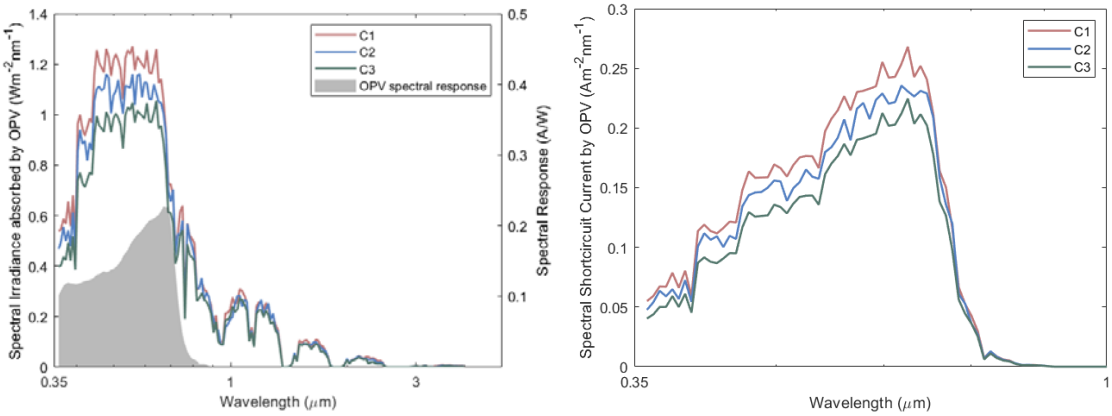

Figure 11. Left: Solar Irradiance absorbed by the OPV in configurations C1, C2 and C3; Right: Spectral short-circuit current density (J_{sc}) for configurations C1, C2 and C3.

By integrating the spectral short-circuit current from Fig. 11 (right), the short-circuit current density can be obtained. The results are given in Table 3.

Table 3. Short-circuit current density (J_{sc}) for configurations C1, C2 and C3.

	J_{sc} (Am^{-2})
C1	65.17
C2	59.85
C3	53.39

4. Conclusions

Optical spectral transmittance and reflectance values for ETFE foils with different thickness and for a commercially available OPV module have been measured from 0.35 µm to 50 µm, covering from the far ultraviolet, visible and far-infrared regions. This radiative characterization allows covering more than 99% of the spectrum emitted by a blackbody at a temperature of 25 ºC.

Spectral emittances, calculated by ray-tracing from using the optical properties (complex refractive index) inferred from measured optical characteristics, are reported for four different horizontal cushion configurations. Configuration C0 refers to a three-layer ETFE cushion and C1-C3 are with three layers but with two layers of ETFE and

one consisting of an OPV module. Position of OPV layer is either at the top (C1), or at the bottom (C3), or in the middle (C2). C0 is highly emissive in the mid-infrared, with an almost 100% emittance over the atmospheric transparency window (8-13 μm), and transmits almost entirely the solar spectrum. Cushions including OPVs (regardless of its position) become much more absorptive in the solar range. The three configurations (C1, C2 and C3) show similar overall reflectance, absorptance and transmittance with minor differences. Regarding the OPV layer, the configuration where the module is at the top (C1) is that with the largest irradiation absorbed by OPV, including the solar fraction.

The CFD model results in thermal transmittances of 2.65 W/m^2K and 1.58 W/m^2K for the two- and three-layer cushions. In the case of the two-layer ETFE cushion, numerical results have been experimentally validated showing a very good agreement. Regarding the three-layer configuration, the mean temperatures of the three layers obtained through the numerical simulations are 4.47 ºC, 9.27 ºC and 14.07 ºC, referred from the outer to the inner layer respectively.

Electrical performance of the OPV cells is influenced by the position of the module. Short-circuit current densities range from around 50 A/m^2 to 65 A/m^2 for the worst and best case.

The thermal results obtained reveal a great potential of this type of glazing for building integration applications since thermal transmittances are similar to those of very high quality double-glass windows. However, in terms of weight, manufacturability and economical and environmental costs, ETFE may be advantageous.

Further investigation is being carried out to fabricate a representative size ETFE/OPV cushion to be characterized outdoors in a test unit. This will better support the obtained results, allowing feedback in the model presented. CFD modelling could be more accurate by including the solar spectrum and radiative exchanges with the cold outer space in clear-sky conditions.

Acknowledgements

This research was supported by the "Generalitat de Catalunya" (grants 2018FI_B1_00136, 2017 SGR 1276 and ICREA Academia) and "Ministerio de Economía y Competitividad" of Spain (grant reference ENE2016-81040-R). The authors would like to acknowledge the collaboration with the company IASO SA.

5. References

[1] European Parliament, "The energy performance of buildings directive factsheet (2019)." .

[2] H. Khandelwal, A. P. H. J. Schenning, and M. G. Debije, "Infrared Regulating Smart Window Based on Organic Materials," *Adv. Energy Mater.*, vol. 7, no. 14,

2017.

[3] A. Cannavale, F. Martellotta, F. Fiorito, and U. Ayr, “The challenge for building integration of highly transparent photovoltaics and photoelectrochromic devices,” *Energies*, vol. 13, no. 8, 2020.

[4] DIRECTIVE (EU) 2018/844, “Directive 2018/844/EU Energy performance of buildings,” *Off. J. Eur. Union*, vol. 2018, no. October 2012, pp. 75–91, 2018.

[5] P. K. Nayak, S. Mahesh, H. J. Snaith, and D. Cahen, “Photovoltaic solar cell technologies: analysing the state of the art,” *Nat. Rev. Mater.*, vol. 4, no. 4, pp. 269–285, 2019.

[6] J. Yu, Y. Zheng, and J. Huang, “Towards high performance organic photovoltaic cells: A review of recent development in organic photovoltaics,” *Polymers (Basel).*, vol. 6, no. 9, pp. 2473–2509, 2014.

[7] D. Hengevoss, C. Baumgartner, G. Nisato, and C. Hugi, “Life Cycle Assessment and eco-efficiency of prospective, flexible, tandem organic photovoltaic module,” *Sol. Energy*, vol. 137, pp. 317–327, 2016.

[8] S. Lizin *et al.*, “Life cycle analyses of organic photovoltaics: A review,” *Energy Environ. Sci.*, vol. 6, no. 11, pp. 3136–3149, 2013.

[9] S. Robinson-Gayle, M. Kolokotroni, A. Cripps, and S. Tanno, “ETFE foil cushions in roofs and atria,” *Constr. Build. Mater.*, vol. 15, no. 7, pp. 323–327, 2001.

[10] S. Afrin, J. Chilton, and B. Lau, “Evaluation and comparison of thermal environment of atria enclosed with ETFE foil cushion envelope,” in *Energy Procedia*, 2015, vol. 78, pp. 477–482.

[11] M. Schäffer and B. Stimpfle, “Large scale ETFE cushion roof covers the Lilienthalhaus in Brunswick, Germany | ETFE-Großkissendach über dem Lilienthalhaus in Braunschweig,” *Stahlbau*, vol. 87, no. 7, pp. 649–656, 2018.

[12] L. S. Babayan, *ETFE plastic application for reconstruction and preservation of architectural structures in Syunik Province, RA*, vol. 828 KEM. 2020.

[13] M. Rychtáriková, R. Šimek, J. Húsenicová, and V. Chmelík, “Prediction of noise levels in large shopping streets covered by glass and ETFE,” *Archit. Eng. Des. Manag.*, 2020.

[14] C. Lamnatou, A. Moreno, D. Chemisana, F. Reitsma, and F. Clariá, “Ethylene tetrafluoroethylene (ETFE) material: Critical issues and applications with emphasis on buildings,” *Renew. Sustain. Energy Rev.*, vol. 82, 2018.

[15] Á. Moreno, D. Chemisana, R. Vaillon, A. Riverola, and A. Solans, “Energy and luminous performance investigation of an OPV/ETFE glazing element for building integration,” *Energies*, vol. 12, no. 10, 2019.

[16] H. M. Zanelli, A.; Beccarelli, P.; Monticelli, C.; Ibrahim, “Technical and Manufacturing Aspects in order to create a smart façade system with OPV integrated into ETFE foils,” in *In Proceedings of the International Symposia IASS-APCS*, 2014.

[17] Z. Fan, M. De Bastiani, M. Garbugli, C. Monticelli, A. Zanelli, and M. Caironi, “Experimental investigation of the mechanical robustness of a commercial module and membrane-printed functional layers for flexible organic solar cells,”

Compos. Part B Eng., vol. 147, pp. 69–75, 2018.

[18] Z. Fan, M. De Bastani, C. Monticelli, and A. Zanelli, "Performance investigation of organic photovoltaic layers on architectural membrane," in *Advanced Building Skins Conference Proceedings of the 9th ENERGY FORUM*, 2014, pp. 1203–1217.

[19] J. Hu *et al.*, "Electrical-thermal-mechanical properties of multifunctional OPV-ETFE foils for large-span transparent membrane buildings," *Polym. Test.*, vol. 66, pp. 394–402, 2018.

[20] InfinityPV, "InfinityPV foil," *OPV brochure*, 2020. [Online]. Available: https://infinitypv.com/. [Accessed: 20-May-2020].

[21] D. Zhao *et al.*, "Radiative sky cooling: Fundamental principles, materials, and applications," *Appl. Phys. Rev.*, vol. 6, no. 2, 2019.

[22] T. P. Otanicar, P. E. Phelan, and J. S. Golden, "Optical properties of liquids for direct absorption solar thermal energy systems," *Sol. Energy*, vol. 83, no. 7, pp. 969–977, 2009.

[23] ASTM, "G173-03 Standard tables for reference solar spectral irradiances: direct normal and hemispherical on 37° tilted surface," *B. Stand.*, vol. 14.04, 2004.

[24] Iasoglobal, "Iasoglobal ETFE cushion," *ETFE cushion brochure*. [Online]. Available: https://www.iasoglobal.com. [Accessed: 15-Nov-2019].

[25] AENOR, "UNE EN 673:2011. Vidrio en la construcción. Determinación del coeficiente de transmisión térmica U. Método de cálculo.," 2011.

Capítulo 7. Conclusiones e investigaciones futuras

1. Discusión general y conclusiones

En la presente tesis se han estudiado y modelado sistemas fotovoltaicos orgánicos semitransparentes incorporados en membranas de ETFE para su integración en edificios como sistemas constructivos translucidos. Este tipo de sistema constituye una alternativa a los materiales convencionales utilizados en la construcción debido a sus propiedades transparentes, energéticas y de baja energía incorporada. En los siguientes párrafos, se muestran las principales conclusiones en el orden lógico en el que se han desarrollado los diferentes capítulos y objetivos.

De la revisión realizada sobres tecnologías fotovoltaicas semitransparentes, se concluye que estas tecnologías están despertando mucho interés debido a los avances tecnológicos que han permitido lograr eficiencias de conversión eléctrica elevadas con valores de transmitancia del espectro visible también altas. La revisión repasa las tecnologías ya maduras como son las basadas en materiales inorgánicos, Silicio, CdTe, CIGS y las tecnologías menos maduras de 3ª generación como las DSSC, perovskitas y orgánicas. Esta última recibe mayor importancia en la revisión ya que es utilizada como tecnología para ser integrada en los cerramientos poliméricos estudiados. Se seleccionó la tecnología orgánica porque, suponiendo todas las ventajas mencionadas, está en una fase mucho más avanzada que las perovskitas, habiendo módulos comerciales. Por otro lado, las eficiencias registradas son de más del doble que las obtenidas en células del tipo DSSC. Se realiza un breve repaso al método de funcionamiento y fabricación y se muestran los avances logrados en investigaciones previas, las cuales muestran que la tecnología orgánica representa una tecnología con gran potencial para ser utilizada en la integración en edificios, presentando eficiencias superiores al 10% y transmitancias en el rango visible de alrededor del 40%.

De la revisión realizada sobre el ETFE, se concluye que es un material prometedor como elemento constructivo de la envolvente de un edificio, puede ser utilizado en tejados, fachadas, lucernarios…Presenta múltiples ventajas como su liviandad, la posibilidad de realizar estructuras flexibles con diferentes formas, material respetuoso con el medio ambiente y compatible con la integración de sistemas fotovoltaicos al poder ser utilizado como sustrato. La revisión repasa las principales propiedades como elemento constructivo, como son las mecánicas, ópticas, térmicas y medioambientales.

Se llevan a cabo unas mediciones del comportamiento eléctrico y lumínico de tres tecnologías orgánicas en condiciones reales de operación. Se concluye que las células orgánicas presentan una alta transmitancia en el espectro visible, obteniendo unos valores de eficiencia de en torno al 4%. También se concluye que las células

orgánicas presentan una estabilidad variable según el tipo de célula utilizada. Por esta razón, el protocolo ISOS establece de forma particular las pruebas pertinentes a realizar en este tipo de módulos.

Se lleva a cabo el modelado y simulación dinámica completa de un sistema plano OPV / ETFE integrado en una fachada sur (hemisferio norte), en el que se caracterizan el efecto sobre la iluminación del espacio interior, las demandas térmicas y la generación de energía eléctrica. Se determinó que el sistema OPV/ETFE representa una alternativa prometedora a los cerramientos de vidrio convencionales, que puede proporcionar energía para cubrir una parte de la demanda energética de la vivienda, que puede ser utilizado como sistema de control solar y lumínico manteniendo un confort visual interior adecuado.

Se ha realizado un modelo físico que contempla las propiedades ópticas de las membranas de ETFE y de las OPVs, de forma que mediante un trazado de rayos completo se hallan las diferentes emitancias de los elementos individuales y de los conjuntos en configuración de cojín hinchable. A partir de esta determinación, se han balanceado los diferentes flujos térmicos, incluyendo de forma explícita los radiativos, para conocer el comportamiento su comportamiento térmico y, en consecuencia, el eléctrico del módulo orgánico implicado.

2. Investigaciones futuras

Se han caracterizado experimentalmente los diferentes elementos del sistema por separado, pero sería interesante fabricar el sistema completo a una escala adecuada e incorporarlo en una celda de testeo de elementos constructivos para poder evaluar y validar los diferentes modelos teóricos realizados, además de evaluar las dificultades posibles que se pueden encontrar en el ensamblaje del conjunto. Por este motivo, la construcción de un prototipo que nos permita realizar un estudio detallado del comportamiento en condiciones reales de operación es uno de los principales hitos futuros, y en los que en la actualidad se está trabajando.

Las células orgánicas, como se ha visto a la revisión, despiertan un gran interés y en consecuencia los avances conseguidos en eficiencia eléctrica y comportamiento lumínico son continuos. Por lo tanto, aunque en la actualidad estos avances conseguidos en eficiencia eléctrica y lumínica sean a nivel de laboratorio, es necesario tenerlos en cuenta para tener una visión real del potencial de esta tecnología.

La simulaciones dinámicas requieren de modelos matemáticos que describan el comportamiento de los sistemas evaluados, hasta el momento los sistemas planos como el estudiado ya disponen de modelo validados, pero es necesario la modelización de nuevos sistemas de cerramiento como son las estructuras en forma

de cojín hinchable, por este motivo, el desarrollo de un modelo matemático y su validación para poder ser utilizado en un programa que permita realizar simulaciones dinámicas es necesario. El modelo físico se corresponde con el capítulo 6 de la tesis, y concretamente la tarea que sería la subsiguiente es su validación experimental, pudiendo de esta forma realimentar el modelo para afinarlo.

Como ya se ha visto, hay muchos estudios sobre la eficiencia de las células solares orgánicas, aunque uno de sus puntos flojos es la estabilidad, la realización de estudios de estabilidad durante periodos largos son necesarios para poder incrementar la confianza del consumidor final en esta tecnología.

La incorporación de sistemas semitransparentes ha sido estudiada para la integración en edificios, nuevos enfoques como el uso en invernaderos u otras aplicaciones pueden ser evaluados.